Synchrotron radiation in materials research

Yuriy Zorenko

**Institute of Physics Kazimierz Wielki University in Bydgoszcz,
85-070 Bydgoszcz, Poland**

Synchrotron radiation in materials research

Lection 2

X-ray imaging using the synchrotron radiation

13.09.2016, Milan, Italy

Outline of lection

1. Introduction – why we need the scintillating screens based on the single crystalline films ?
1. Development of the visible emitting SCF scintillation screens on the base of different oxide compounds
3. Example of X-ray imaging using the traditional X-ray sources and synchroton radiation excitation
4. New generation of the SCF scintillators for X-ray imaging:
   - multi-layer scintillators;
   - K-edge engineering;
5. Shortly about development of SCF scintillating screens based on the mixed garnet compounds
6. Conclusions

Application of luminescent materials based on the SCF of oxide compounds

1. Laser media
2. Cathodoluminescent screens of electron beam tubes;
3. Thin film scintillators for α- and β–particles registration;
4. **Screens for visualization of X ray image with high spatial resolution – hot topic of research related to my lecture**

ESRF

T. Martin group

Crytur Ltd, Czech Republic

13.09.2016, Milan, Italy

Indirect X-ray detection principle

A Light for Science

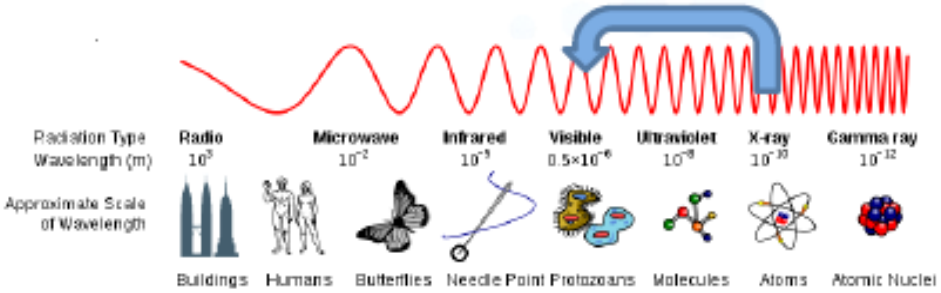

X-ray photons are not detected directly by the imaging camera; a material is used to convert x-ray photons to **visible wavelengths**.

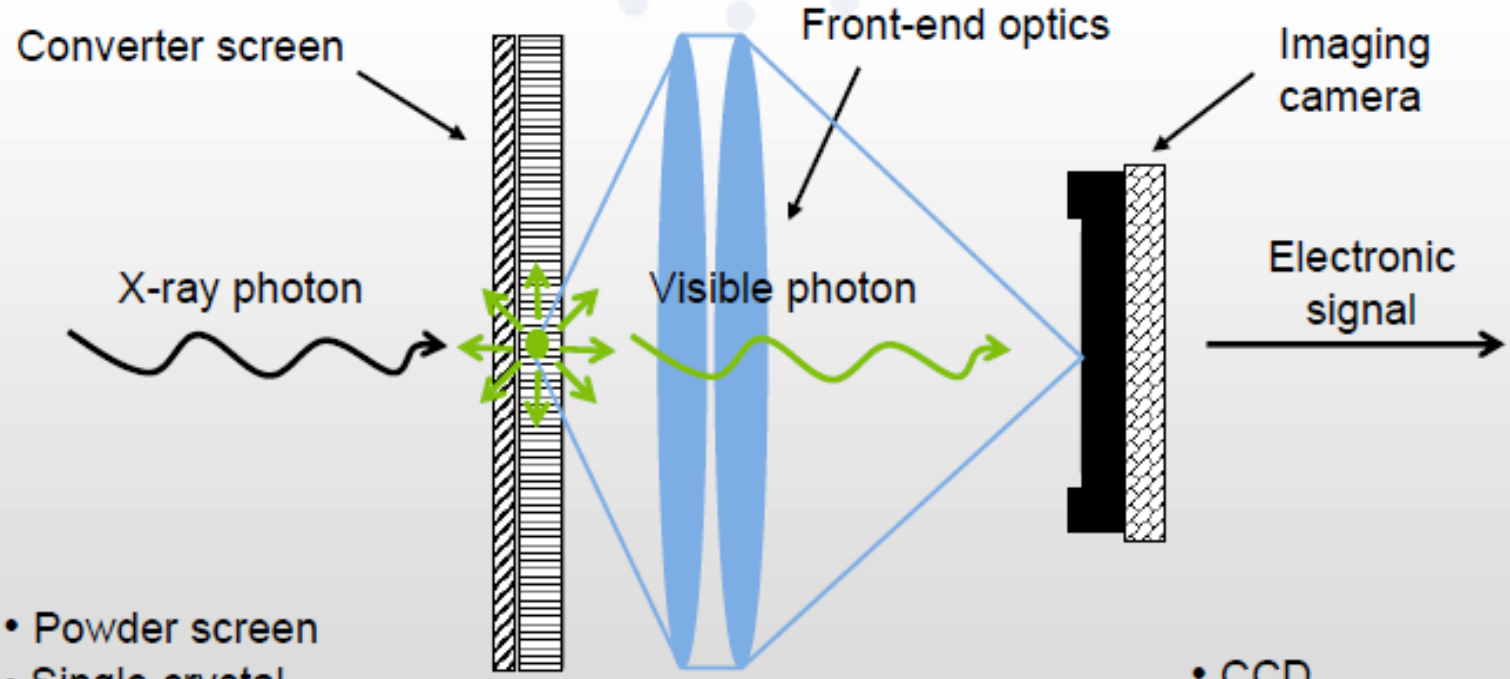

- Powder screen
- Single crystal
- Structured scintillator
- Transparent ceramic

- Fiber optics
- Refractive lenses
- Reflective lenses

- CCD
- CMOS

Converter screen: technologies

Spatial resolution (thin) vs. absorption efficiency (thick)

- Powder screen

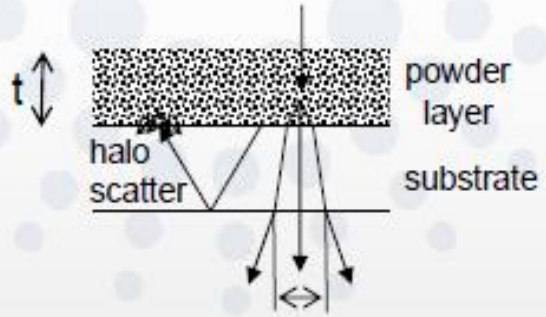

R ~ t ≥ 2(grain size)
R ~ 5 µm

- Structured scintillator

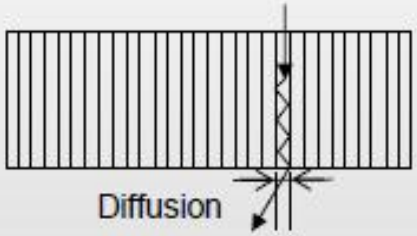

R < t
R ~ 10 µm

- Transparent ceramics

Under development

(R ~ 2 µm)

- Single crystal:

  Single crystal film, massive crystal

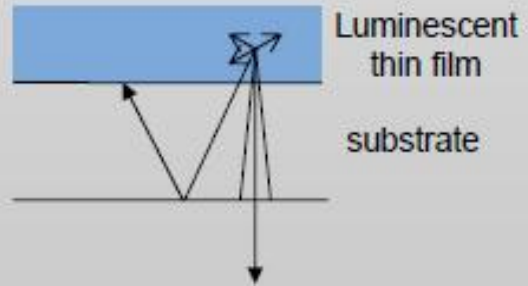

R < t
R < 1 µm

Comparison of the resolution of the powder (a) and SCF (b) screens

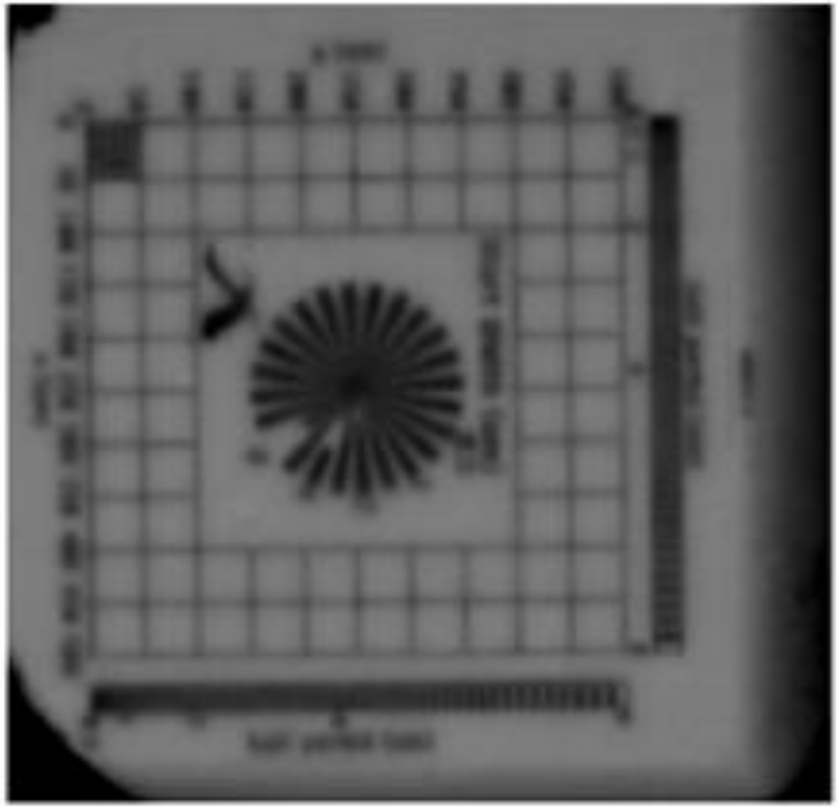

(a) Gadox powder 5µm

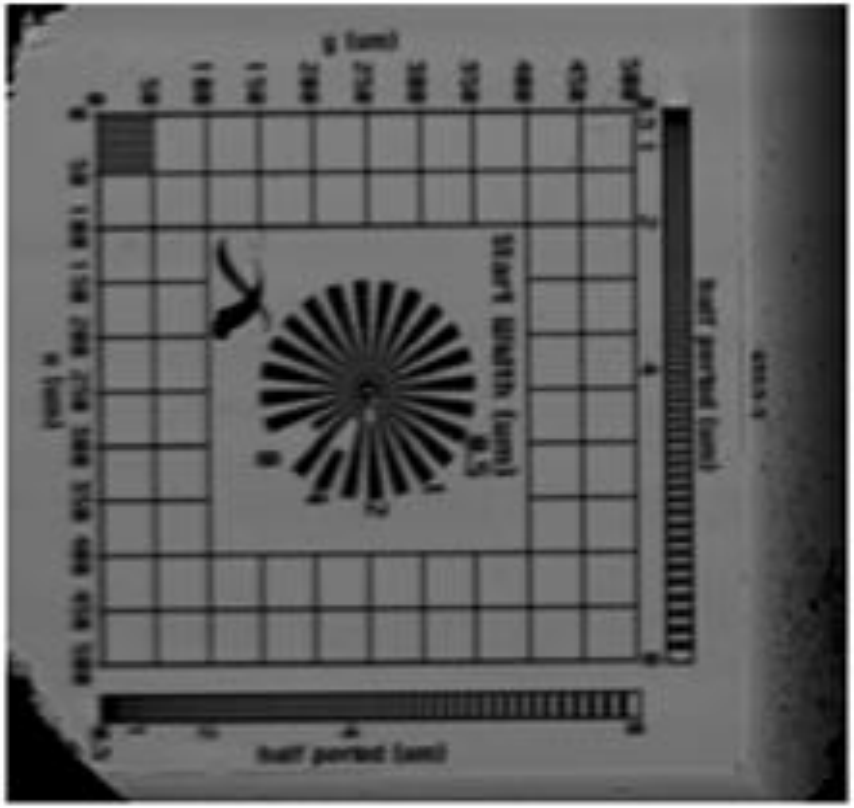

(b) LSO:Tb SCF 48µm

X ray tomography using the traditional X ray sources

13.09.2016, Milan, Italy

High resolution 2D-imaging under X-ray excitation

J. Tous, Nucl.Instr.Meth.Phys.Res. A 591 (2008) 264–267

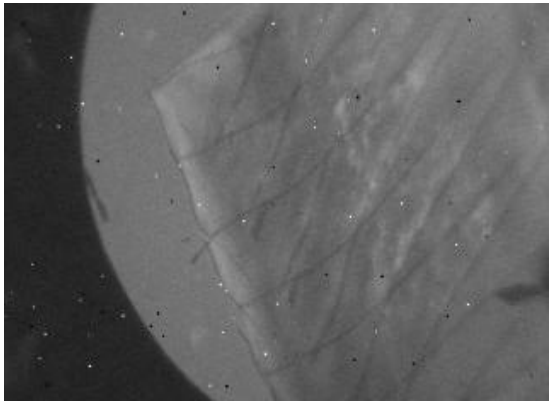

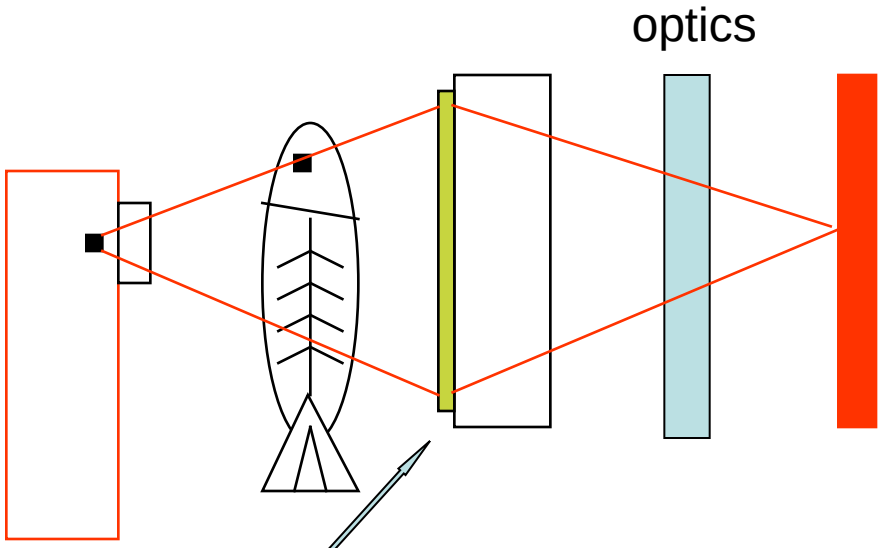

Sub-μm resolution needed!
Better 2D-resolution requires thinner scintillator

Experimental set-up for 2D imaging

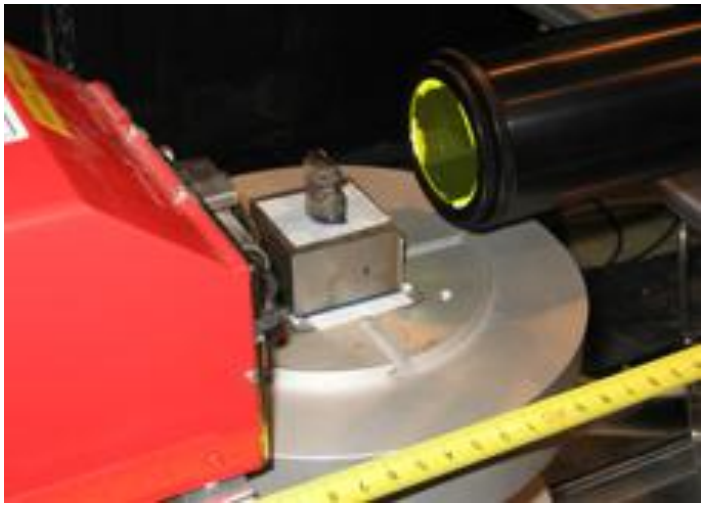

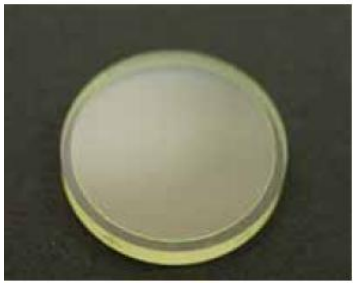

Made by CRYTUR Ltd, CR

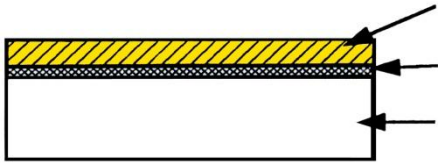

X-ray radiography of a spider (left) and a mouse brain (right). In the last image the bloodstream within the brain is resolved (J. Tous, http://iopscience.iop.org/1748-0221/6/01/ C01048)

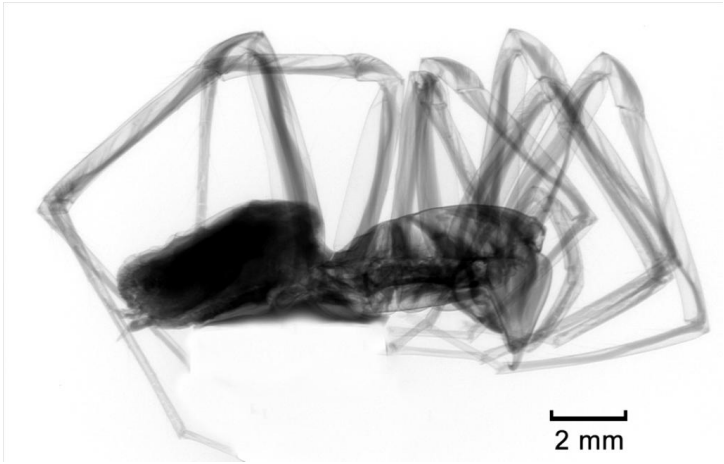

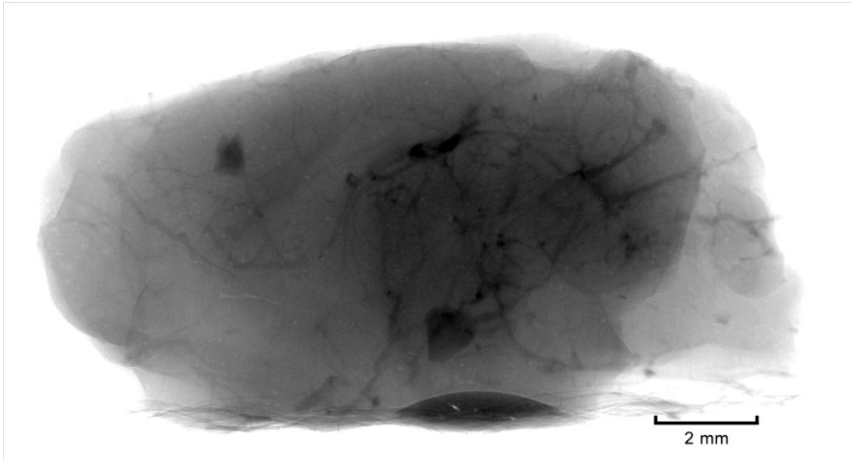

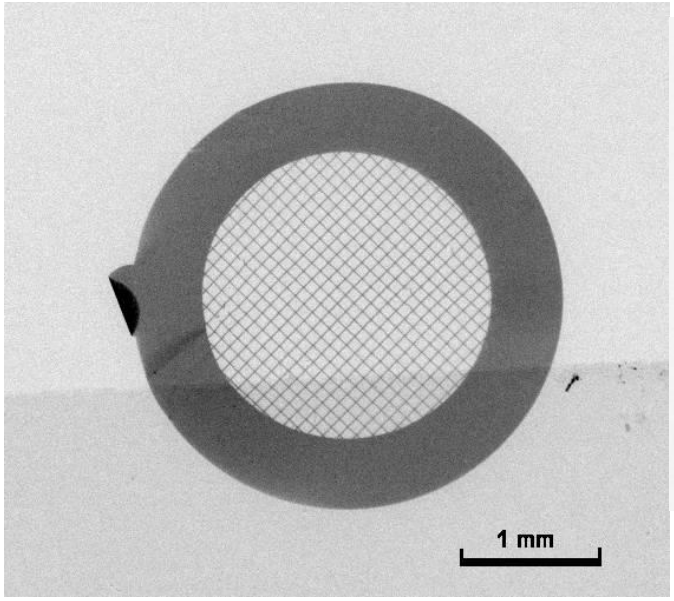

X-Ray Images of the grid

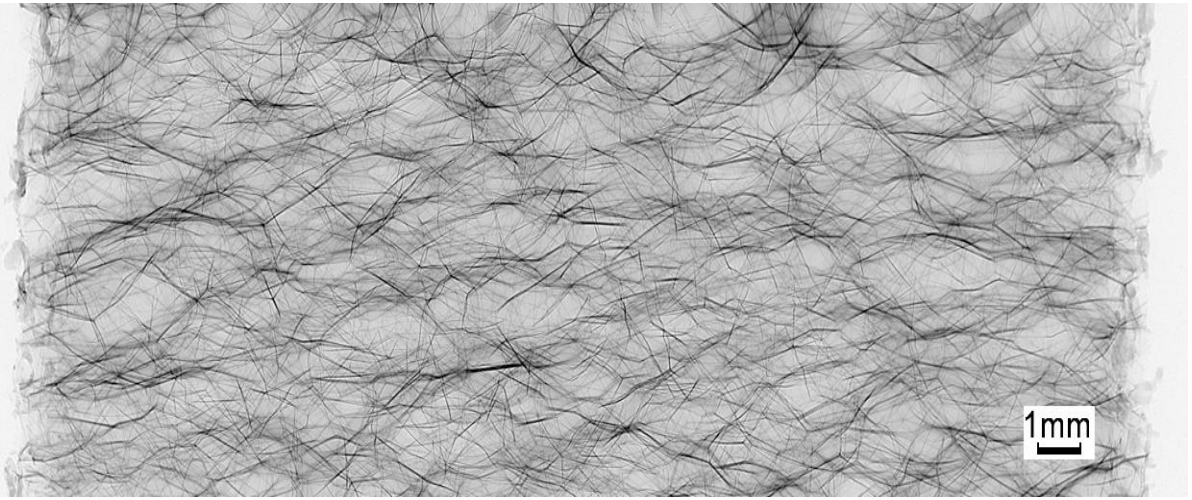

High Resolution and High Contrast Image of Plastic Foam

J. Tous, prented at NDT in Aerospace 2010

Some more images by LuAG:Ce SC plate sensor

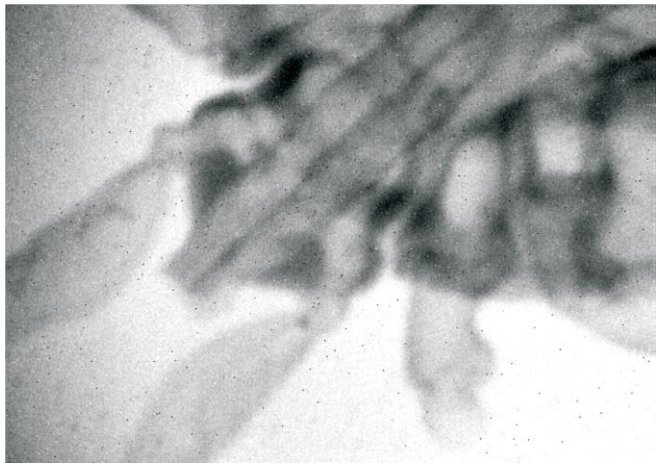

A tick

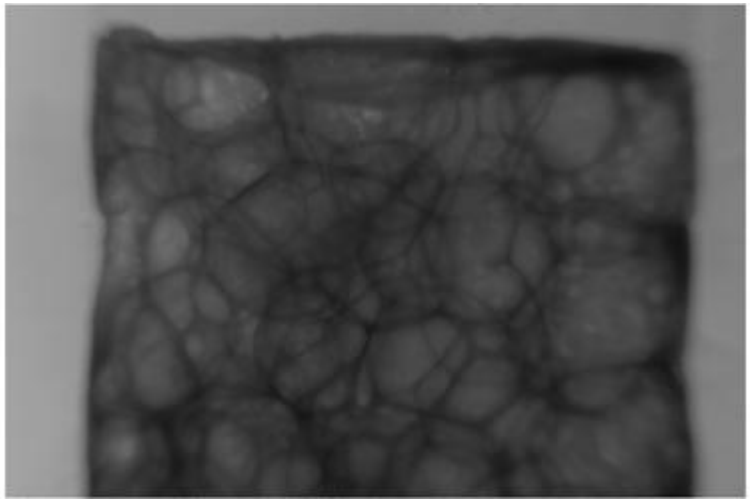

Aluminum structure

Coaxial cable with
BNC connector

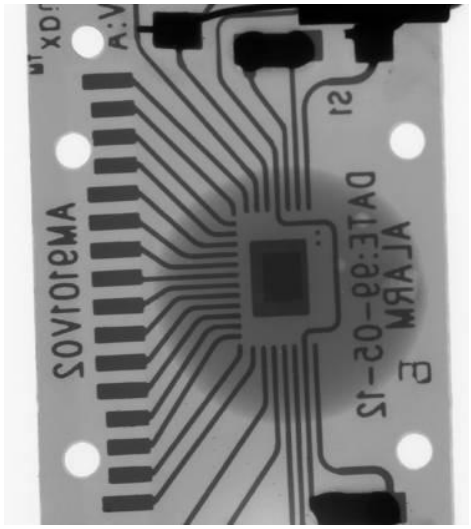

A circuit from calculator

Imaging with typical X-ray sources

Screens for visualization of X-ray images

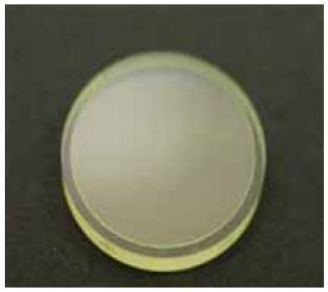

Visual appearance of LuAG:Ce LPE-grown film samples Lu-6,9,11,16.
On the right the bulk sample is displayed with the LuAG:Ce plate on the top surface.

Crytur Ltd, Czech Republic

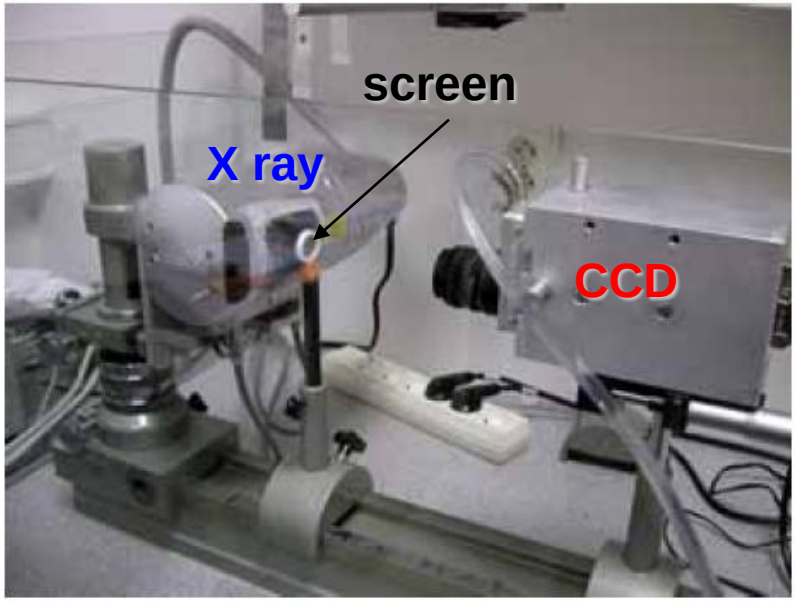

2D X-ray imaging experiment is composed of microfocus X-ray source (on the left), sample holder and digital CCD camera with high 2D-resolution.

M. Nikl, et al., Proc. SPIE, 2009, 7310, 731008.

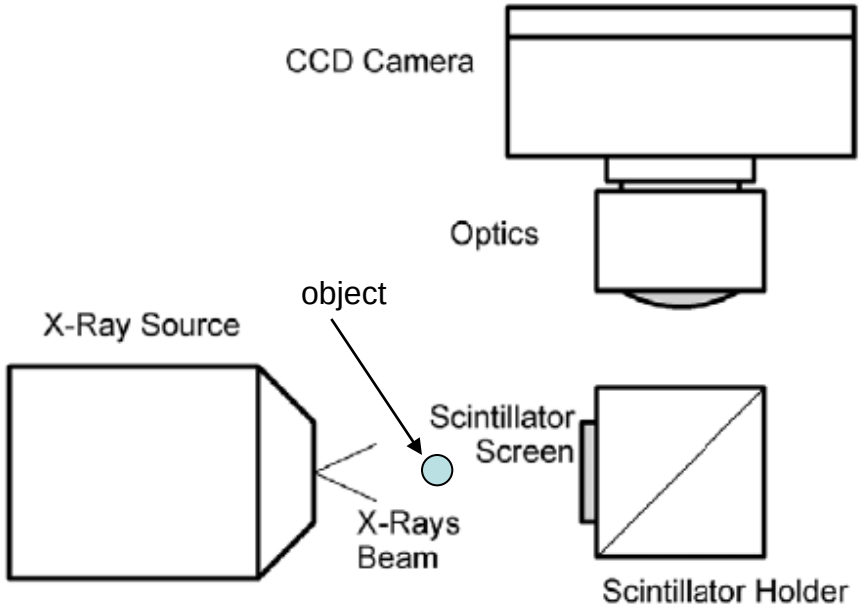

J. Tous, *Rad. Measur.*,10.1016/j.radmeas.2012.01.015

Imaging with typical X-ray sources

Crystal and film screens for visualization of X-ray images

Image of Pt wire-net with thickness of ~8 μm obtained with help of screens based on LuAG:Ce film (a) and crystal (b) with thickness of ~20 μm. The images were obtained in Crytyr Ltd, Turnov, Czech Republic

M. Nikl, et al., Proc. SPIE, 2009, 7310, 731008.

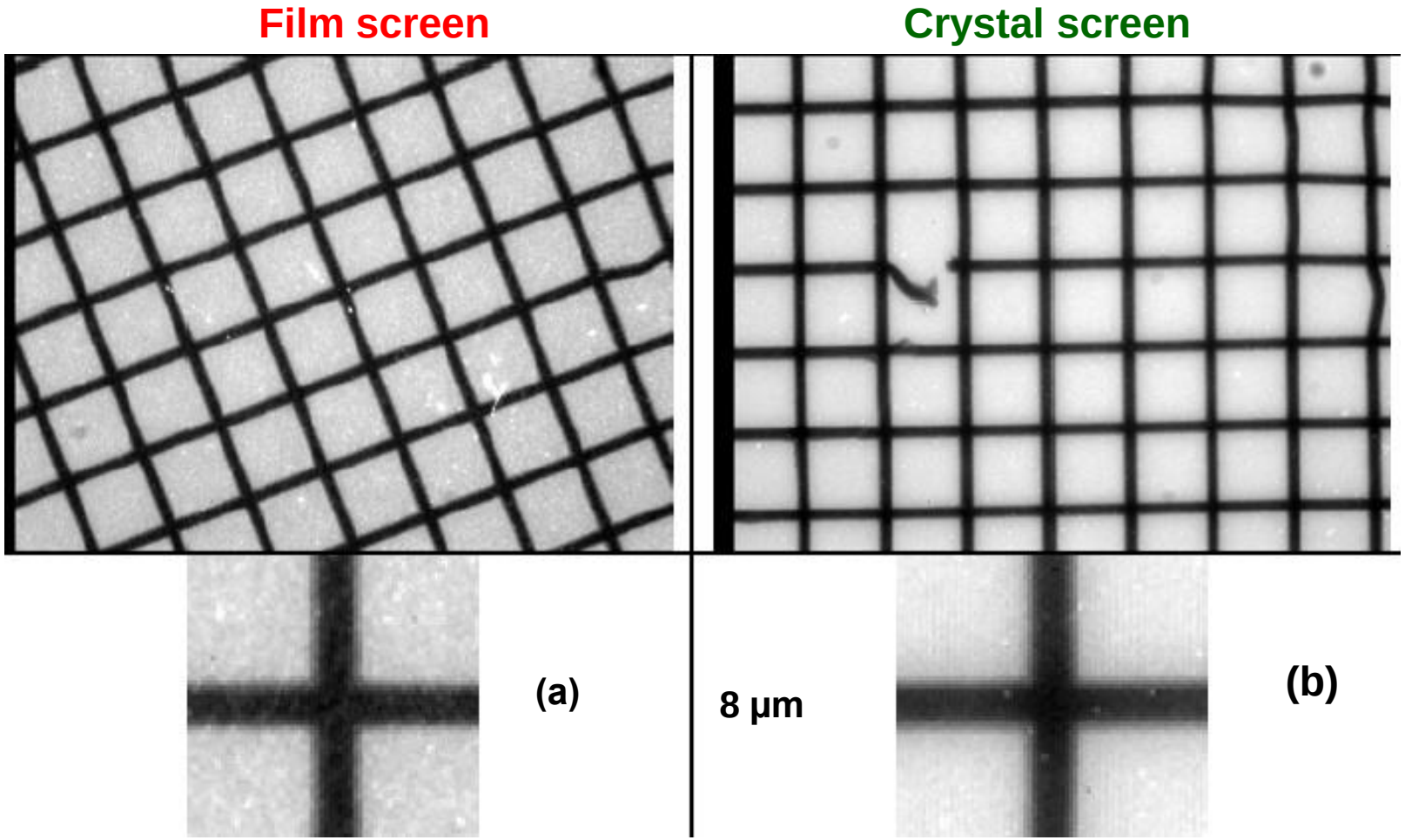

Spatial resolution of SCF screens

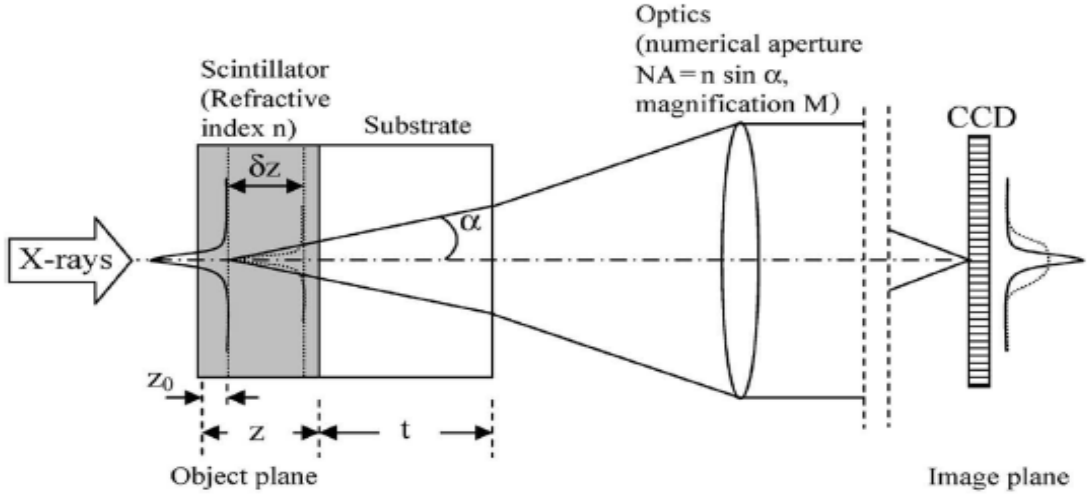

Figure 8
X-ray imaging with scintillators and lens coupling. Identical visible-light images are created by the X-ray beam in different planes of the scintillator. An image in plane z_0 is focused onto the CCD. An image in plane $z_0 + \delta z$ is out of focus at the CCD.

T. Martin,
J. Synchrotron Rad.
13, (2006) 180–194

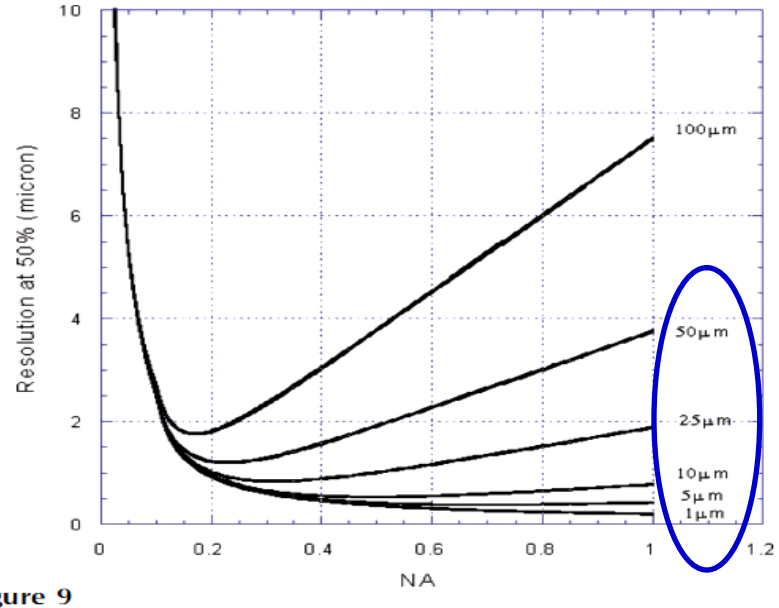

Figure 9
Spatial resolution *versus* numerical aperture NA of an optical system fo different thicknesses of the scintillator.

Resolution of images is proprtional to scintillator thickness !

Application of scintillators based on the SCF of oxide compounds

- **Screens for visualization of X ray image with high spatial resolution**

LPE grown SCF scintillating screens is without any concurence from the side of other methods in 1-5 μm range !

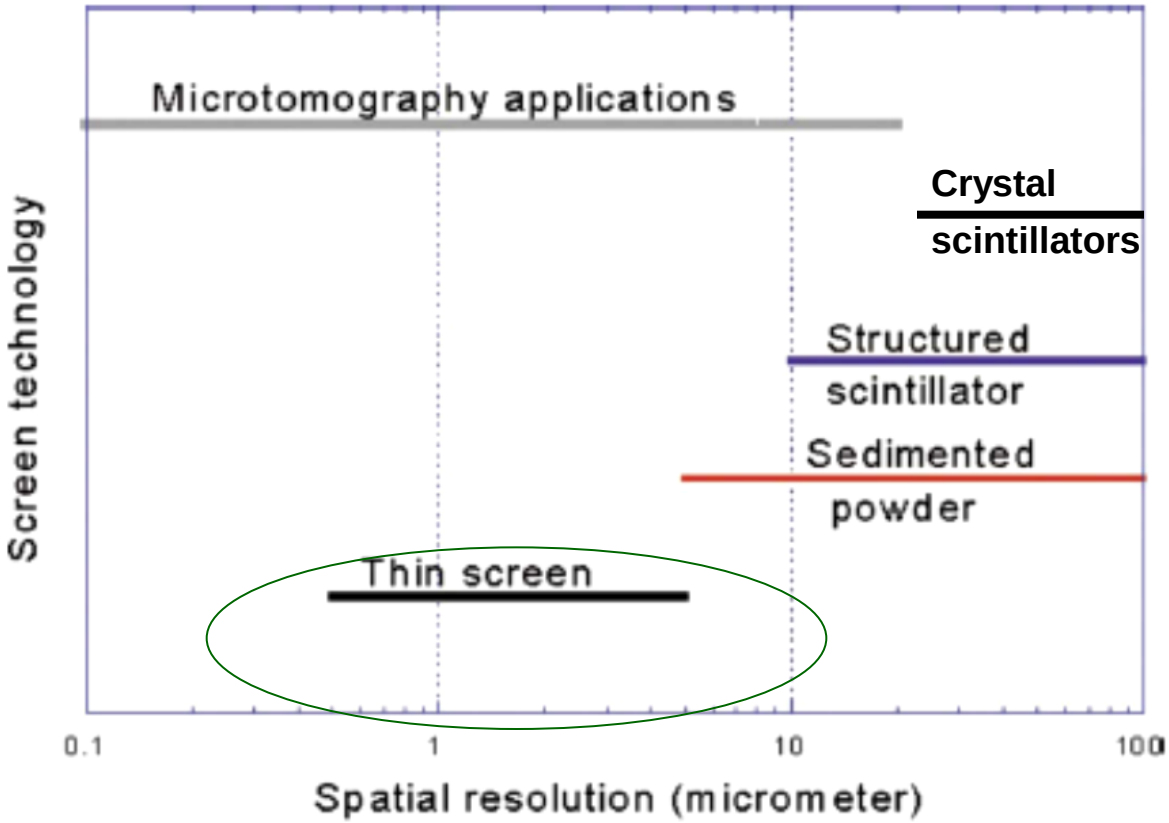

Figure 1
Film requirements for a high-resolution detector based on a CCD.

Single crystalline film (SCF) : Liquid Phase Epitaxy (LPE) technology

LOM, Lviv University

Institute of Physics UKW

Time control of Ω, z, T, δT

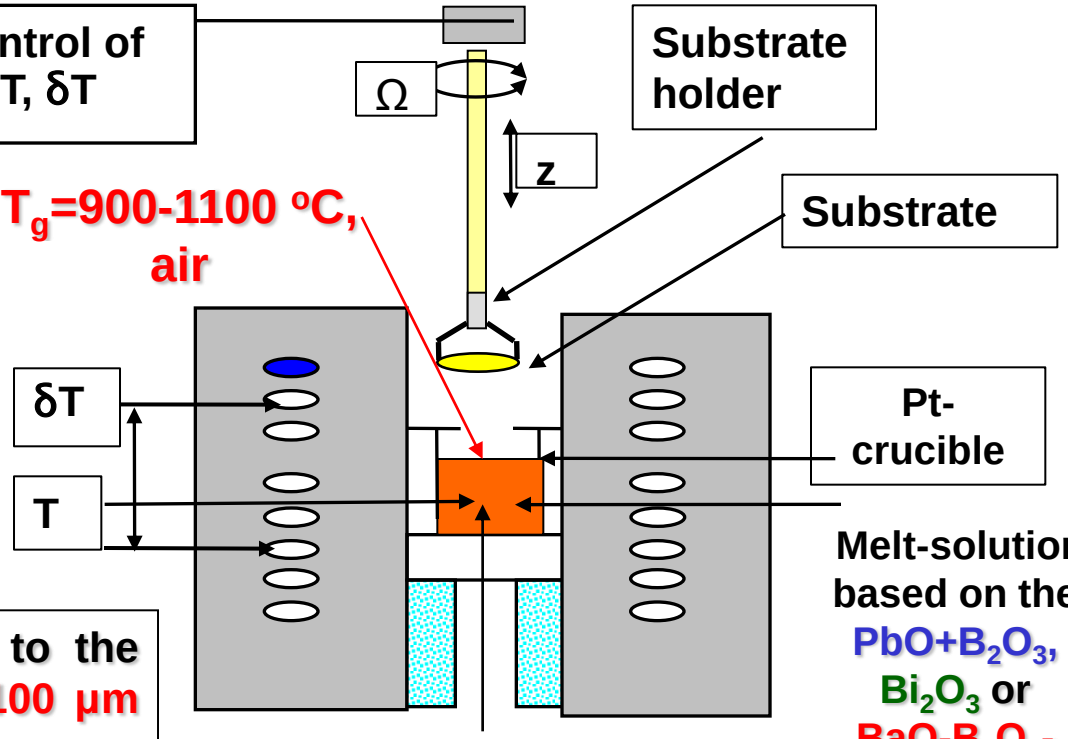

Growth parameters

- T : temperature of melt-solution
- Ω : substrate rotation
- z : substrate translation

LPE process is very well adapted to the required SCF thickness between 1…100 μm up to 200 μm for different applications

Melt-solution based on the $PbO+B_2O_3$, Bi_2O_3 or $BaO-B_2O_3-BaF_2$ fluxes + SCF-forming oxides

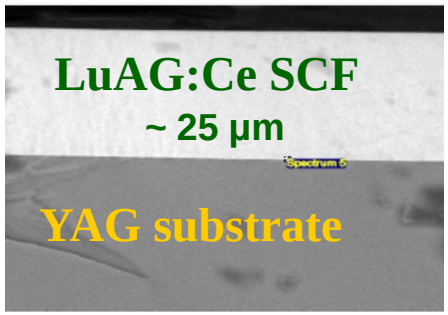

Cross section of LuAG:Ce/ YAG epitaxial structure

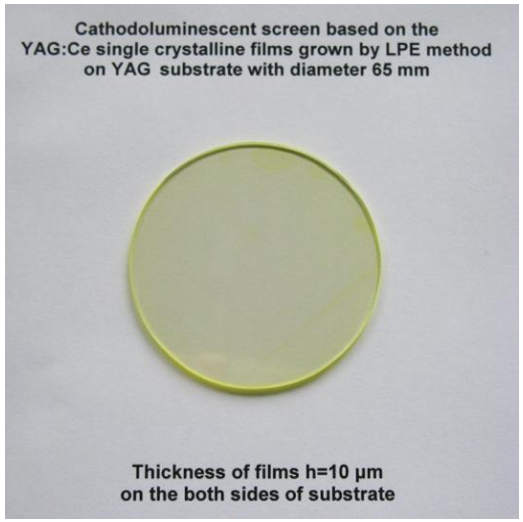

X-rays absorption efficiency

For SCF scintillating screens we need the materials with highest as possible absorption ability of X-rays !!!

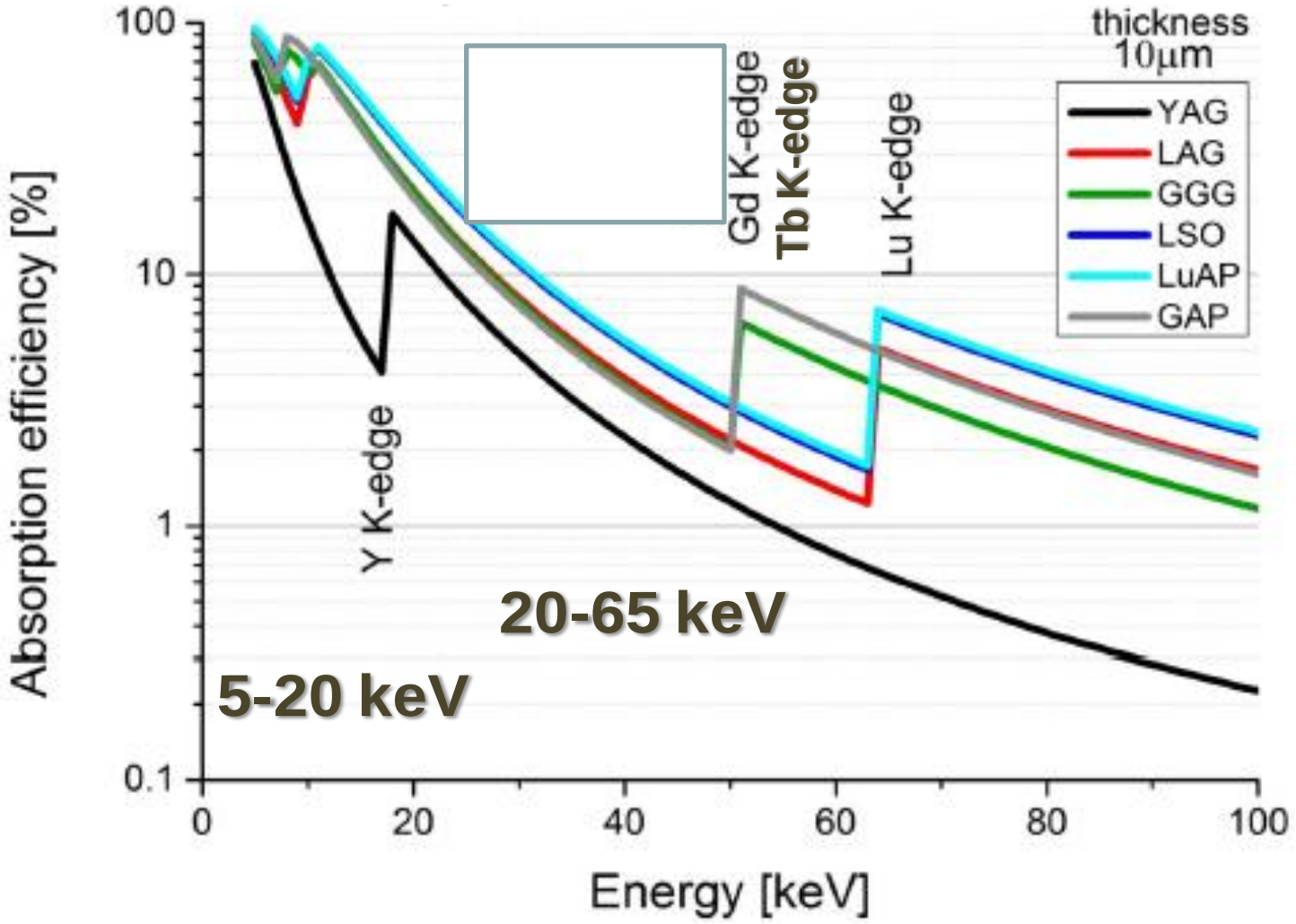

Heavy Lu based materials possesses the largest absorption efficiency

X-rays absorption efficiency

$$\mu \sim \rho Z_{eff}^{4}$$

Crystal	Z_{eff}	ρ	$\rho Z_{eff}^{4} * 10^{6}$	
Lu_2SiO_5 (LSO)	65.2	7.4	136	
$Lu_3Al_5O_{12}$ (LuAG)	61	6.73	93	films
$LuAlO_3$ (LuAP)	64.9	8.34	148	
Y_2SiO_5 (YSO)	44	4.54	17	
$YAlO_3$ (YAP)	34	5.5	7.35	substrates
$Y_3Al_5O_{12}$ (YAG)	32	4.55	5	

Film Formation II

Experimentally we can observe 3 growth modes of film growth

1. Island growth (Volmer - Weber)

- form the dimensional islands
- source:
  - film atoms more strongly bound to each other than to substrate
  - and/or slow diffusion

2. Layer by layer growth (Frank - van der Merwe)

- **generally highest crystalline quality**
- **source:**
  - **film atoms more strongly bound to substrate than to each other**
  - **and/or fast diffusion**

3. Mixed growth (Stranski - Krastanov)

- initially layer by layer
- then forms three dimensional islands
- => change in energetics

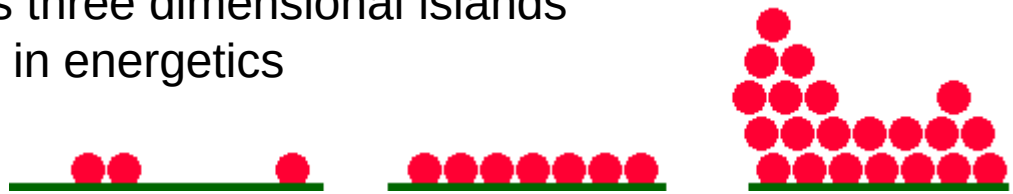

When would we expect to see each of these ?

Condition of growth single crystalline films by LPE methods

I. Misfit between the and films substrate

$$\Delta a = a_{film}\text{-}a_{sub}/a_{sub}*100\ \%$$

1. **Homo-epitaxial growth, for instant, the growth of LuAG:Ce SCF on LuAG substrate or LSO:Ce SCF on LSO substrate; usually $\Delta a \approx 0$;**
2. **Quasi- homo-epitaxial growth, for instant, growth of LuAG:Ce SCF on YAG substrates or LuAP:Ce SCF on YAP substrates, usually $\Delta a \leq 0.02$ Å (0.15 %) for growth of SCF; but that is not truthful demand !**
3. **Hetero-epitaxial growth, for instant, growth of YAG:Ce films on Al_2O_3 (sapphire) substrates, usually $\Delta a \# 0$;**

II. Substrate orientation;

III. Surface energies, which depends on the substrate polishing and cleanness of their surface, content of solution, chemical potential of dissolving ions and ions of substrate and details of growth procedure

Visible–emitting $R_3Al_5O_{12}$ (R = Lu, Y, Tb) SCF scintillators

Boundary conditions for misfit between the SCFs and $Y_3Al_5O_{12}$ substrate at growth of RE based $R_3Al_5O_{12}$ (R=Lu, Gd, Tb, Eu) garnets

Misfit of lattice constants of RAG SCF and YAG substrate and condition of their growth

Type of RAG SCF	Δa, Å	Condition of growth
$Lu_3Al_5O_{12}$ film	−0.12	good
$Y_3Al_5O_{12}$ sub	0	good
$Lu_2GdAl_5O_{12}$ film	0	good
$Tb_3Al_5O_{12}$ film	+ 0.064	good
$Gd_3Al_5O_{12}$ film	+0.85	good
$Eu_{2.15}Y_{0.85}Al_5O_{12}$ fim	+ 0.12	average
$Eu_3Al_5O_{12}$ film	+ 0.14	bad

$$-0.12\ \text{Å} < \Delta a < +0.12\ \text{Å}$$

$$-1\ \% \leq \Delta a \leq +1\ \%$$

Misfit between the LuAG:Ce and TbAG:Ce films and YAG substrate

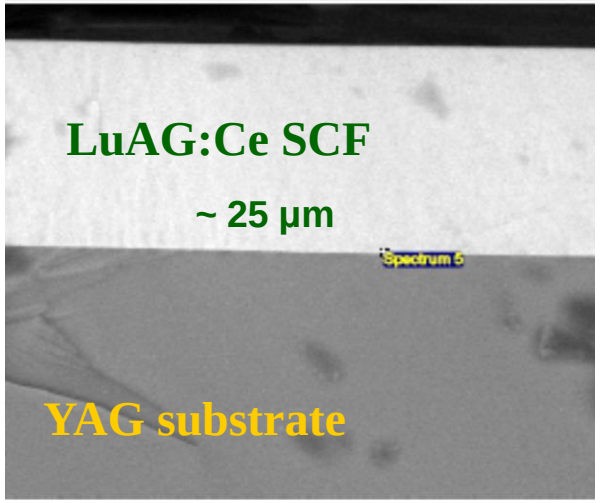

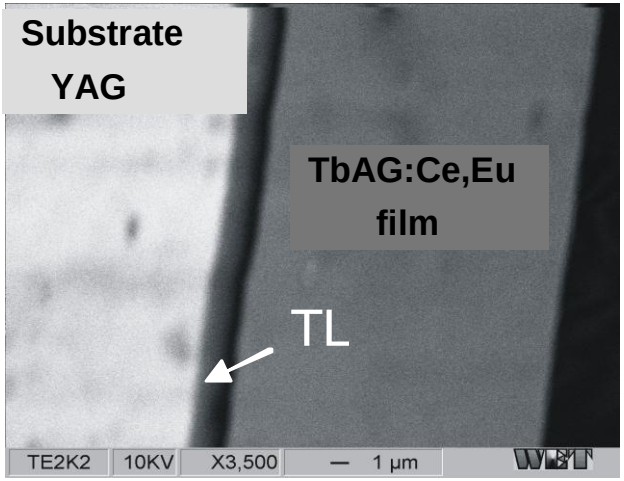

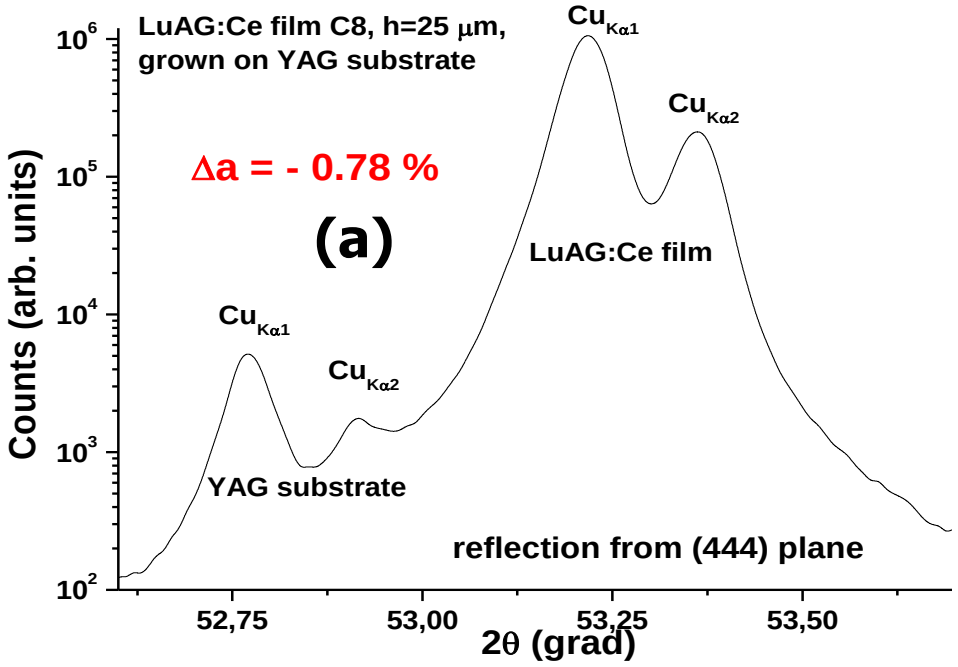

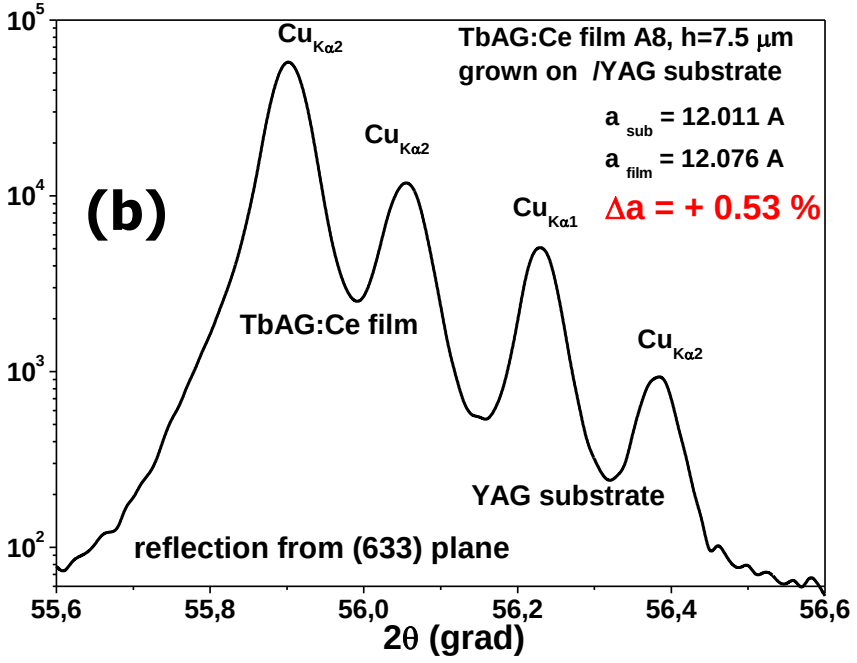

The cross sections (on the top) and XRD patterns (on the bottom) of LuAG:Ce (a) and TbAG:Ce (b) SCFs with thickness of 25 and 7.5 μm, respectively, grown on the YAG substrates.

Formation of transition layers betwen the SCF and substrate

The maim mechanism which help to reduce the misfit between the lattices of $Tb_3Al_5O_{12}$ SCF and YAG substrate is the formation of transition layer (TL) on the border of the substrate/ SCF during the first stage of LPE growth.

The composition of the TL can be presented as $(Tb_{1-x}Y_x)_3Al_5O_{12}$ solid solutions, where the value of x in the TL is changed between 1 and 0.

1 – TbAG (SCF)

2 – $(Tb_{0.7}Y_{0.3})$AG (TL)

2 – YAG (substrate)

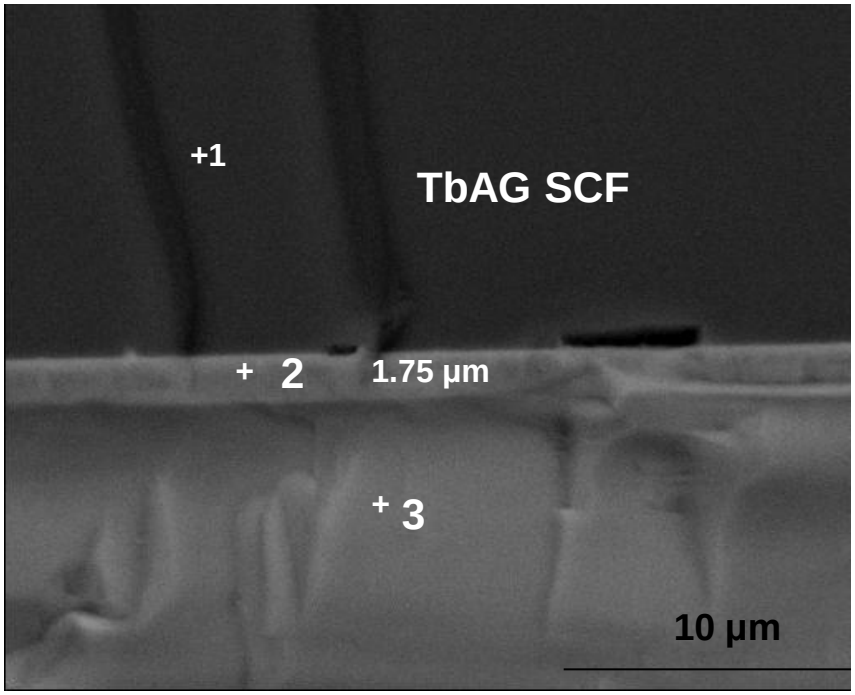

Formation of transition layer (TL) on the border of TbAG SCF and YAG substrate and his content. The crosses indicate the places for measurements

Visible–emitting $R_3Al_5O_{12}$ (R = Lu, Y, Tb) SCF scintillators

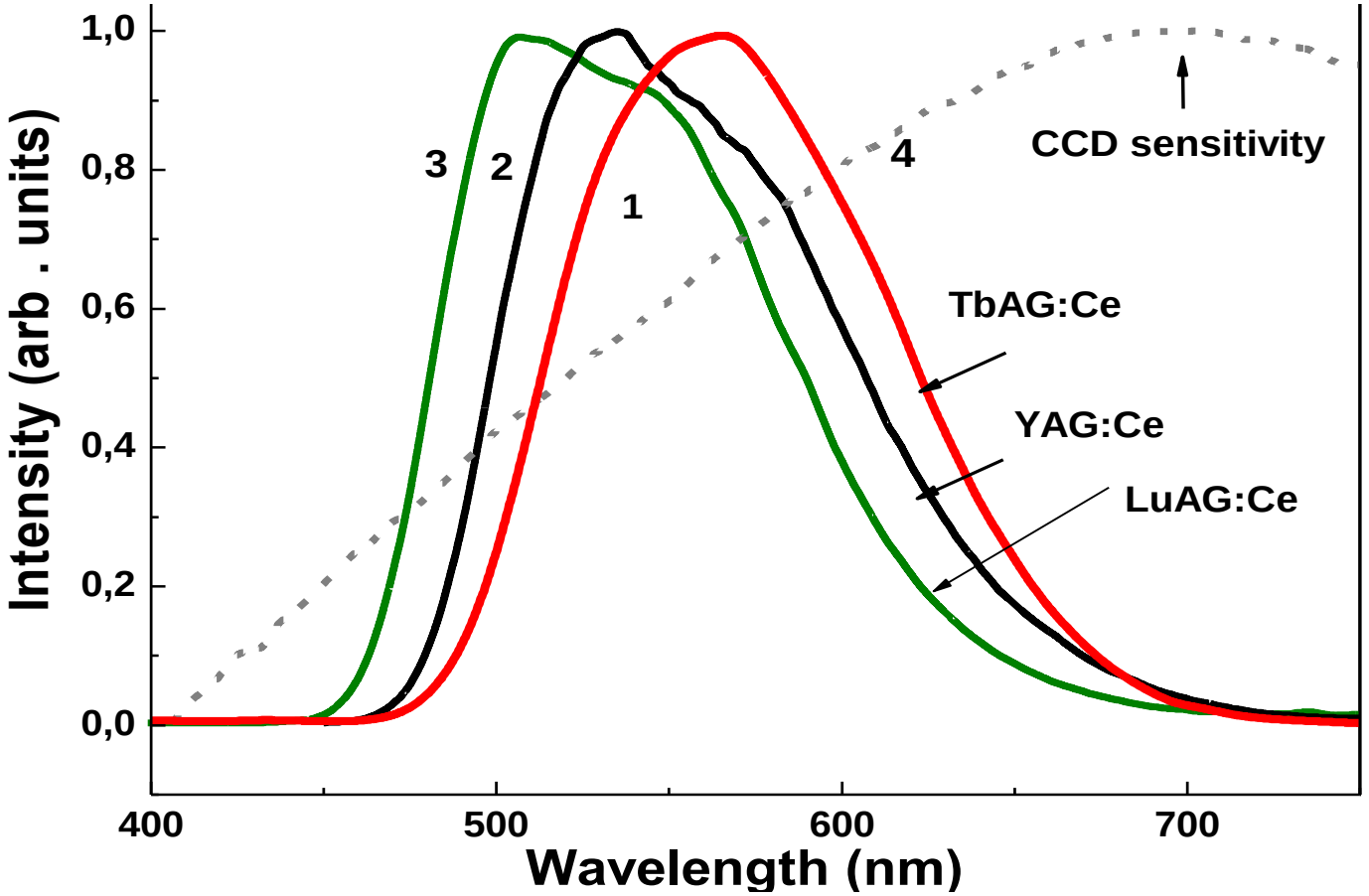

CL spectra of TbAG:Ce (1), YAG:Ce (2) and LuAG:Ce (3) in comparison with the spectrav sensitivity of front-side illuminatated CCD as recording devices (4)

Garnet	CL LY	RL LY (under α-particles excitation of ^{239}Pu source in 12 μs time interval)
LuAG:Ce	1.07	2.0
YAG:Ce	1.0	1.0
TbAG:Ce	0.82	2.43

Scintillation decay of $R_3Al_5O_{12}$:Ce (R = Lu, Tb, Gd) SCF

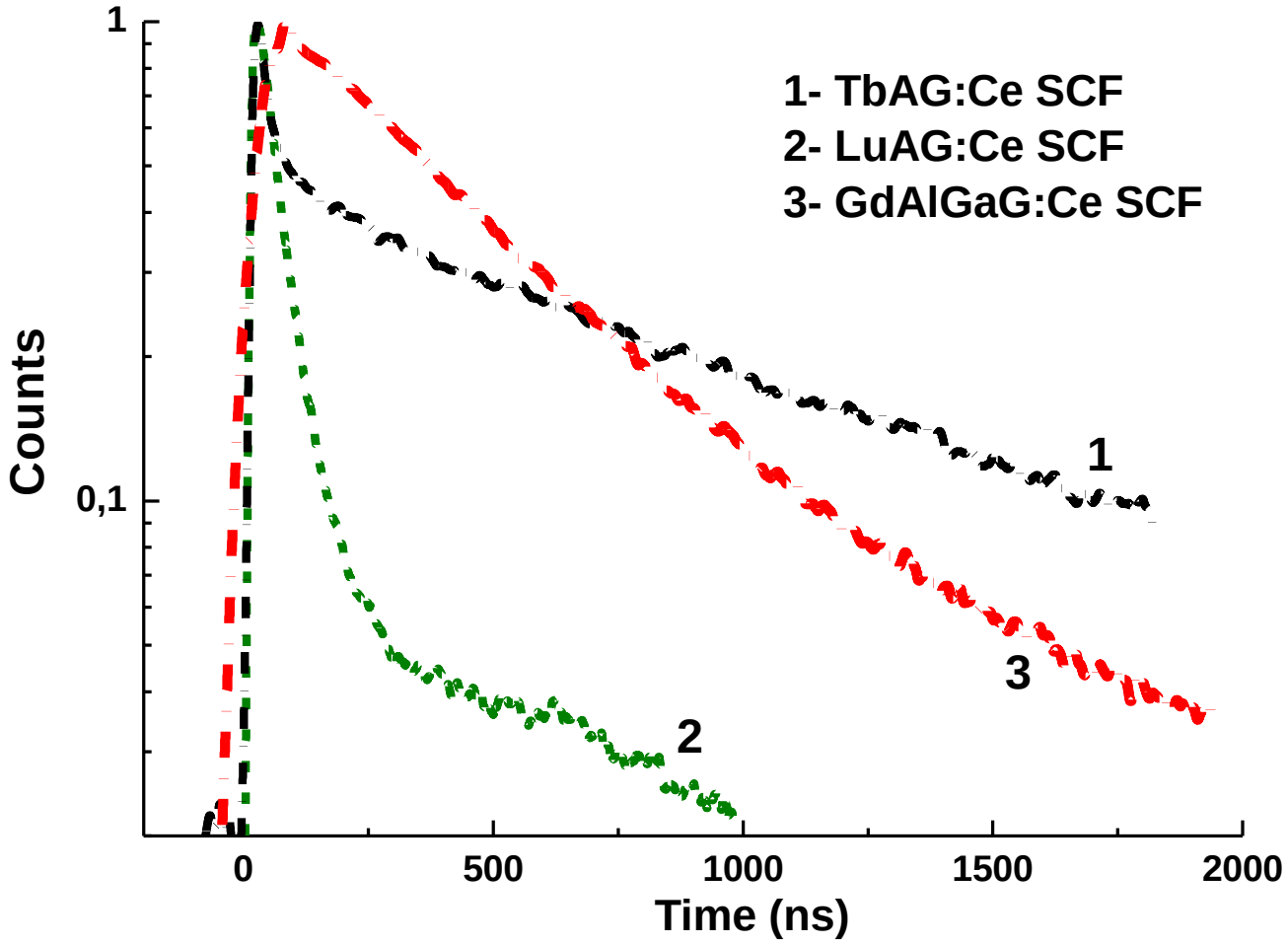

Scintillation decay kinetics of $Tb_3Al_5O_{12}$:Ce SCF (1), $Lu_3Al_5O_{12}$:Ce (2) and $Gd_3Al_{2.5}Ga_{2.5}O_{12}$:Ce (3) under α-particles excitation of ^{239}Pu source.

X-ray imaging ability of LuAG:Ce screens

X-ray images were recorded at 8 keV (CuKα) X rays and PCO Sensicam SVGA CCD camera (1024x1080 pixels, 6.7 μm pixel size).

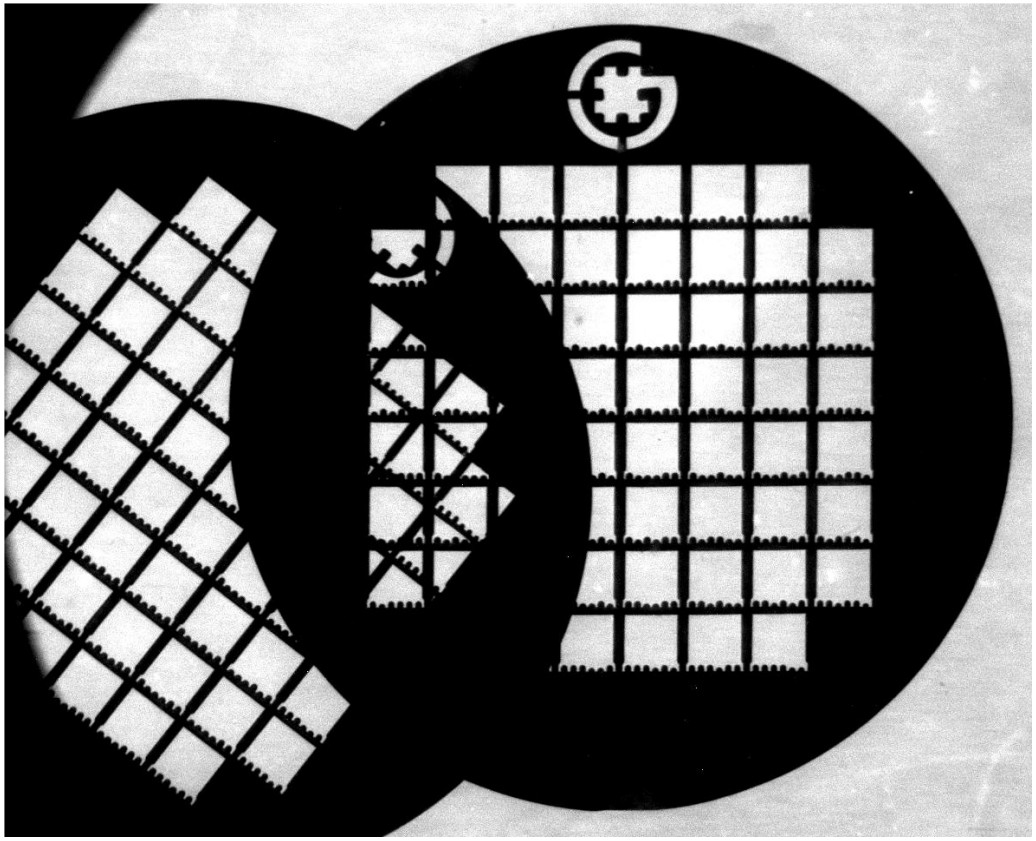

X-ray image of gold targets (G2480A, from Oxford Inst.) obtained with a 2x (NA=0.08) magnification objective. The image is not flat field corrected. The target has a 3.05 mm diameter, with 40 μm bar width and 210 μm hole width.

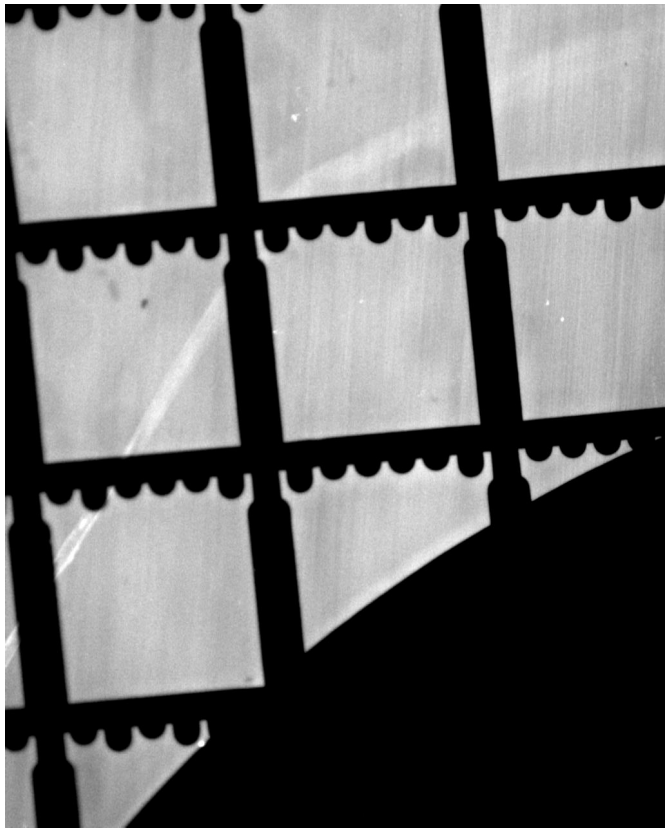

X-ray image of gold target obtained with a 10x (NA = 0.3) magnification objective. The image is not flat field corrected. The bar width is 40 μm and the hole width is 210 μm. The smallest patterns are 25 μm wide.

LY and afterglow of X ray excited luminescence

The afterglow level of TbAG:Ce SCF is very low comparable with LY of best quality LSO:Ce,Tb SCF. The LY of X ray excited luminescence of TbAG:Ce SCF is also comparable with LSO:Ce,Tb counterpart.

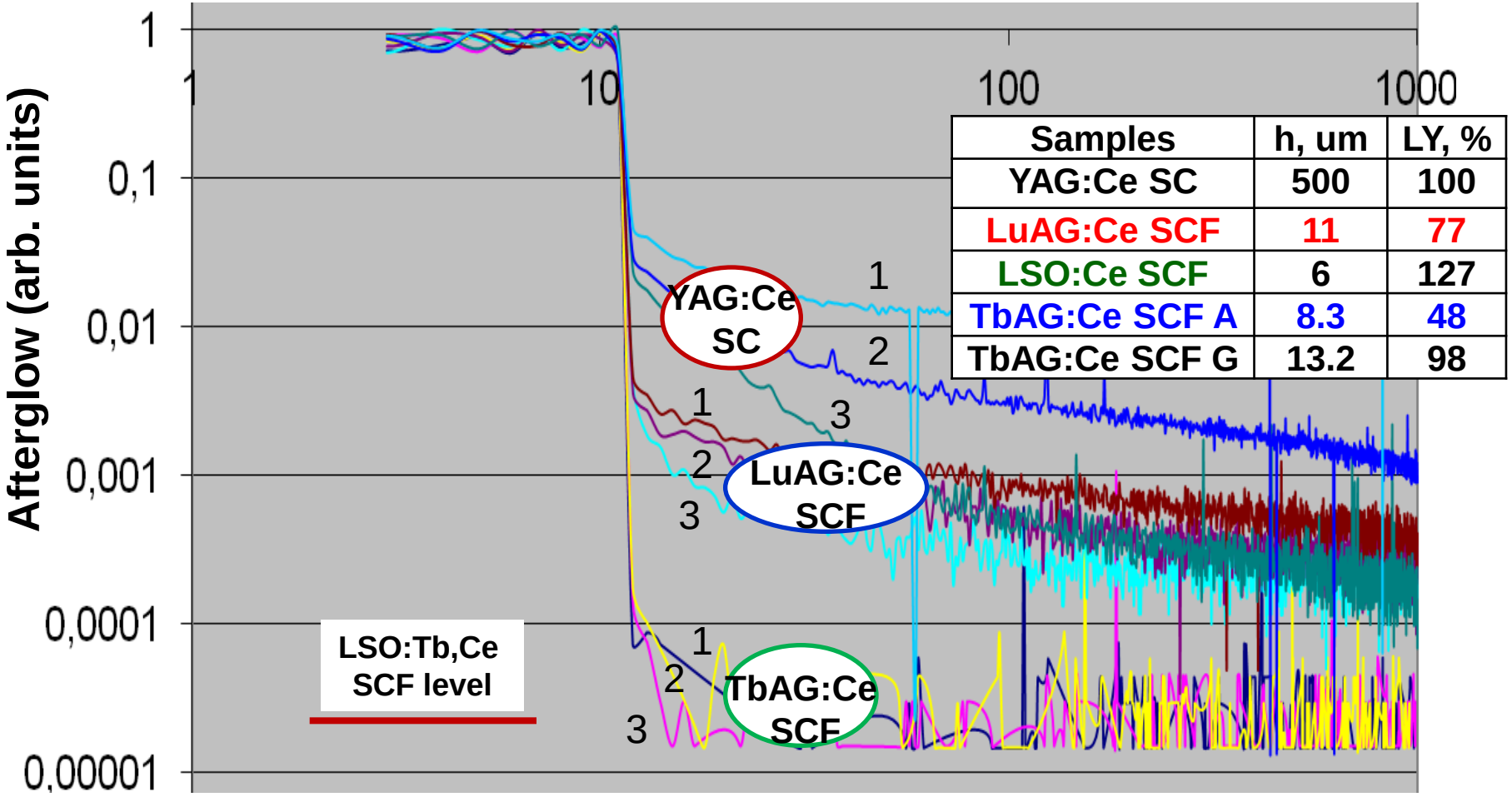

Samples	h, um	LY, %
YAG:Ce SC	500	100
LuAG:Ce SCF	11	77
LSO:Ce SCF	6	127
TbAG:Ce SCF A	8.3	48
TbAG:Ce SCF G	13.2	98

Afterglow under 8 keV X-rays ($Cu_{K\alpha}$) of YAG:Ce SC, LuAG:Ce SCF in comparison with TbAG:Ce SC counterpart. The X-ray burst duration is 0.1, 1 and 10 s, respectively.

Visible–emitting $(Lu,Gd)_2SiO_5$ SCF scintillators

Boundary conditions for misfit of SCF and substrate at growth of SCF of silicates

Table 3 Misfit of lattice constants of A_2SiO_5 SCF and Y_2SiO_5/Lu_2SiO_5 substrates and condition of their growth

SCF content	a, Å	b, Å	c, Å	Misfit, %	Growth conditions
Y_2SiO_5 sub	10.410	6.721	12.490	-	good
$LuSiO_5$ films				- 1.44	good
$Lu_{0.8}Gd_{0.2}SiO_5$ films				+ 0.55	good
$Lu_{0.3}Gd_{0.7}SiO_5$ films				+ 1.36	good

$-1.44\ \% \le \Delta a \le +1.36\ \%$ for silicates

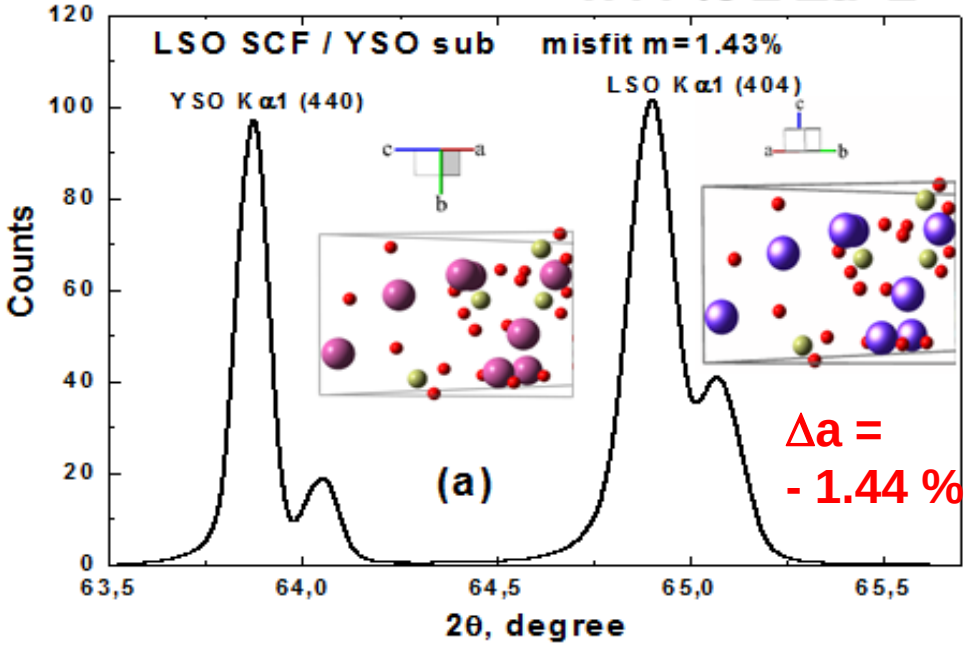

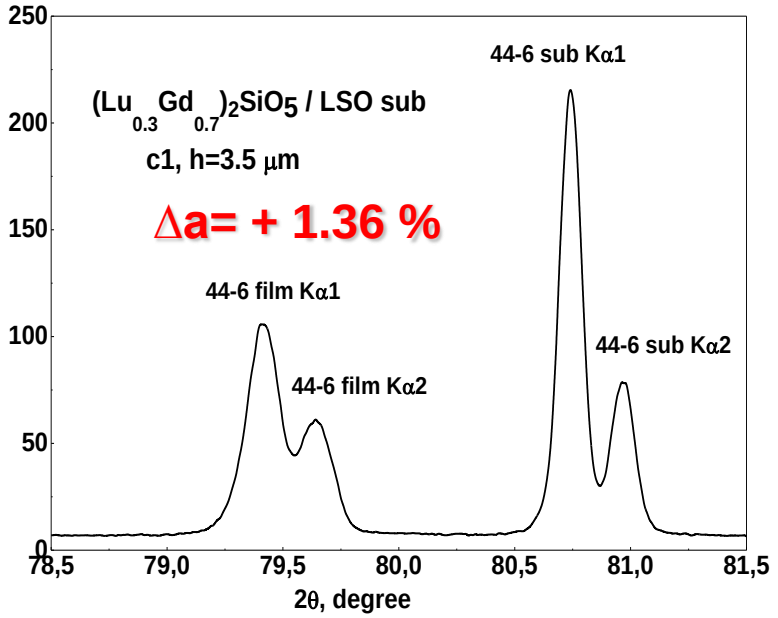

Fig.3. XRD pattern of $Lu_{0.8}Gd_{0.2}SO$:Ce and $Lu_{0.3}Gd_{0.7}$ SO SCFs grown by LPE onto LSO substrates. The difference between peak positions for SCF and substrate is proportional to misfit SCF-substrate

Ce-doped SCF of LSO orthosilicate

Emission spectra and decay kinetic of LSO SCF and crystal

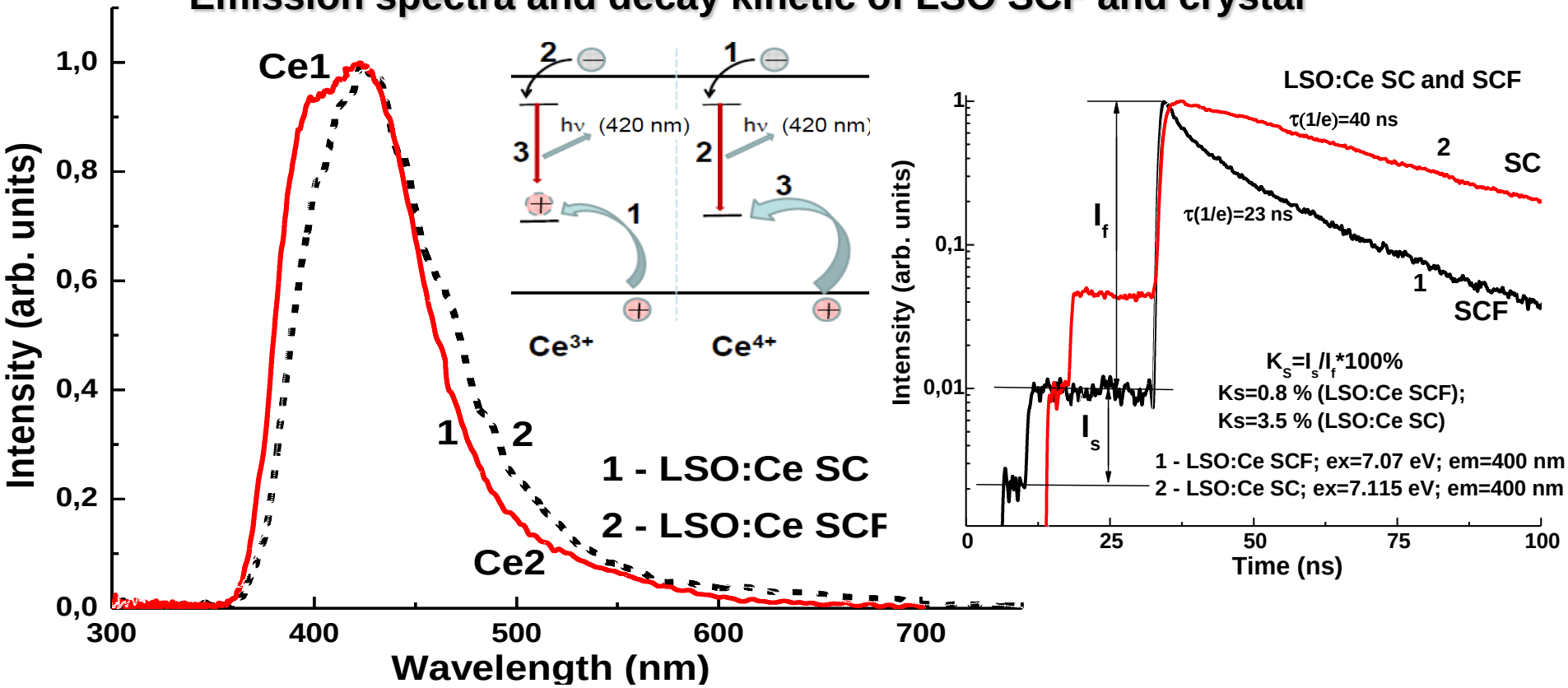

Emission spectra (a) and decay kinetics of Ce^{3+} luminescence at 400 nm (b) in LSO:Ce SCF (1) and crystals (2) at 300 K under excitation by synchrotron radiation with energy of 7.1 eV .

The film scintillators shows the significantly faster luminescence decay and smaller contribution of slow emission components Ks under high-energy excitation in comparison with crystal analogue due to the absence of vacancy type defects as emission and trapping centers. The shift of the emission spectra in LSO:Ce film with respect to crystal counterpart is also caused by the different concentration of Ce^{3+} ions in the Lu1 and Lu2 positions of LSO host in crystal and films.

Light Yield of Ce doped Lu_2SiO_5 and $(Lu,Gd)_2SiO_5$ based SCFs

LY of LSO:Ce SCF is about 15-20 % in comparison with LY of LuAP:Ce crystal analogues

The lower LY of Ce doped YSO and LSO SCF scintillators is caused by:

- **the low segregation coefficient of Ce ions in LSO hosts at LPE growth (0.015-0.025). As result, the Ce/Pb ions ratio in these SCF is only ~1.4-2.5.**
- **the strong quenching influence of Pb^{2+} flux dopant onto the Ce^{3+} luminescence;**
- **the preferable formation of Ce^{4+}-Pb^{2+} centers instead Ce^{3+} ones in LSO and YSO SCF scintillators (PbO based flux).**

Local conclusions: **It is strongly desirable to use :**

- **the alternative lead free fluxes, for instant BaO-based fluxes, for producing of the Ce doped LSO SCF scintillators to achieve higher LY;**
- **co-doping with other RE activators with significantly higher segregation coefficient then Ce^{3+} ions.**

Ce-Tb doping of LSO SCF

The problem with low LY of Ce-doped (Y,Lu)SO SCFs can be partly eliminated by doping these SCF with Tb^{3+} ions with significantly larger (of about 0.6) segregation coefficient in LPE growth process. Such type of screens can simultaneously emit in the blue and green ranges.

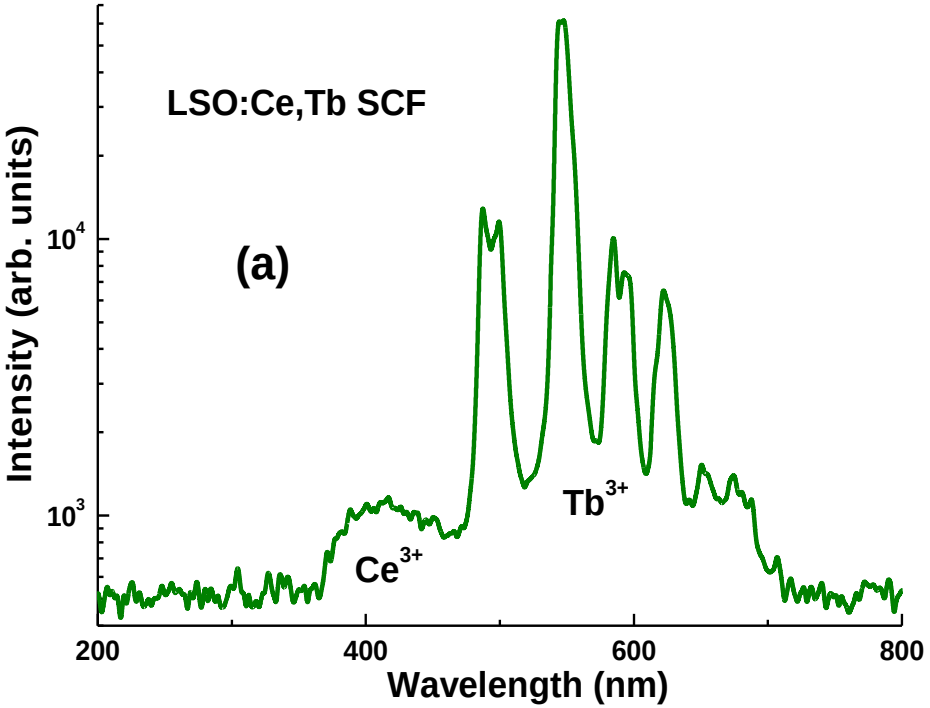

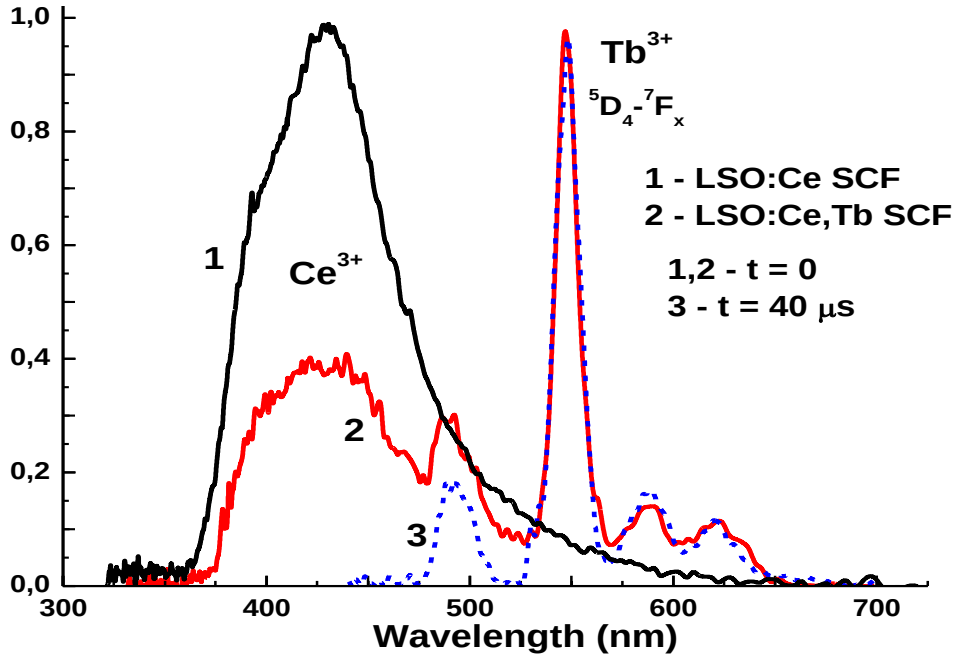

Fig.11. (a) CL spectra of LSO:Ce,Tb SCF at 300 K; (b) - normalized CL spectra of LSO:Ce (1b) and LSO:Ce,Tb (2b, 3b) SCFs at delays Δt=0 (1, 2) and Δt=40 μs (3).

The effective Ce-Tb energy transfer is observed in LSO:Ce,Tb SCF which result in the notable increase of the intensity of X ray excited luminescence in these SCF scintillation screens

X-Ray microimaging with SCF scintillators

Resolution of images

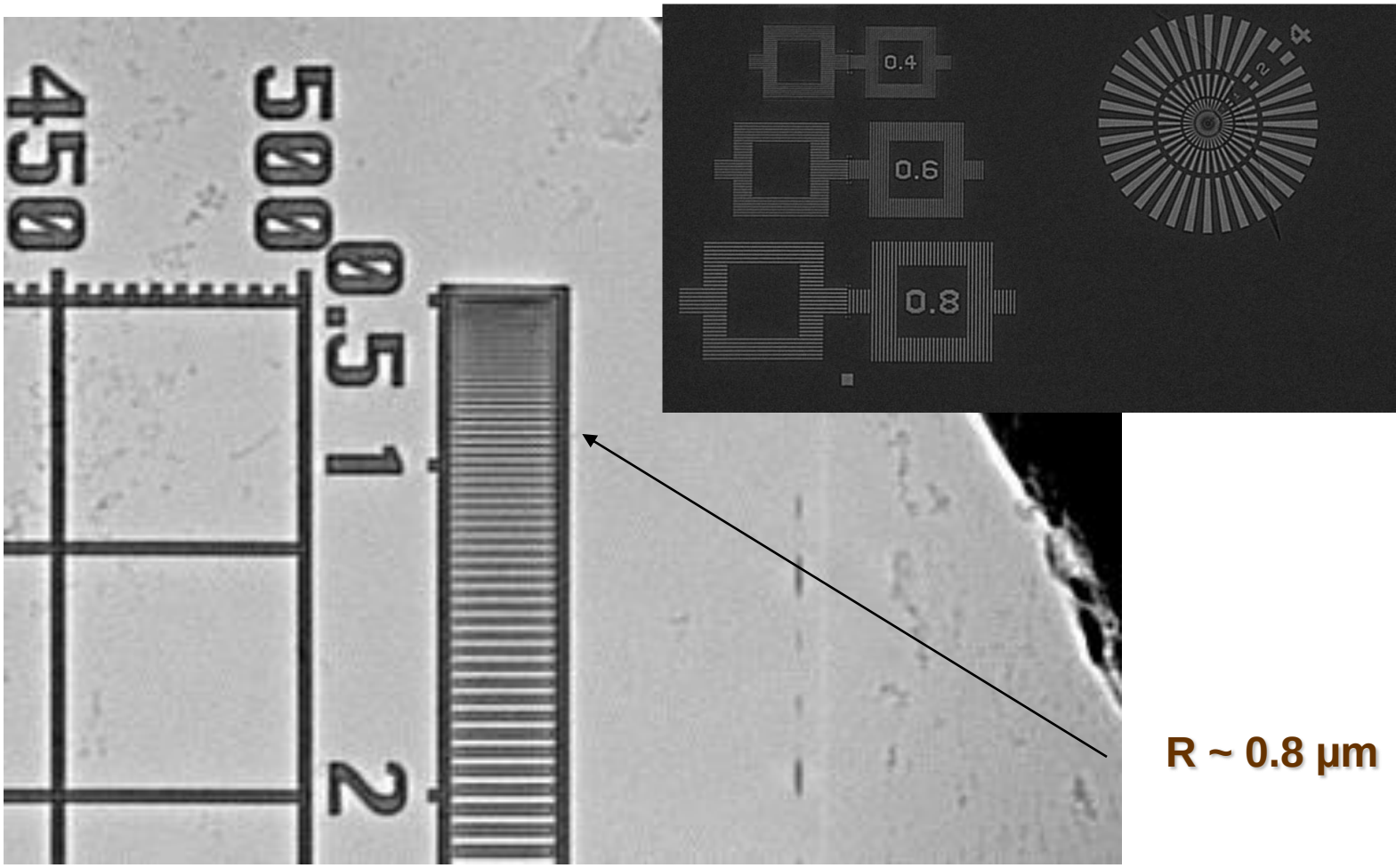

R ~ 0.8 µm

Images of resolution target obtained using the visible emission of LSO:Ce,Tb SCF scintillators [T. Martin, IEEE TNS 56 (2009) 1412-1418].

UV and visible–emitting SCF of $(Lu,Gd)_2SiO_4$ SCF perovskites

Boundary conditions for misfit between the SCF and substrate at growth of RE based perovskites

Table 2. Mismatch of lattice parameters of RAP SCF and YAP substrate and condition of their growth

SCF content	a, Å	Δa, Å (Δa, %)	b, Å	Δb, Å (Δb, %)	c, Å	Δc, Å (Δc, %)	Condition of growth
$YAlO_3$	5,18004	-	5,30842	-	7,36301	-	good
$TbAlO_3$	5,22961	+ 0,04957 (+ 0,957)	5,30692	- 0,0015 (- 0,028)	7,41543	0,05243 (+ 0,71)	good
$GdAlO_3$	5,2482	(+0,106) (+1,34)					good
$LuAlO_3$	5,10564	- 0,0744 (- 1,436)	5,33417	+ 0,02575 (+ 0,484)	7,30532	- 0,05747 (- 0,743)	good

- 1.44 % < Δa < + 1.34 %;
+ 0.48 % > Δb > - 0.03 %;
- 0.74 % < Δc < + 0.71 %
for perovskites (Table 2)

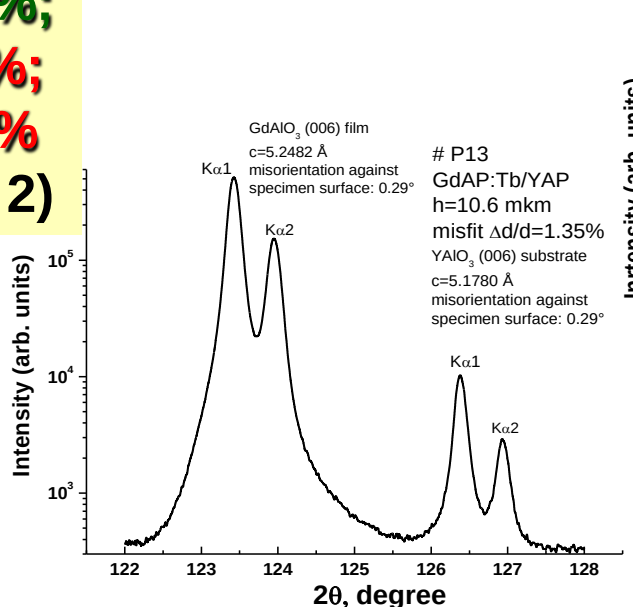

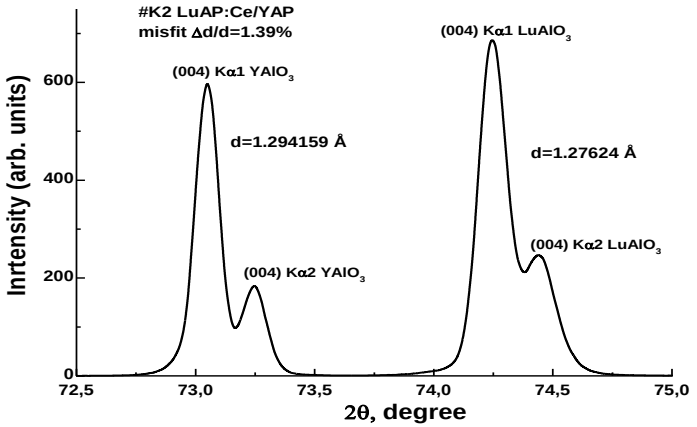

Zorenko, Yu., Gorbenko, V., 2009a., Physics of Solid State, 51, 1800-1808.

XRD pattern of the LuAP (a) and GdAP:Tb (b) SCFs grown onto YAP substrates

Development of SCF of LuAP:Ce perovskite

Emission spectra and LY of LuAP:Ce SCF grown by LPE method onto YAP substrates from PbO- and lead free BaO-based fluxes

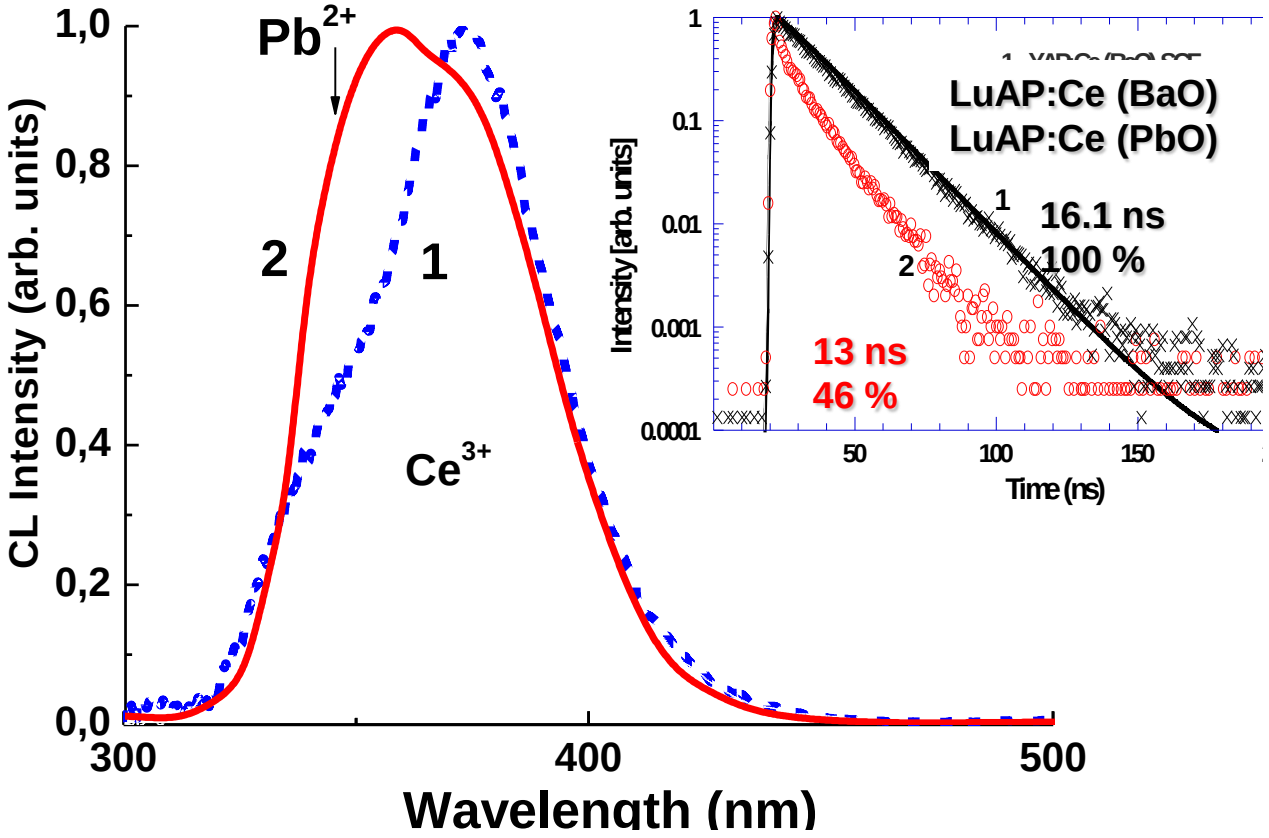

Normalized CL spectra (a) and decay kinetic (b) of LuAP:Ce *SCF*; grown from the BaO- (1) and PbO- (2) based fluxes under excitation in Ce3+ absorption band at 300 nm; T=300 K.

LY of LuAP:Ce SCF is about 8-10 % in comparison with LY of LuAP:Ce crystal analogue

Influence of Pb^{2+} flux dopant

1. Ce^{3+} emission in LuAP:Ce (PbO) *SCF* is strongly distorted by the UV emission band of Pb^{2+} ions at 340 nm.

2. Non-exponential decay kinetic of the Ce^{3+} emission occurs in LuAP:Ce (PbO) *SCF*, caused by the energy transfer from Ce^{3+} ions to Pb^{2+}-related centers.

3. The losses of more than 50% excitation energy take place LuAP:Ce (PbO) *SCF* due to the energy transfer away from the Ce^{3+} excited state to Pb^{2+}-based centers. Such huge losses explain low LY of LuAP:Ce *SCF*, grown from the PbO-based flux

Development of LuAP:Tb, and LuAP:Ce,Tb based scintillators by LPE method onto YAP substrates

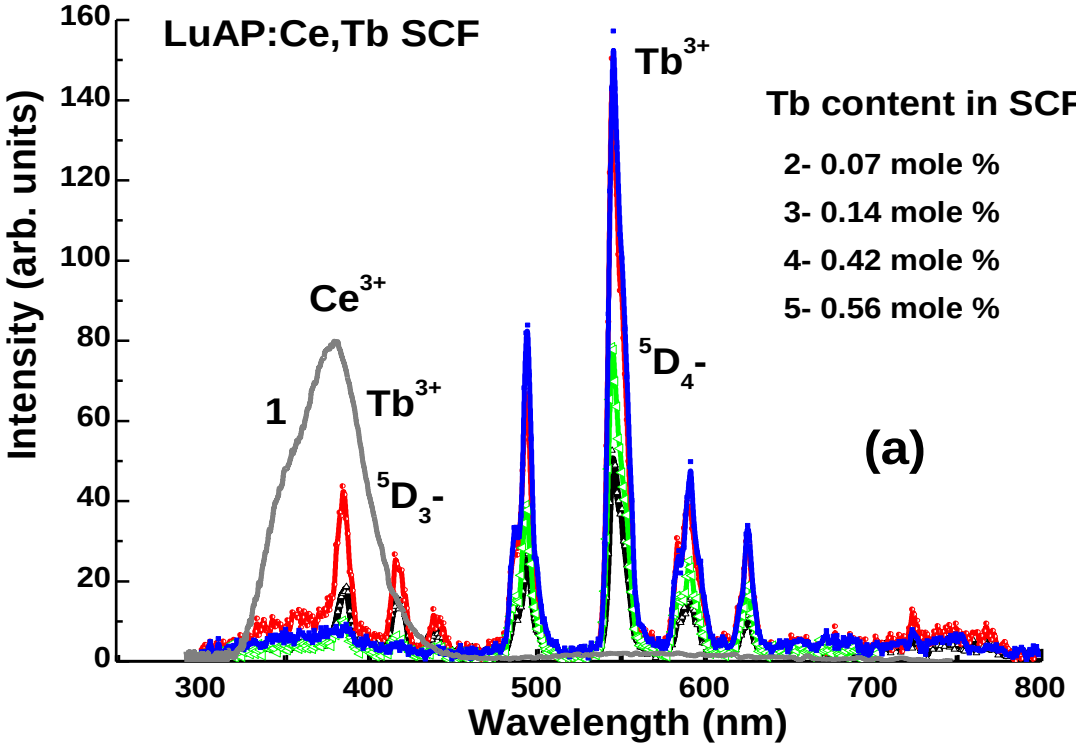

Effective Ce^{3+} to Tb^{3+} energy transfer is observed in LuAP:Ce,Tb

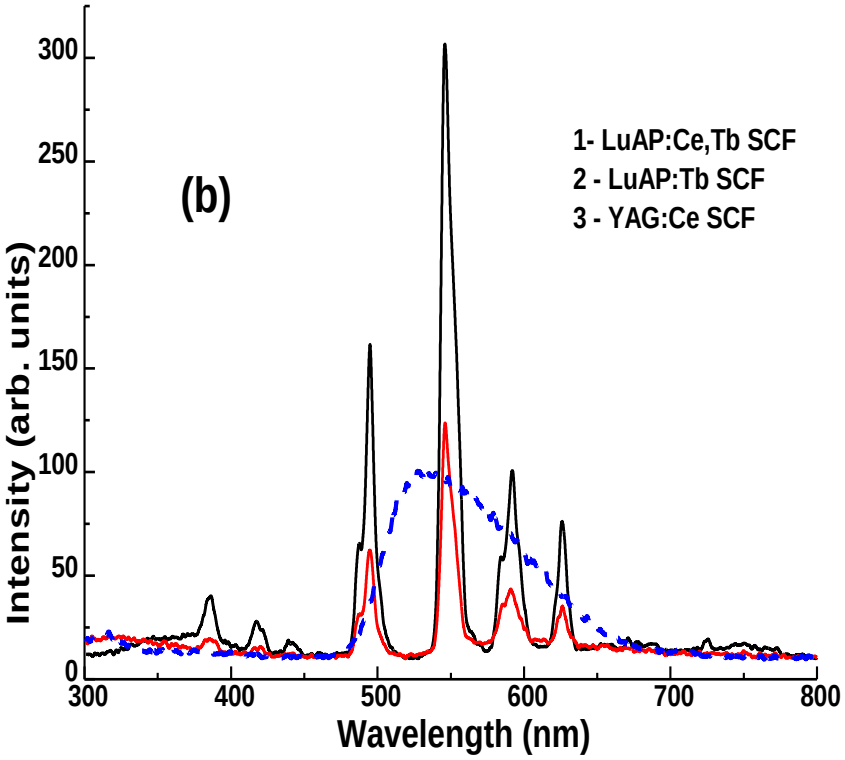

(a) - CL spectra of LuAP:Ce SCF (1) and LuAP:Ce,Tb SCF (2-5) grown with different molar contents of Tb activator in MS; (b) – comparison of the intensity of X-ray excited spectra of LuAP:Ce,Tb SCF (1) and LuAP:Tb (2) SCF with a 500 μm thick YAG:Ce SC (3).

X-Ray microimaging with SCF scintillators

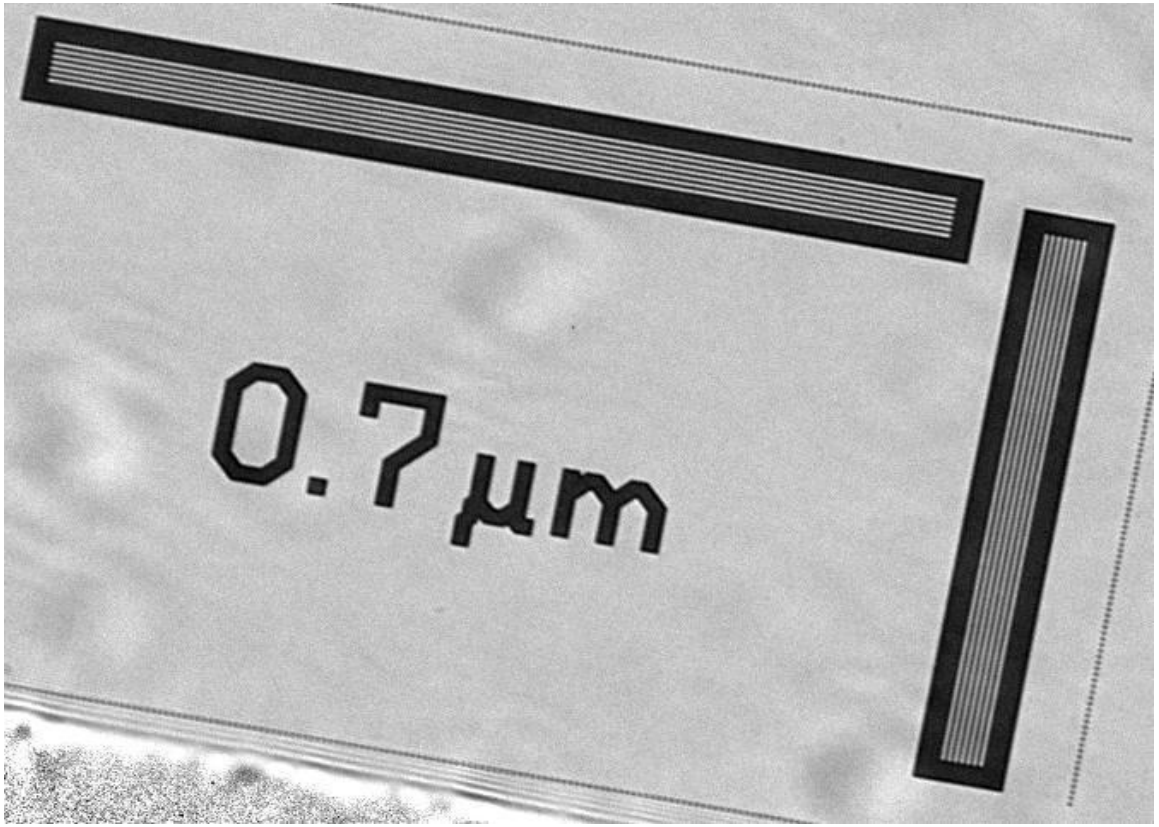

Image of resolution target obtained on the the BM05 beamline at ESRF with a PCO1600 CCD camera, a 40x objective (NA=0.45) and a 4 µm thick LuAP:Tb,Ce.

Matching the emission spectra of SCF scintillators with CCD sensitivity range

13.09.2016, Milan, Italy

State of the art: LSO or GGG?

LSO: Tb / YbSO vs GGG: Eu / GGG

😐Match λ_{emis} / camera QE

Due to the long-time SR pulse registration (about of 10 ms) the Tb^{3+} and Eu^{3+} activators can be used !!!

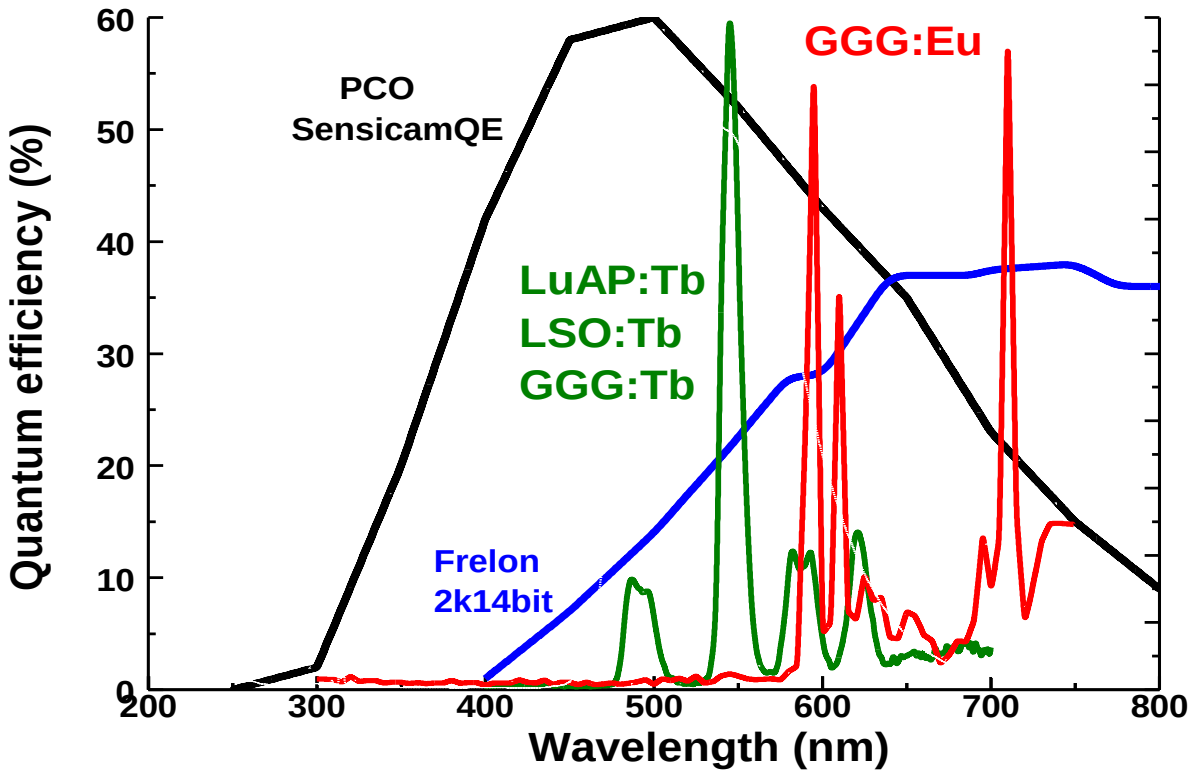

LuAP:Tb, LSO:Tb, GGG:Tb and LuAP:Ce,Tb SCFs are more suited to back-illuminated sensors and GGG:Eu is more suited to front-illuminated sensors.

Matching the emission spectra of SCF scintillators with CCD sensitivity ranges

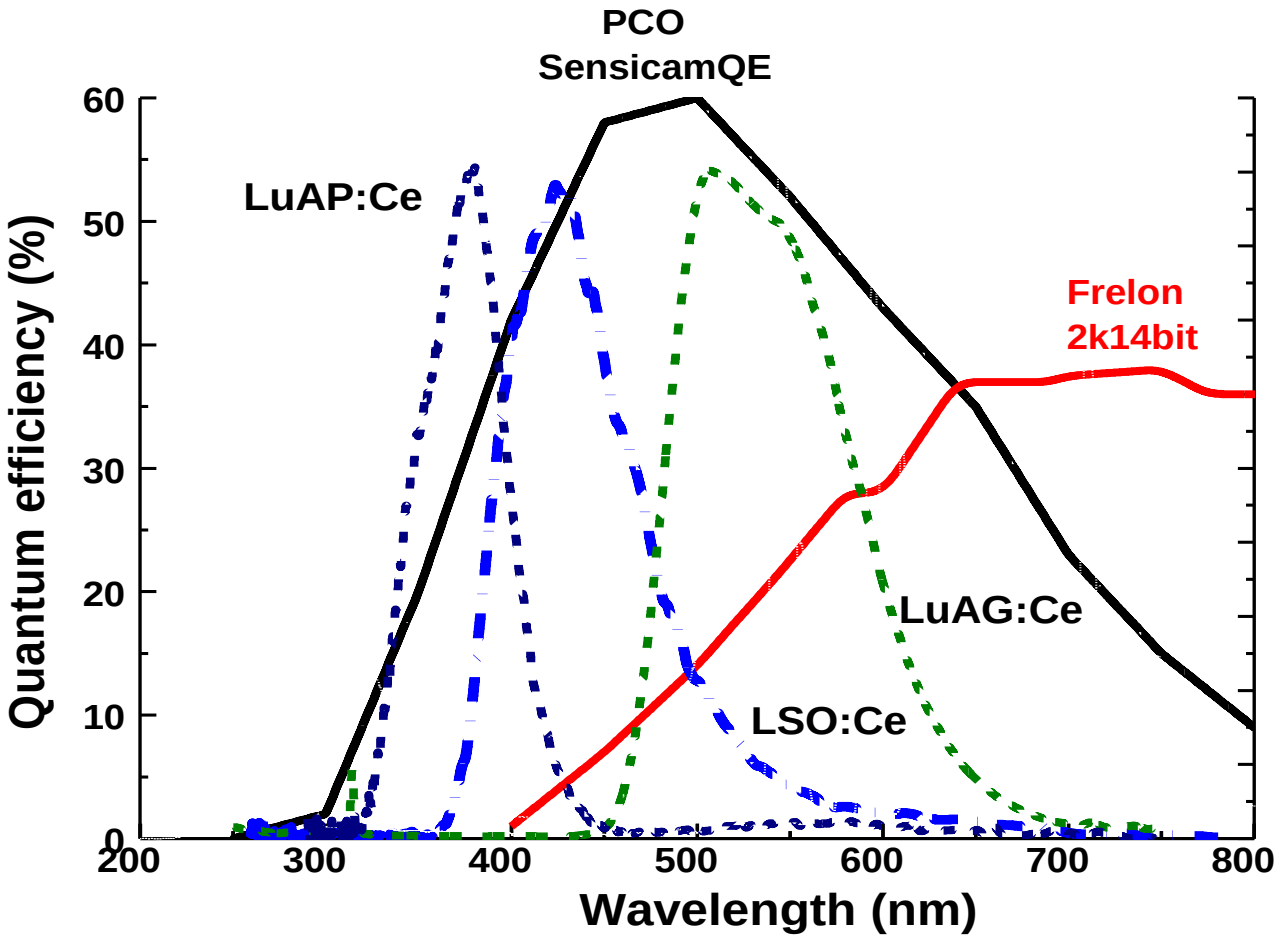

Emission spectra of the SCFs scintillators. LuAG:Ce, LSO:Ce and LuAP:Ce SCFs are more suited to back-illuminated sensors

X ray tomography using the synchrotron radiation in the X-ray range

13.09.2016, Milan, Italy

X-Ray imaging at ESRF, Grenoble France

Grenoble, France

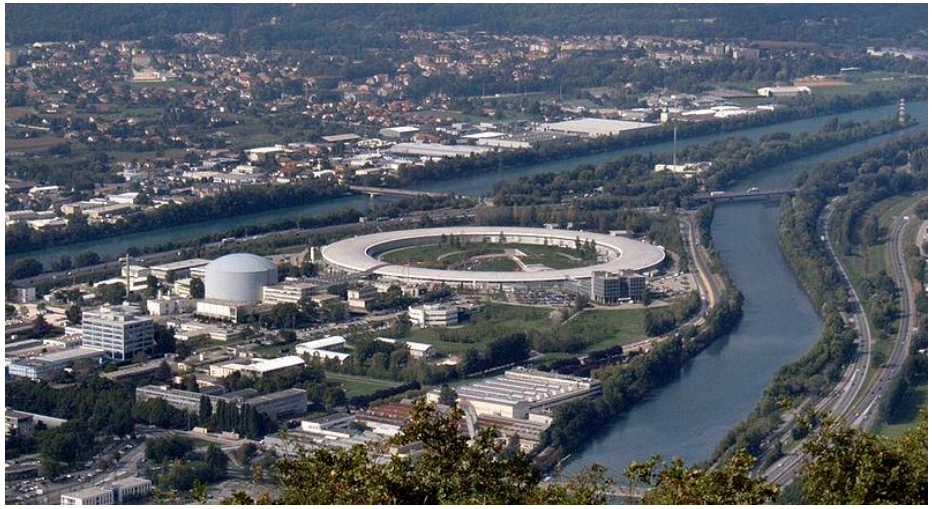

Scientific polygon in Grenoble

ESFR

Microtomography with synchrotron radiation at ESRF

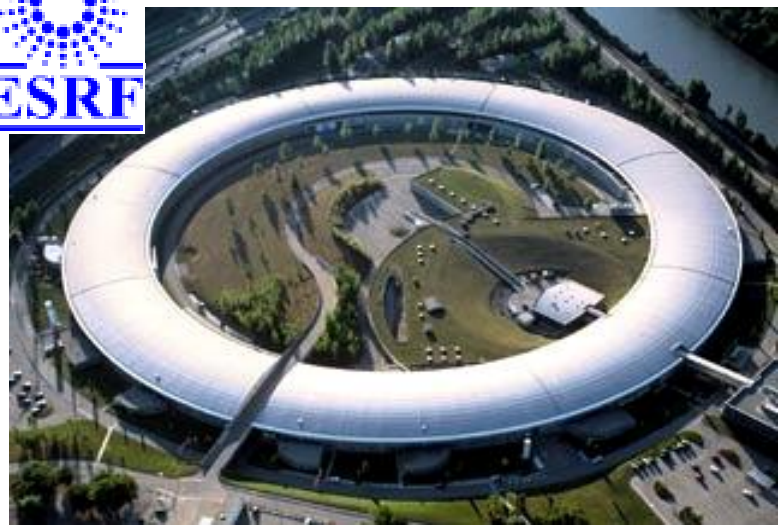

Collaboration with dr Thierry Martin group from ESRF, Grenoble

„Creation of SCF scintillation screens by LPE method”

LuAG:Ce; LuAP:Ce,Tb;
LYSO:Ce,Tb ; LuAG:Eu SCFs

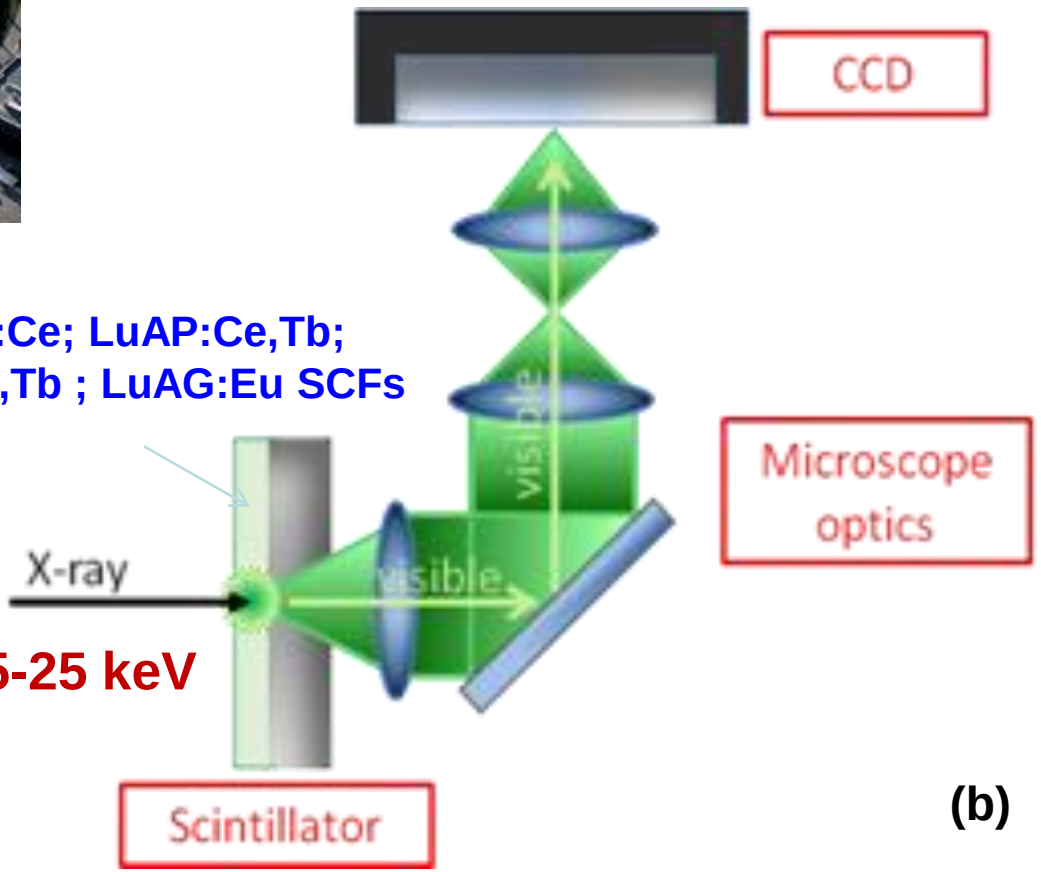

SR > 5-25 keV

(a) **(b)**

Fig.1. Detector for microtomography developed in ESFR, Grenoble, France (a) and functional scheme of detector (b);

LPE lab at ESRF

EPI lab (created since 2010)

LPE lab at ESRF mainly specialized on the developed of Tb^{3+} and Eu^{3+} dopes SCF screens

(a)

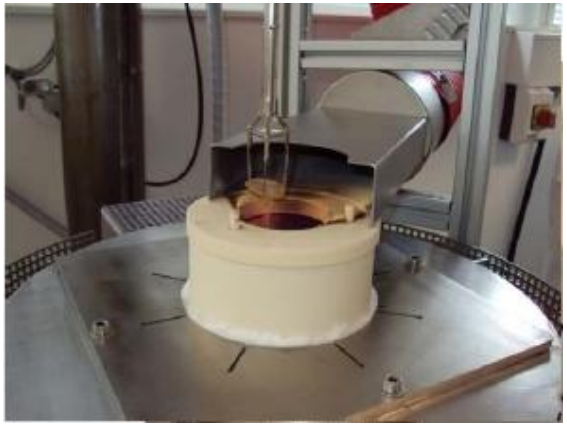

(b)

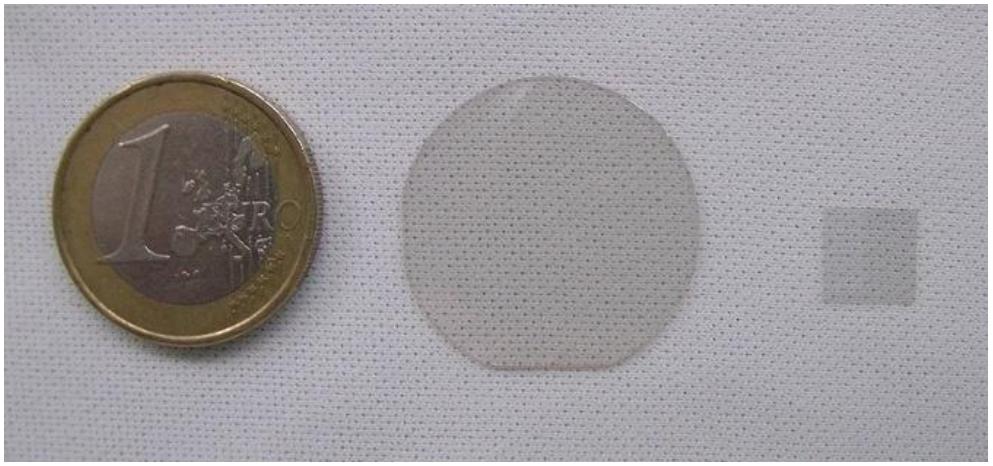

LPE technique used at the ESRF, Grenoble, France (a); GGG:Tb SCF is grown on a GGG substrate from a superrsaturated melt (b)

Imaging with synchrotron radiation at ESRF, Grenoble, France

Applications

- material science;
- biology
- archeology;
- medicine

13.09.2016, Milano, Italy

Application: science and industry

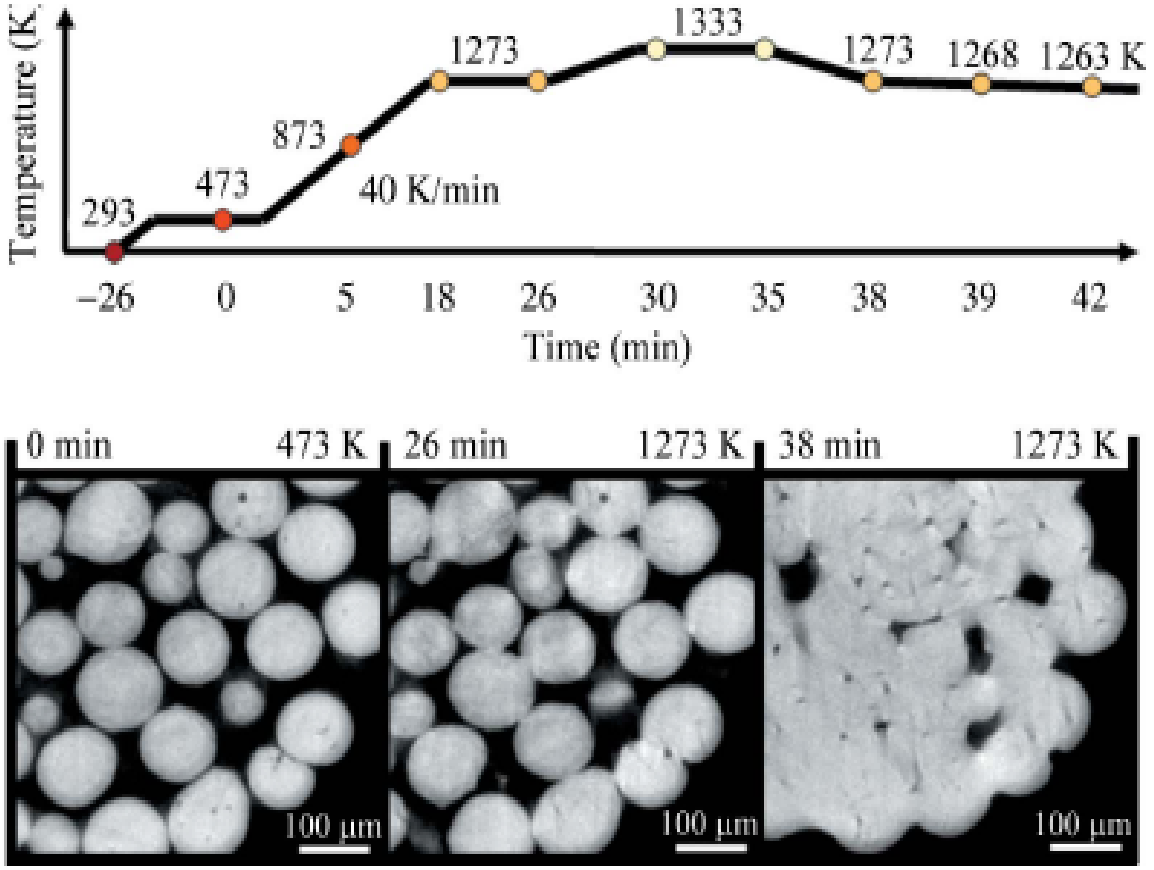

Figure 15
Thermal cycle for copper powder sample and two-dimensional projections of Cu particles at different stages of the sintering.

Imaging with synchrotron radiation at ESRF, Grenoble, France

Application: material science

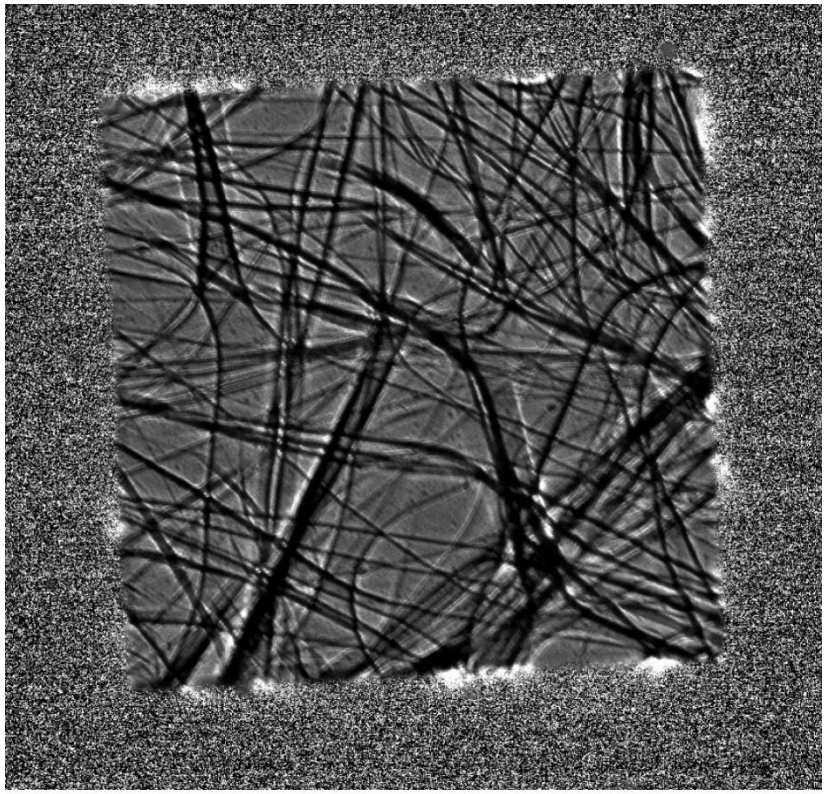

(a)

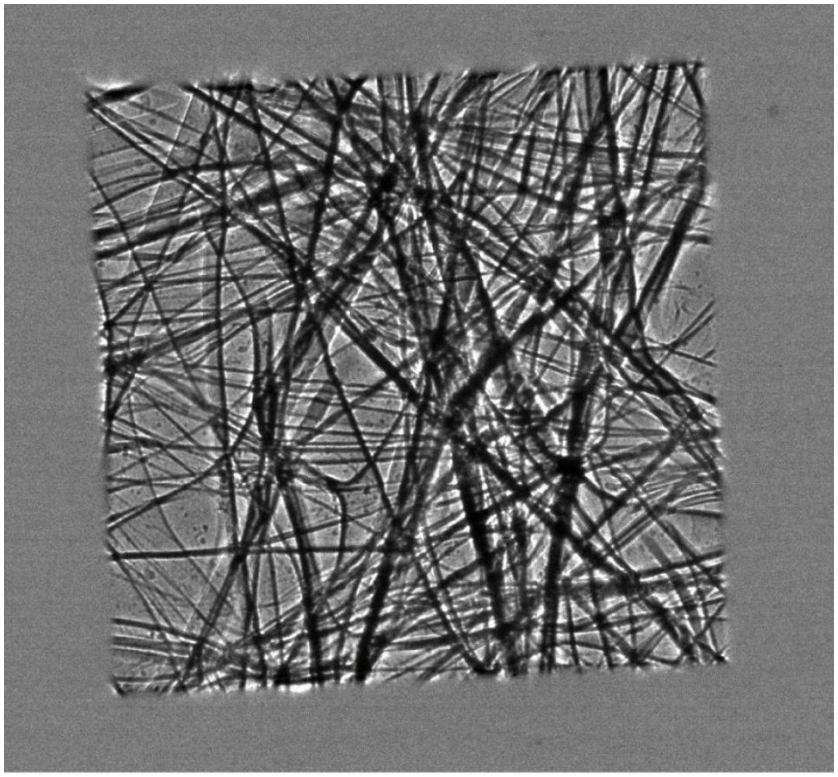

(b)

Images of a foam obtained under X-ray at the BM05 beamline at 10 keV with the LuAP:Tb and LuAP:Tb,Ce SCF screens (with SCF thicknesses of 11 and 4.2 µm, respectively).

Paul-Antoine Douissard, Thierry Martin, Federica Riva, Eric Mathieu, Yuriy Zorenko, Volodymyr Savchyn, Tanya Zorenko, Alexander Fedorov,, IEEE Transaction on Nuclear Science, 2014, Vol.61, Is.1, P. 433 - 438.

Application: biology

The microtomography is a powerful tool for non-destructive testing in biology.

The advantage is to perform the anatomical studies without sectioning in order to save the native structure.

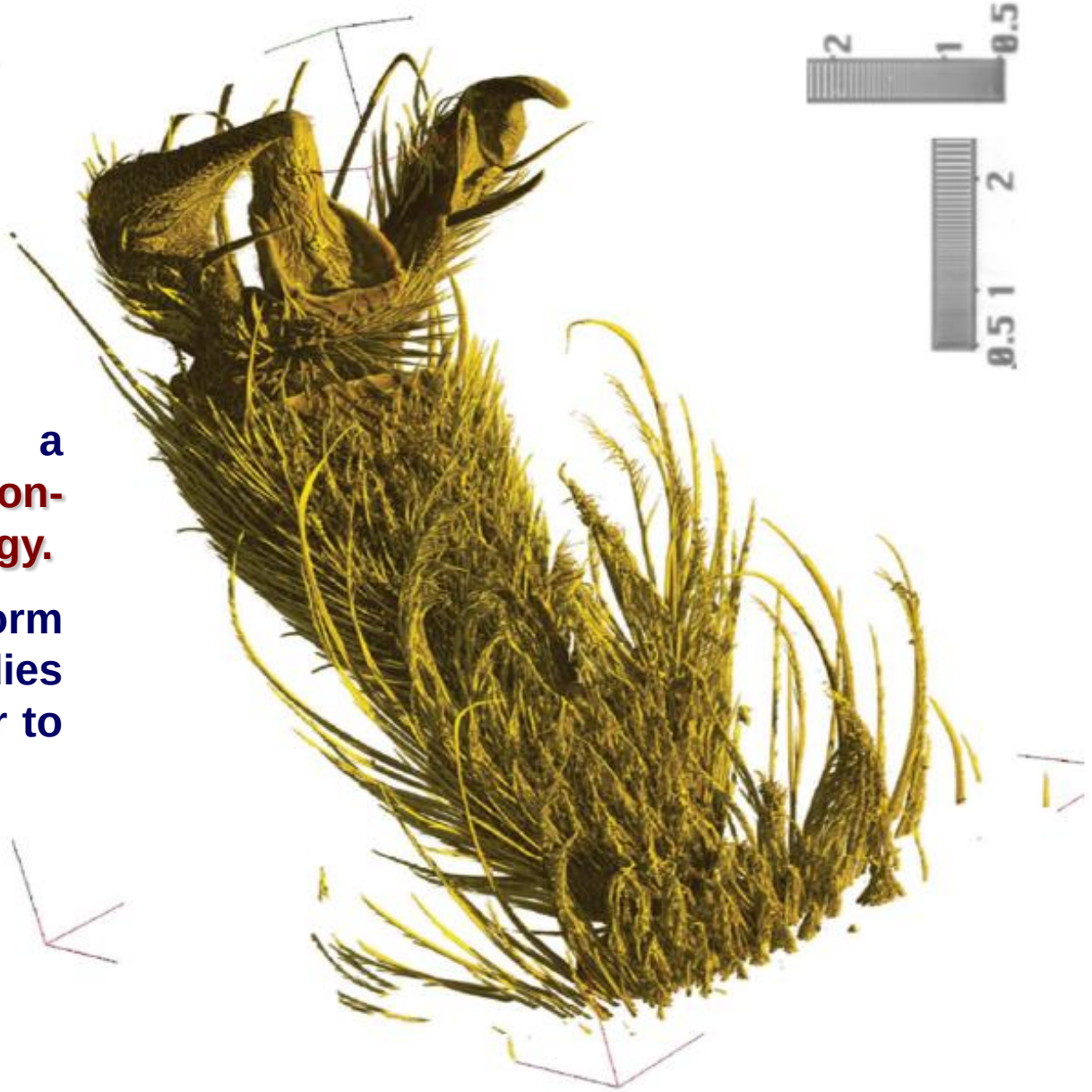

A section of the tarsus of a honey bee (*apis mellifera*), which is a prominent distinguishing feature in insect science. As an insect the honey bee has an exoskeleton (external skeleton). The muscles are attached to the inside of the skeleton. The horizontal and vertical line pairs (size given in micrometers) to demonstrate the spatial resolution reached.

Figure 1: Pieces of opaque amber. Image credits: V. Girard/ D. Néraudeau, UMR CNRS 6118

Application: biology / archeology

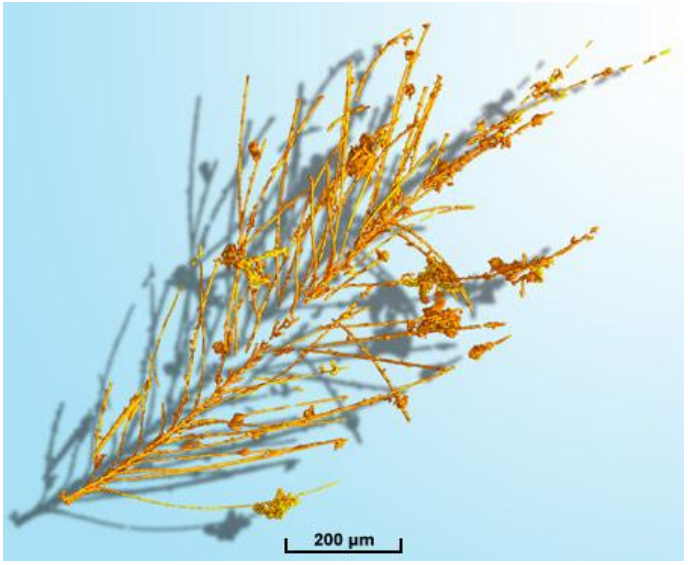

Figure 4: 3D reconstruction of the basis of one of the feathers. Credits: Paul Tafforeau/ESRF.

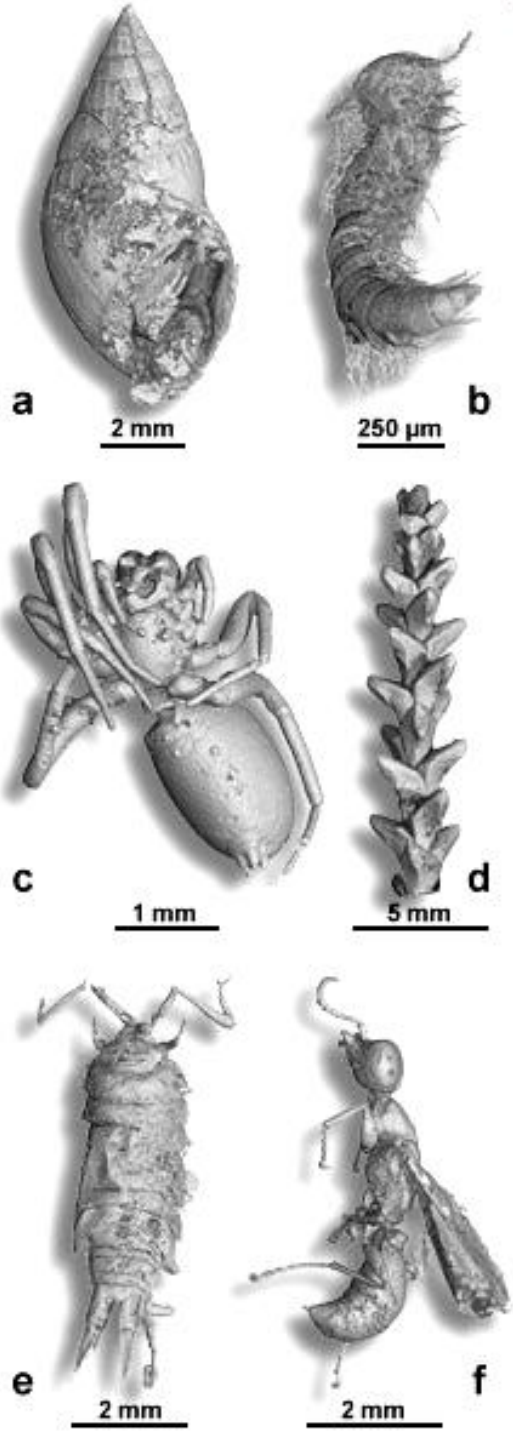

Figure 3: Examples of virtual 3D extraction of organisms embedded in opaque amber:

a) Gastropod Ellobiidae;
b) Myriapod Polyxenidae;
c) Arachnid;
d) Conifer branch (Glenrosa);
e) Isopod crustacean Ligia;
f) Insect hymenopteran Falciformicidae.

Credits: M. Lak, P. Tafforeau, D. Néraudeau (ESRF Grenoble and UMR CNRS 6118 Rennes).

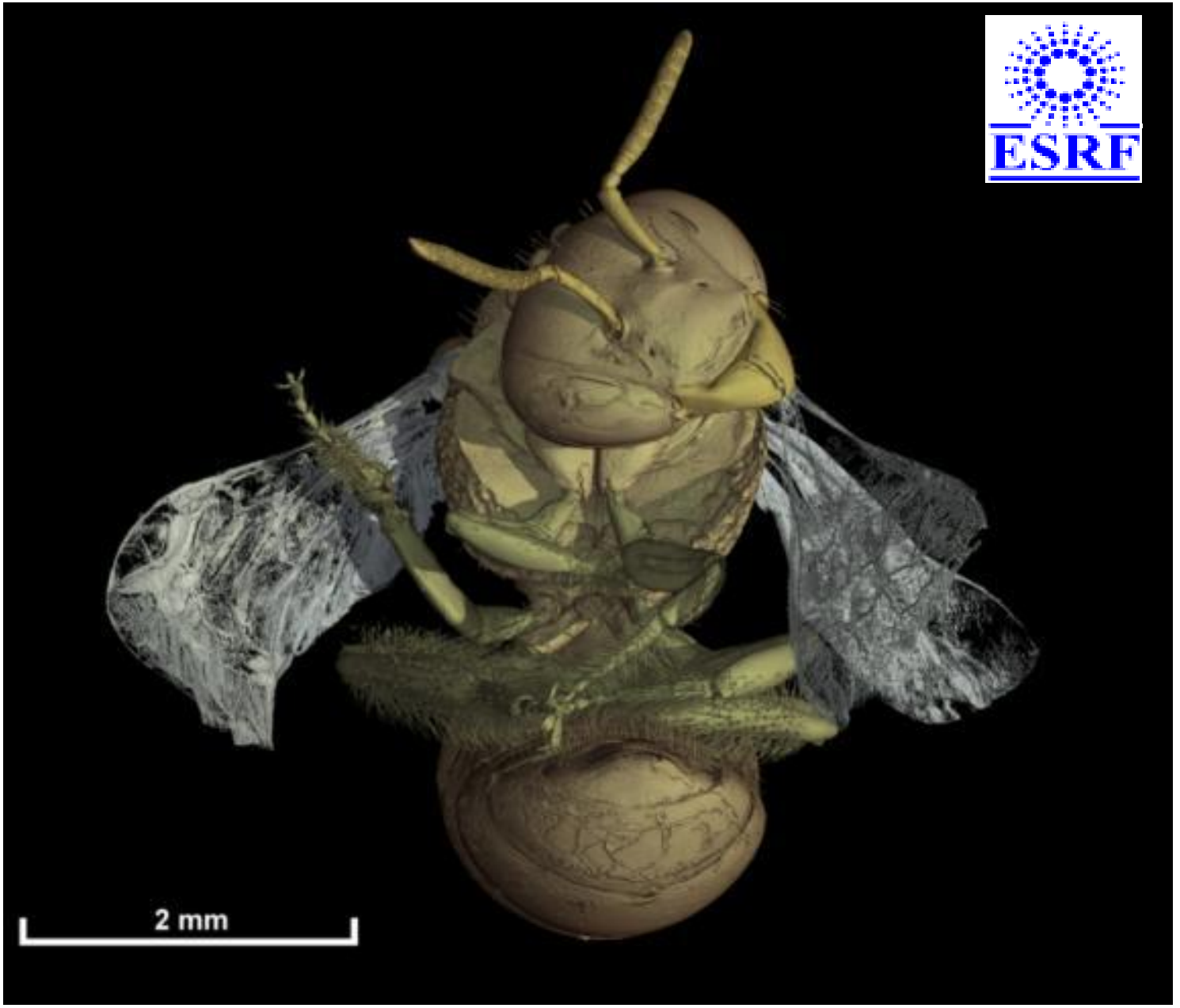

3D reconstruction of insect embedded in the natural amber

Credits: Paul Tafforeau/ESRF.

Application: archeology

Investigation of microstructure of teeth of Neanderthal human

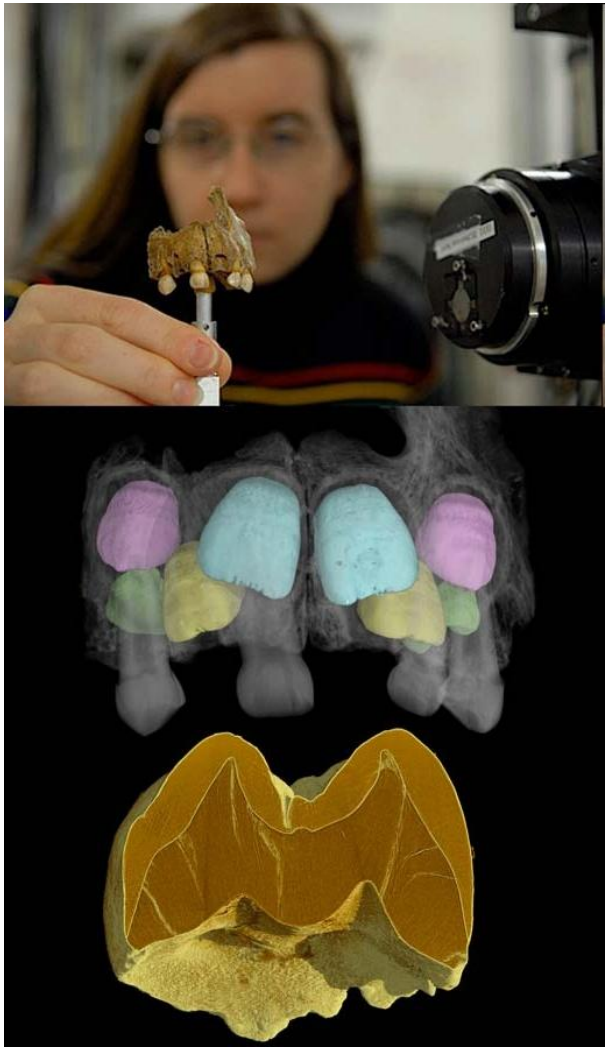

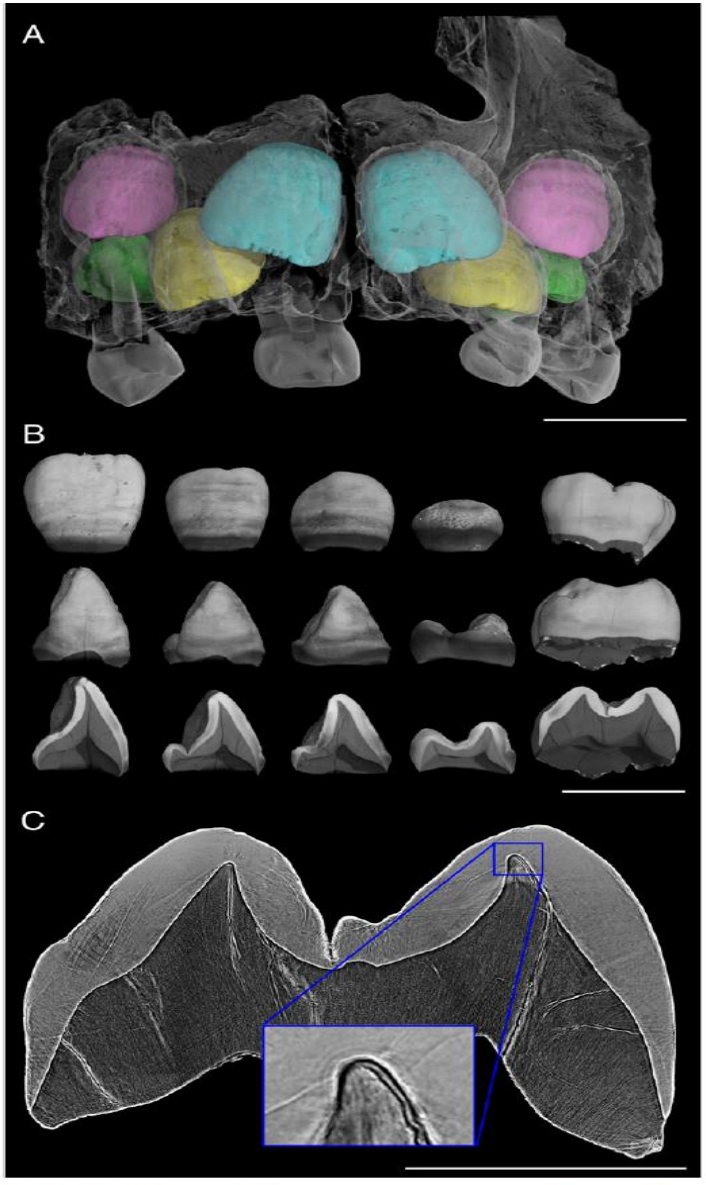

State-of-the-art synchrotron imaging of the tiny upper Neanderthal allows scientists to virtually isolate the permanent teeth inside the bone (center image), count tiny growth lines inside the first molar teeth (lower image), and determine that it died at age 3.

Application: medicine

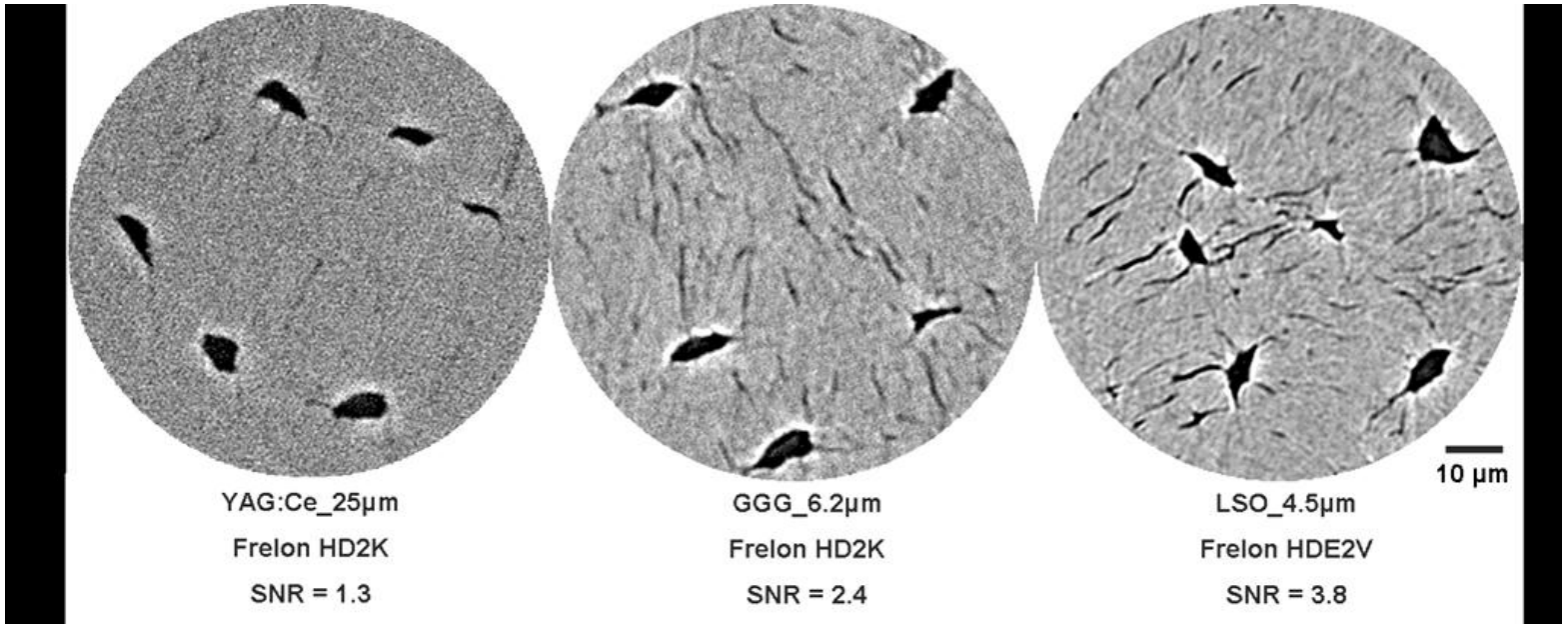

Courtesy of Dr. A. Pacureanu and Dr. F. Perrin [4]

The authors achieved the first 3D images of human bone canaliculi (300-600nm) network in an area covering several osteons.They optimised the imaging setup and acquisition parameters to obtain simultaneously a radiation dose reduction and an inrcease of the S/N ratio in the images.

Visibility of canaliculi with three different scintillators coupled with a CCD camera. While using 25µm thick YAG:Ce, the image resolution is affected and the signal to noise ratio is low, despite the high number of projections (3500) acquired for the scan (nominal pixel size 280 nm). With 6.2 µm GGG:Eu, the canaliculi are visible but the image is still quite noisy (nominal pixel size 280 nm). 4.5 µm LSO:Tb, combined with the HDE2V camera, gives simultaneously better resolution and good SNR (nominal pixel size 300 nm).

X-Ray imaging with SCF scintillators

Application:biology

ANKA Topo/tomo beamline, Karlsrue, Germany

Courtesy of Dr. A.Cecilia

Those images of the amber fossil weevil were obtained on the **ANKA Topo/tomo beamline** for an investigation by the Staatliches Museum fur Naturklunde Karlsruhe (Dr. A Riedel). The tomography acquisition time was 30s with the Photron Fastcam SA-1 camera, a 12.5x magnification optics, 1.6 µm pixel size and **24 µm thick LSO:Tb,Ce**.

Imaging with synchrotron radiation at BESY-II, Berlin, Germany

hard X-ray beamline (BAMline)

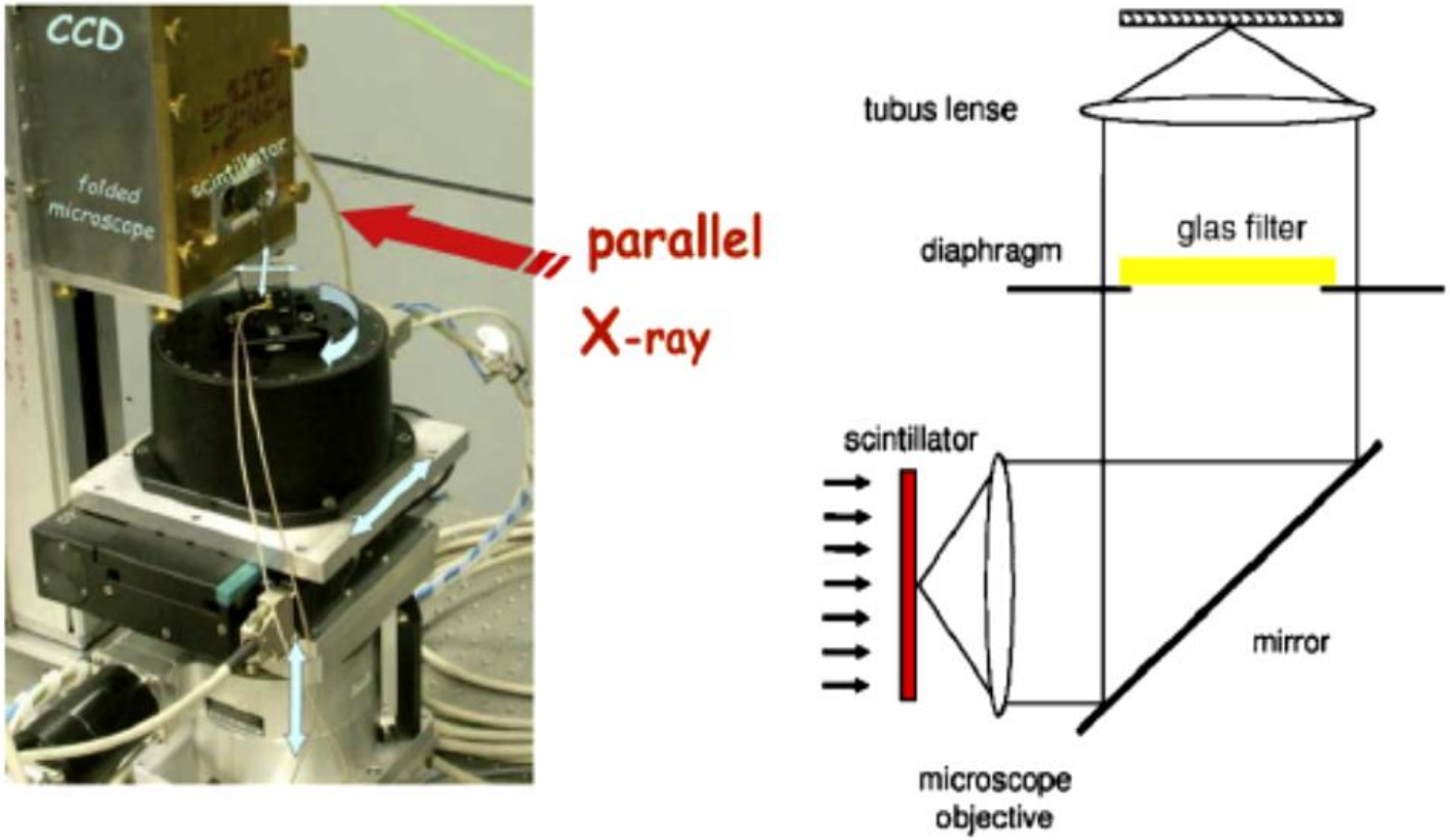

Left: photo of the aligned microscope at the BAMline with sample manipulator and right: principle sketch of the X-ray imaging detector with additional glas filters and a diaphragm in the beam path of the visible light.

SCF for imaging with synchrotron radiation at BESY-II, Berlin, Germany

Application: material science

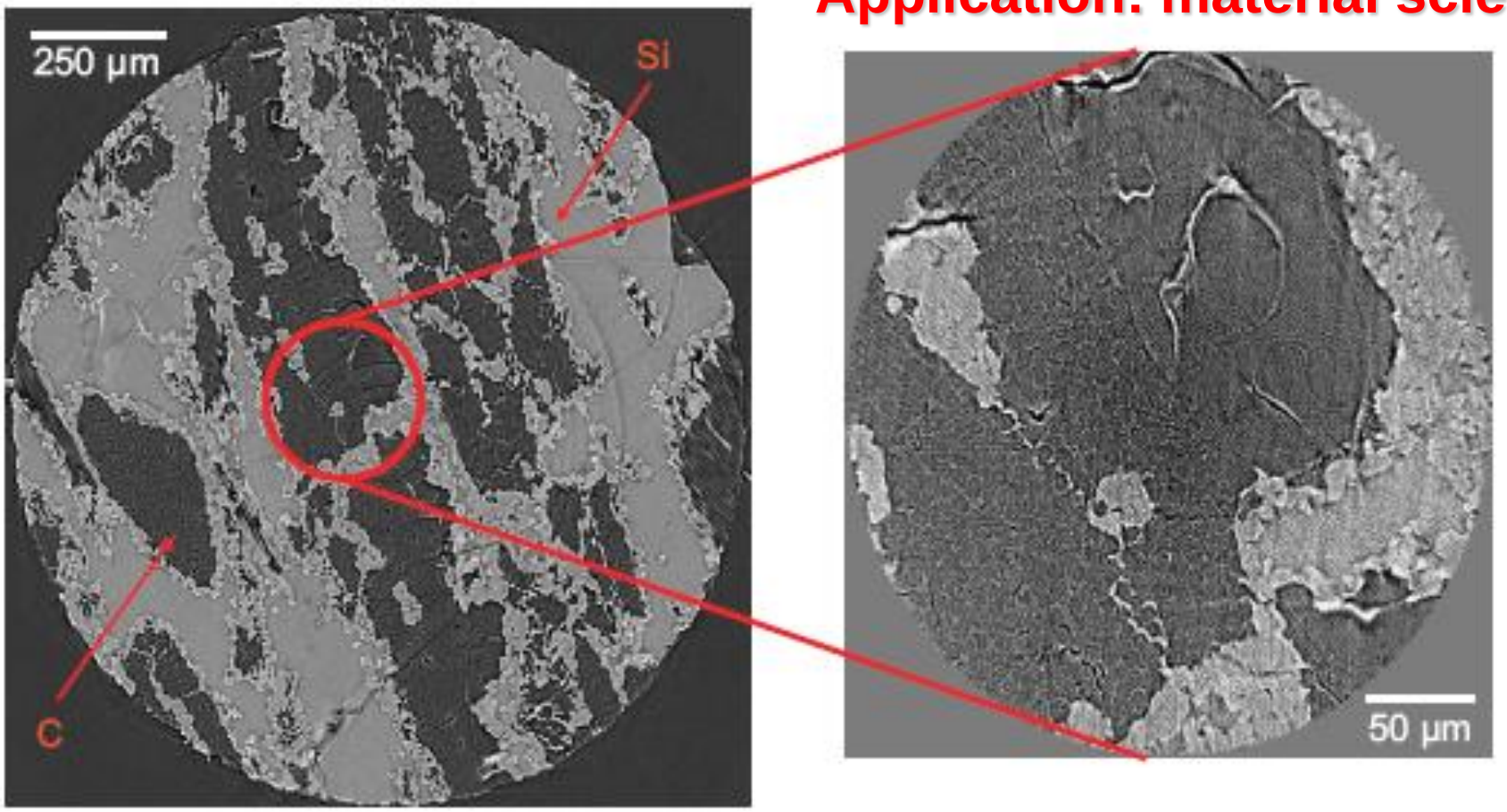

Cross-sections of a fiber reinforced C/SiC ceramic.

The left image is taken with a resolution of < 4 µm with $CdWO_4$ single crystal screens; the right image (local tomography) uses a resolution of < 2 mm with LuAG:Eu SCF screens, 4 µm thick. The carbon fibers, silicon, microcracks and SiC crystals are visible.

SCF for imaging with synchrotron radiation at BESY-II, Berlin, Germany

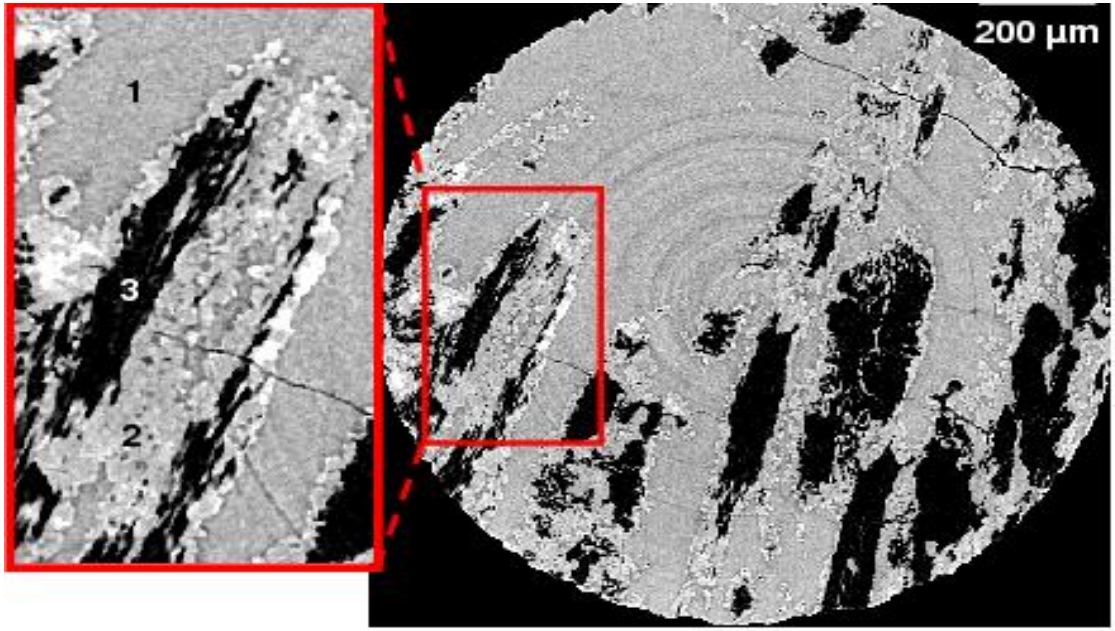

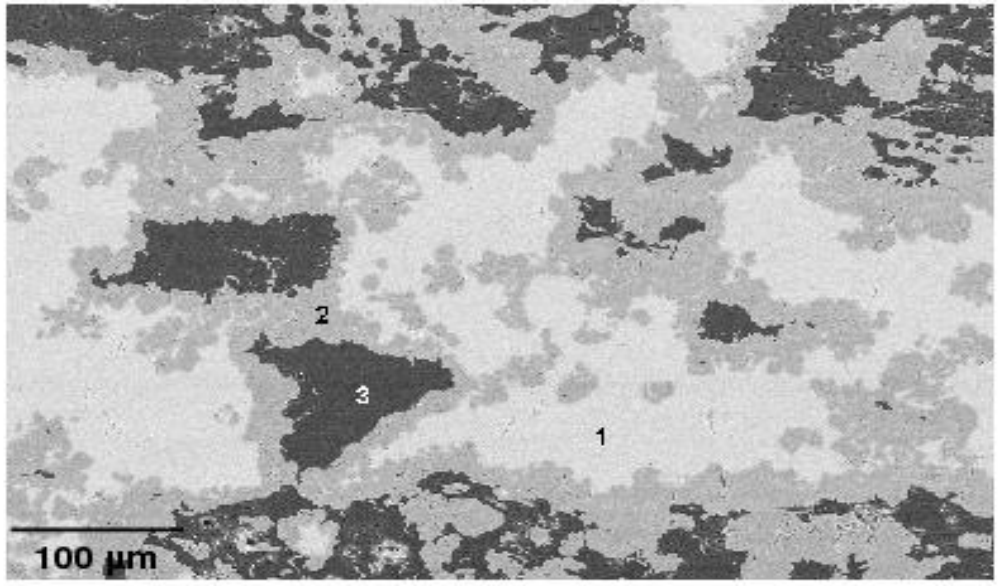

Courtesy of Dr. A. Rack [5]

Top: tomographic slice showing a **fibre-reinforced C/SiC ceramic**, acquired by means of high resolution synchrotron-based microtomography. The inset shows a zoom-in with three material phases marked: Si (1), SiC (2) and C (3). Cracks throughout the sample are visible as well.

Bottom: image of a comparable sample acquired by scanning-electron microscopy. The same phases as in the upper image have been marked.

The **scintillator screen consists of a GGG:Eu SCF (20 µm thick) grown on an undoped GGG substrate.** A 5× objective (0.15 NA) was used and combined with a 2.5× eyepiece. The ESRF inhouse camera FReLoN (type e2v) was used leading to an effective pixel size of the detector of 1.1 µm.

Can we obtain the scintillating screens with higher absorption coefficient of X-rays and better spatial resolution in the submicron range ?

New concepts of creation of the SCF screens

1. Development of **complex multilayer-film scintillators** with separate pathway for registration of the optical signal from each film scintillators;
2. Engineering **„K-edge of X-ray absorption”** multilayer-film scintillators.

Stage of development of SCF scintillators

1st stage: single emitting:**YAG:Ce, GGG:Eu, LuAG:Eu or LSO:Tb SCF;**

2d stage: double emisting YSO:Ce,Tb, LuAP:Ce,Tb SCF; LuAG:Ce,Tb

3d stage: double and triple emitting SCF in the different spectral ranges

Future – microimaging tomography !

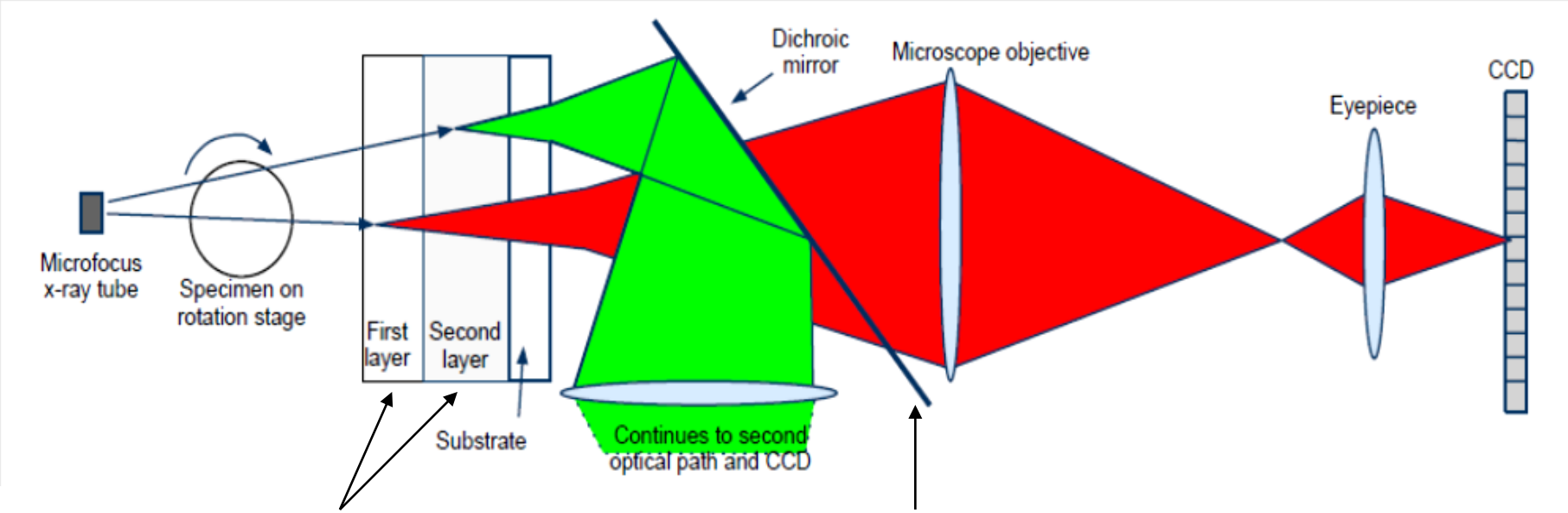

Two scintillator layers each doped to emit a different wavelength

Dichroic mirror to split emission toward different optics + CCD systems

Visualisation with double SCF scintillating screens based on the double LSO:Ce and LYSO:Tb layers

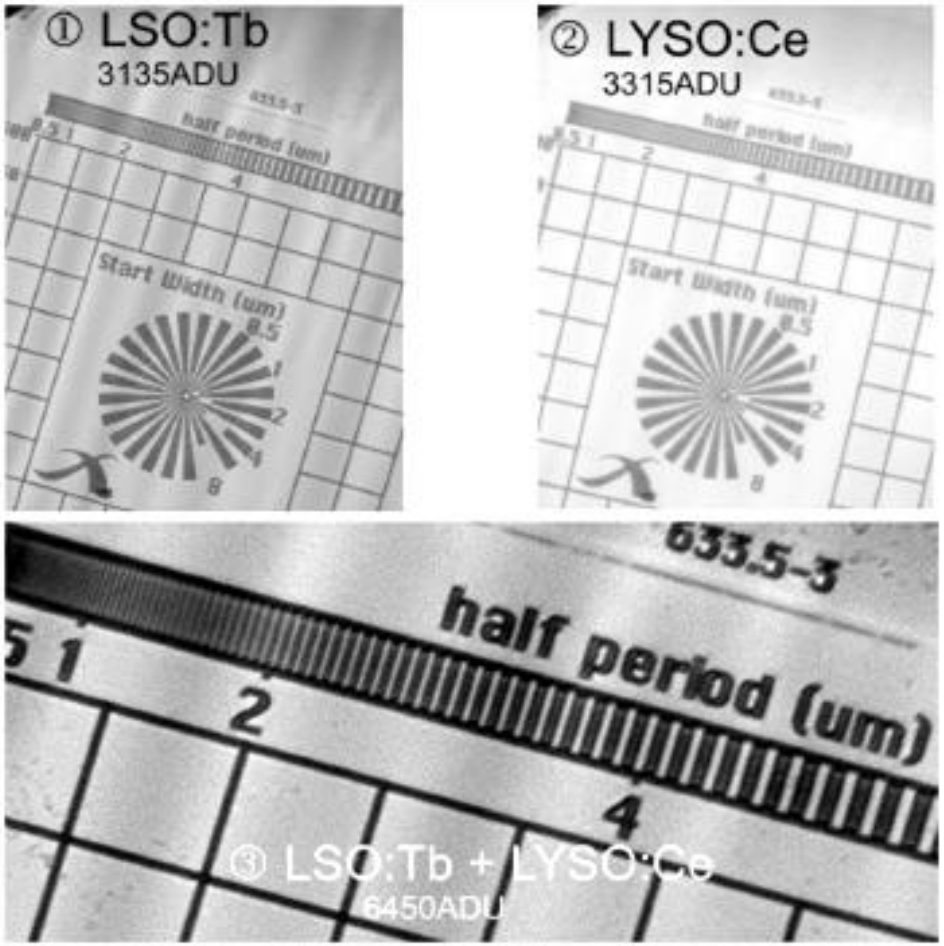

Fig. 8. Demonstration of the spatial resolution achieveable with a scintillator stack consisting of two layers ($15\times$ magnification/NA $= 0.28$ objective). The image ③ is a summation of image ① and ② detected by selecting the different emissions of the scintillator multi-layer via optical filtering.

K-edge engineering

Choice of elements in order to **boost absorption efficiency**

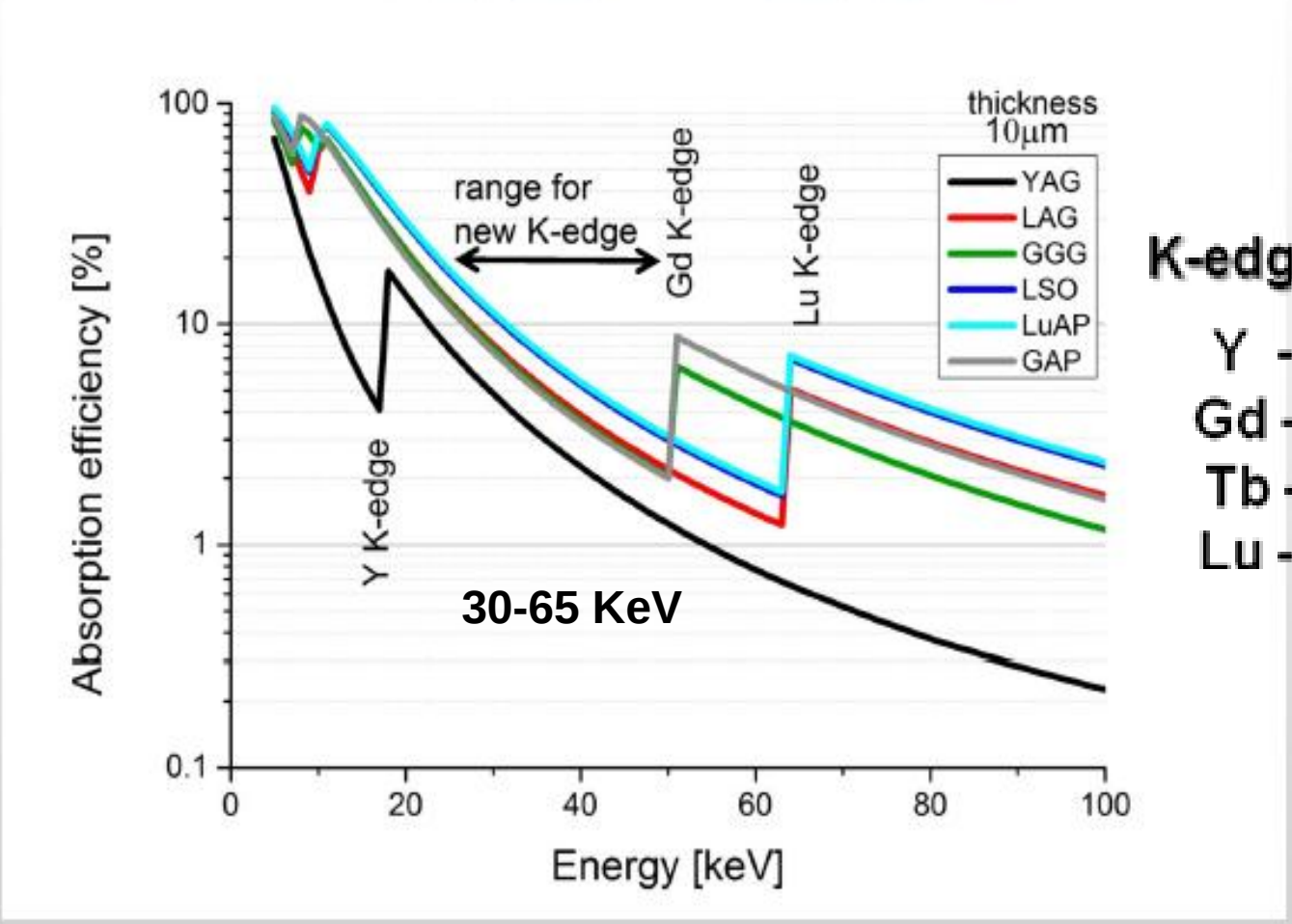

K-edge of cations

Y - 17.04 KeV
Gd - 50.24 KeV
Tb - 52.0 KeV
Lu - 63.61 KeV

Need to take into account absorption properties but also **lattice mismatch** with the substrate and **effects on the emission**

Resolution of images

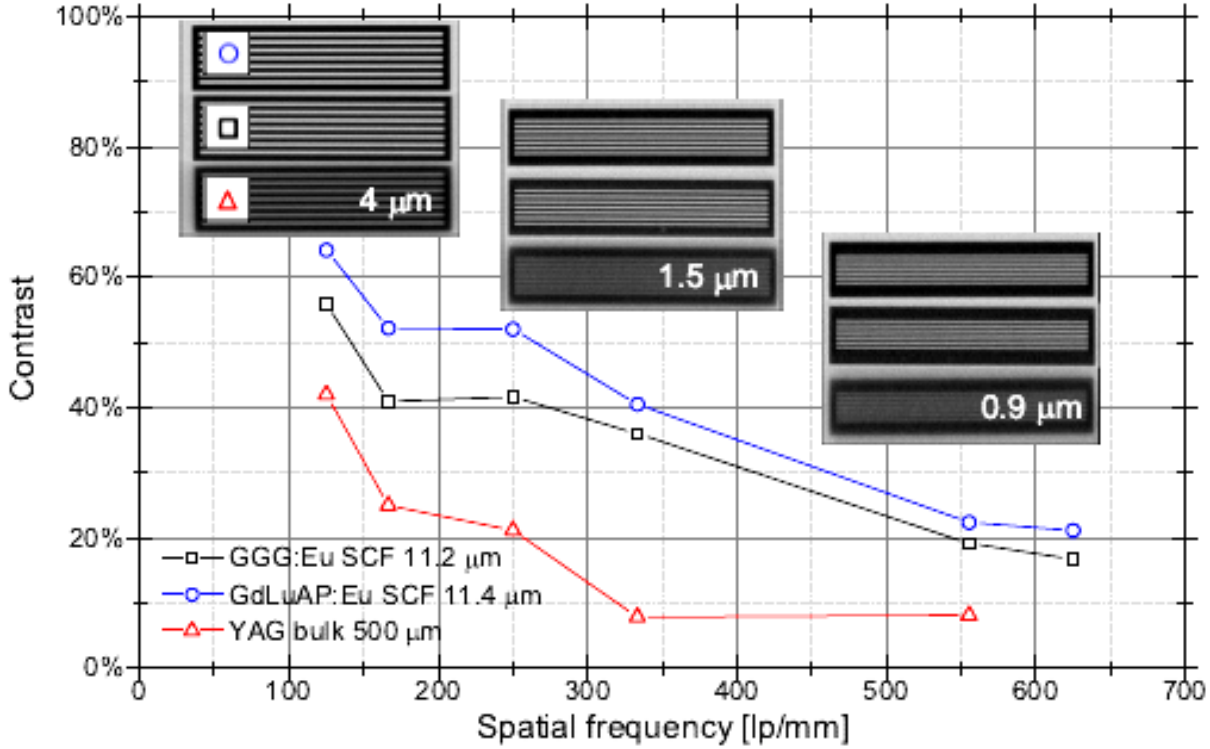

X-Ray microimaging with $(Lu_{1-x}Gd_x)AP:Eu$ SCF scintillators

F. Riva, P-.A.Douissard, T. Martin, F. Carla, Yu. Zorenko, C. Dujardin,
ChystEngComm. 2016; V.18, P. 608–615.

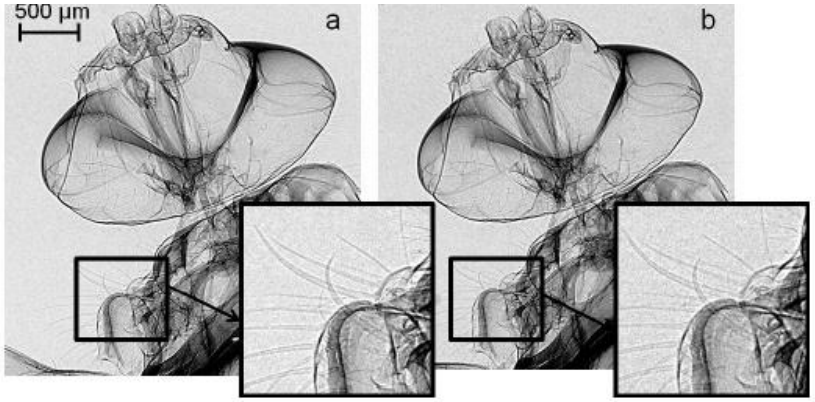

Fig. 9 Top: Images of a tungsten pattern and deduced contrast as a function of the spatial frequency, recorded using a PCO2000 camera coupled with a 20X objective, NA = 0.4. Bottom: Image of a fly with GdLuAP:Eu 11.4 μm scintillator (a) and with a 11.2 μm GGG:Eu scintillator (b), recorded using a PCO2000 camera coupled with a 2X microscope objective, NA = 0.08 (bottom).

SCF scintillators based on the Ce doped $(Gd, Lu, Tb)_3(Al, Ga)_5O_{12}$ mixed garnet compounds grown by LPE method onto YAG and GAGG substrates

13.09.2016, Milan, Italy

SCF scintillators based on the Ce doped $(Gd,Lu,Tb)_3(Al,Ga)_5O_{12}$ mixed garnet compounds grown by LPE method onto YAG and GAGG substrates

Compounds

YAG substrate ; a=12.00 Å

$Lu_{3-x}Gd_x\ Al_{5-x}Ga_xO_{12}$:Ce;
x=0÷1.5; y=0÷2.0;

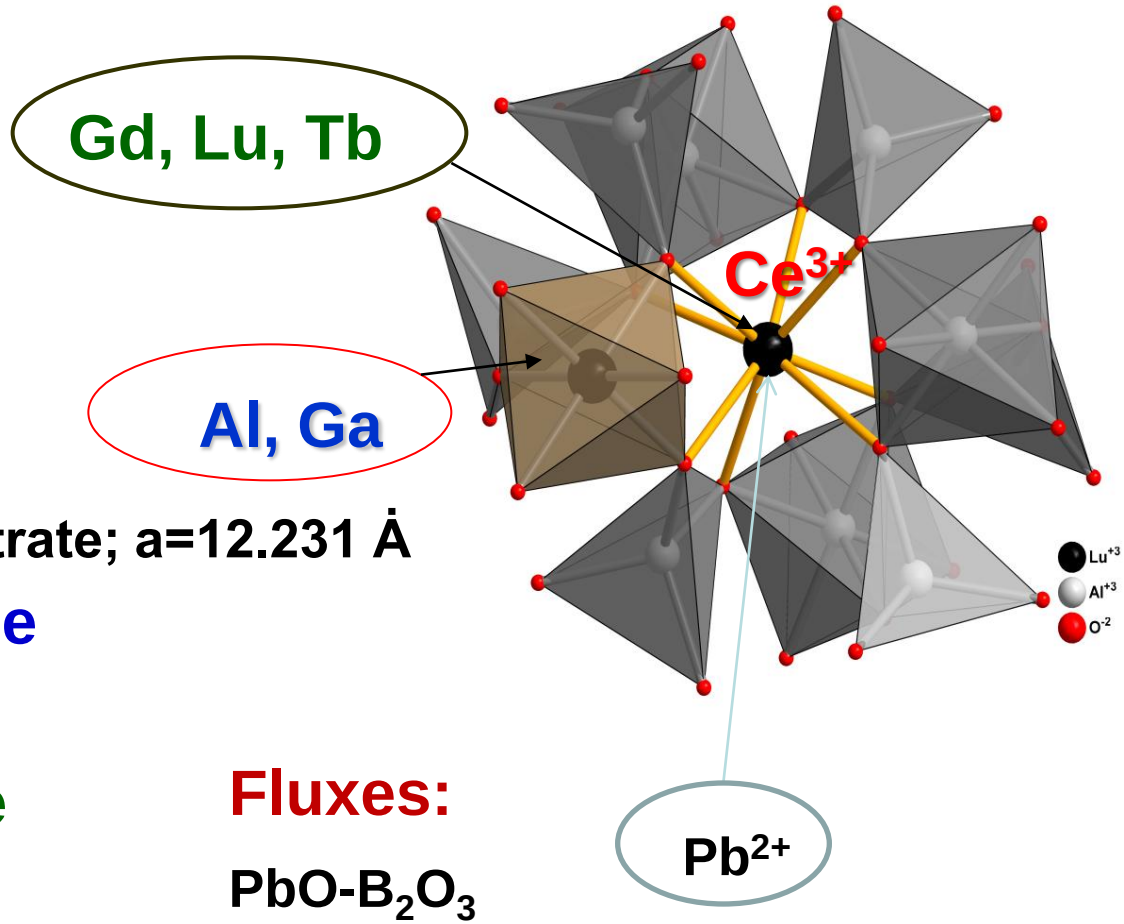

$Gd_3Al_{2.5}Ga_{2.5}O_{12}$ (GAGG) substrate; a=12.231 Å

$Gd_{3-x}Lu_xAl_{5-y}Ga_yO_{12}$:Ce
x=0÷3.0; y=2÷4;

$Tb_{3-x}Gd_xAl_{5-y}Ga_yO_{12}$:Ce
x=0÷3.0; y=1.5÷3.0;

Fluxes:

$PbO\text{-}B_2O_3$
$BaO\text{-}B_2O_3\text{-}BaF_2$ (lead free)

Conceptual aproach in the development of $(Gd,Lu,Tb)_3(Al,Ga)_5O_{12}$ multicomponent garnet SCF scintillators

Producing the SCF analogues of very efficient bulk crystal scintillators (LY up to 60 000 ph/MeV) and optimisation their properties using:

1. **Engineering of the garnet band gap value by the Ga doping;**
2. **Engineering of the energy structure of Ce^{3+} ions by the change of garnet crystal field strength to keep the Ce^{3+} radiative level inside of band gap of garnet;**
3. **Transfer of the part of excitation energy to Ce^{3+} ions using RE cation (Gd^{3+}, Tb^{3+}) sublattices**

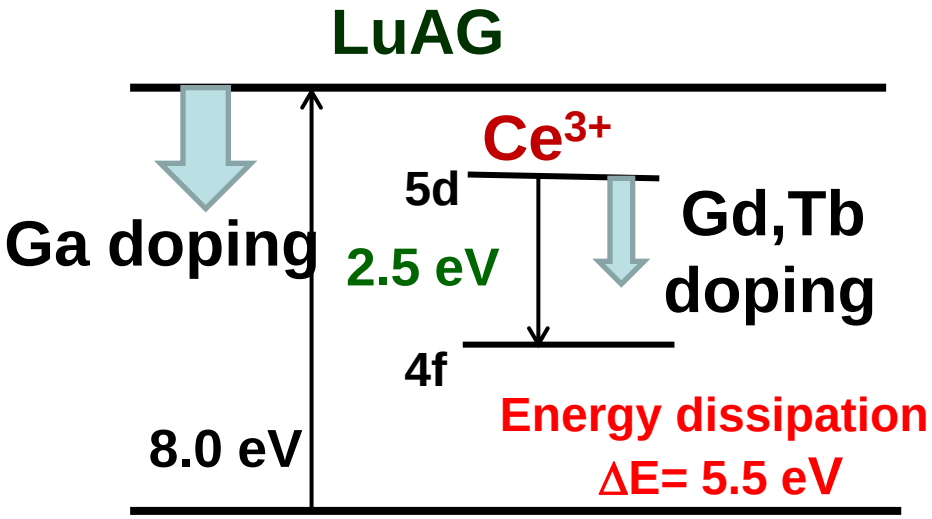

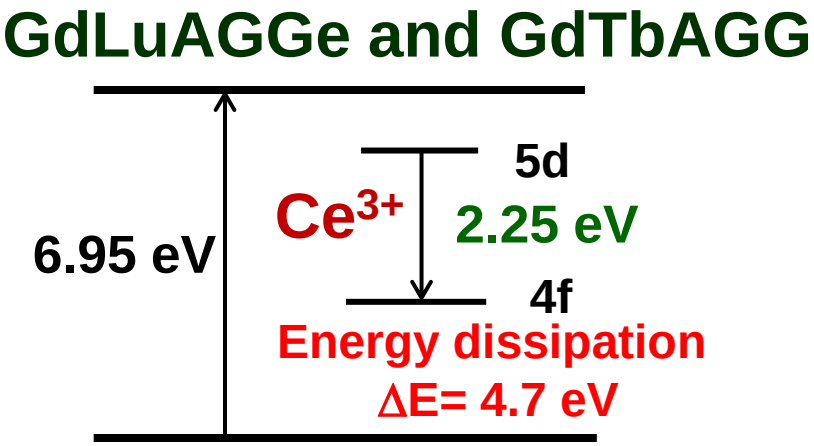

Growth of $(Lu_{3-x}Gd_x)Al_5O_{12}$:Ce SCF onto YAG substrates

- We have found that the full set of $Lu_{3-x}Gd_xAl_{5-y}O_{12}$:Ce SCF with x values from 0 up to 3.0 in principle can be crystallized onto same YAG substrates
- **Lattice constant and misfit m** between SCFs and YAG substrate depend linearly on Gd content.

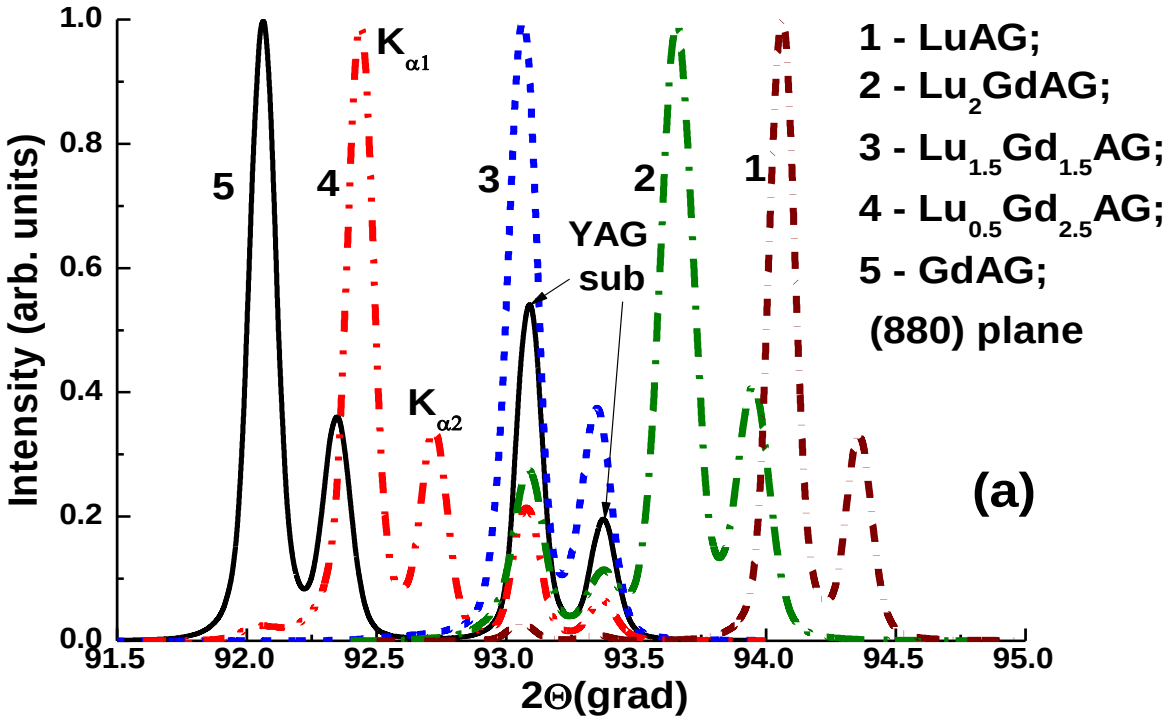

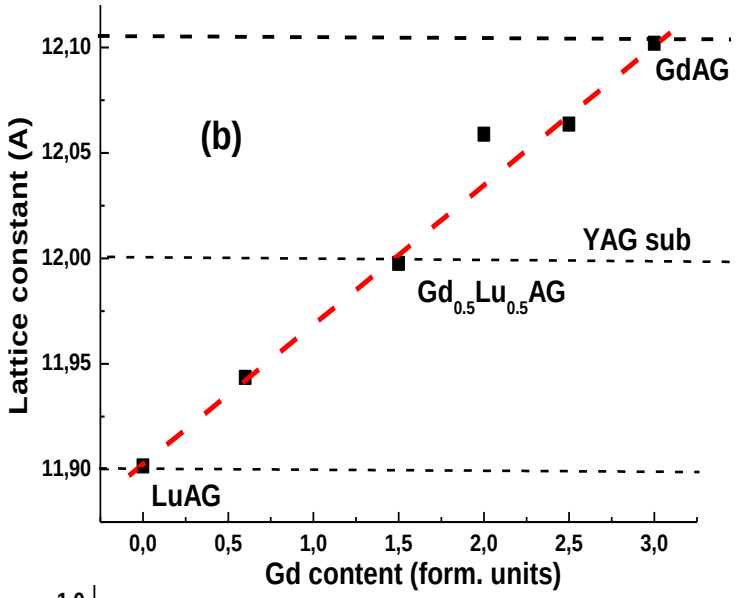

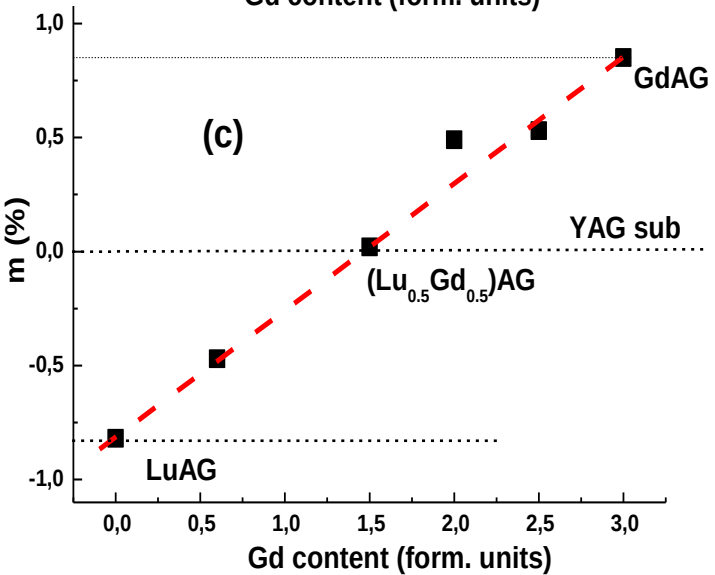

XRD pattern of (880) planes of the $Lu_{3-x}Gd_xAG$ SCFs with different x values: x=0 (1), 1.0 (2), 1.5 (3), 2.5 (4) and 3.0 (5); b, c) – dependence of the lattice constants (b) and misfit m (c) of $Lu_{3-x}Gd_xAG$ SCF on the Gd content x

Growth of $(Lu_{3-x}Tb_x)Al_5O_{12}$:Ce SCF on YAG substrates

- We have found that the full set of $Lu_{3-x}Tb_xAl_{5-}O_{12}$:Ce SCF with x values from 0 up to 3.0 in principle can be crystallized onto same YAG substrates
- The **lattice constant and misfit m** between SCFs and YAG substrate depend linearly on Tb content.

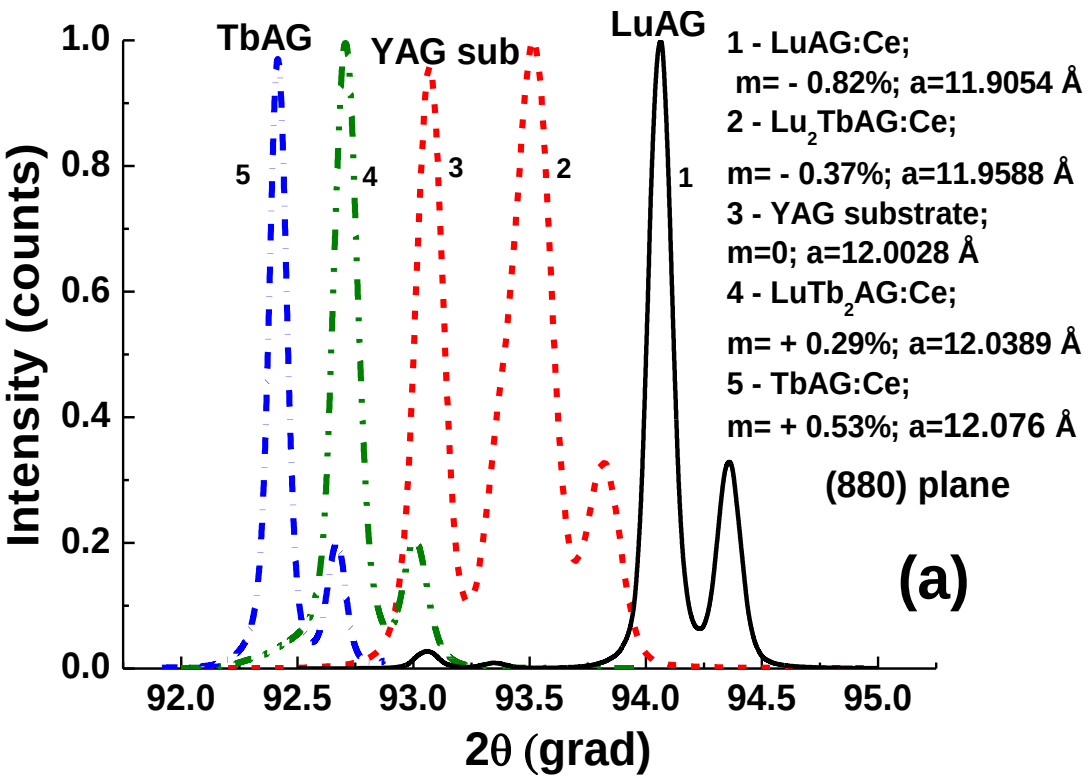

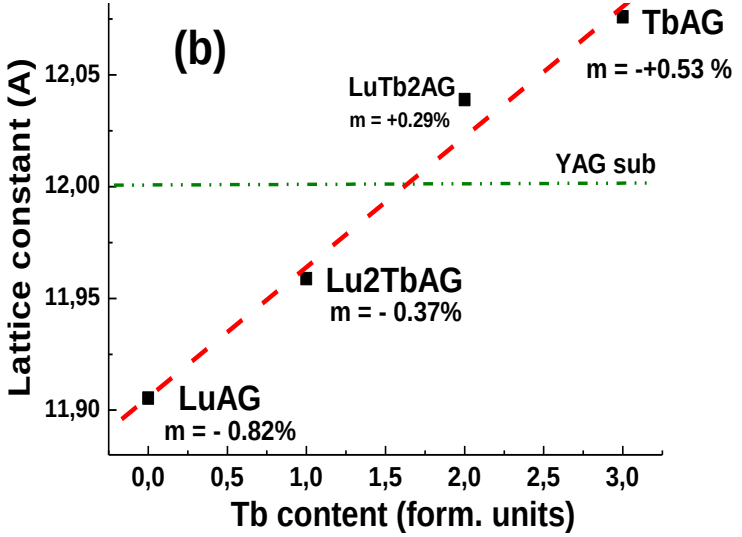

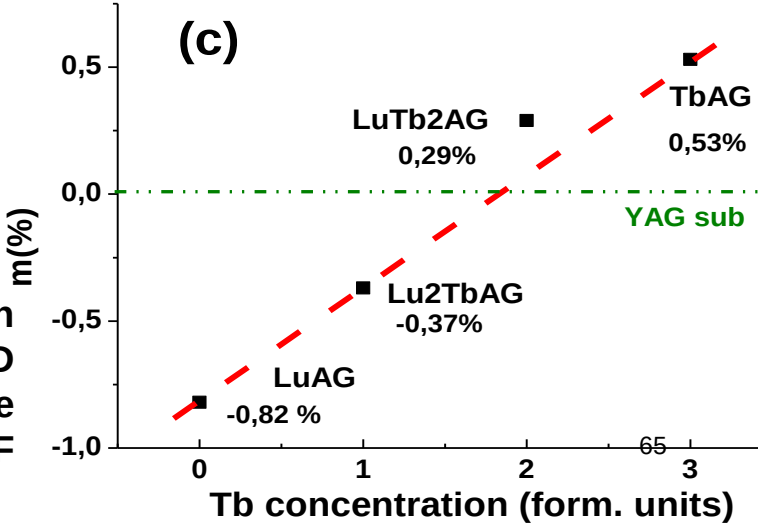

XRD pattern of (880) planes of the $Lu_{3-x}Tb_xAG$ SCFs with different x values: x=0 (1), 1.0 (2), 2.0 (4), 3.0 (5), (3) - XRD from YAG substrate; (b, d) – dependence of the lattice constants (b) and misfit m between the lattice constants SCF and substrate (d) of Lu_{3-x}TbxAG SCF on the x value.

Lattice constants and SCF/substrate misfit of $Lu_{3-x}Gd_xAl_{5-y}Ga_yO_{12}$:Ce SCF / YAG

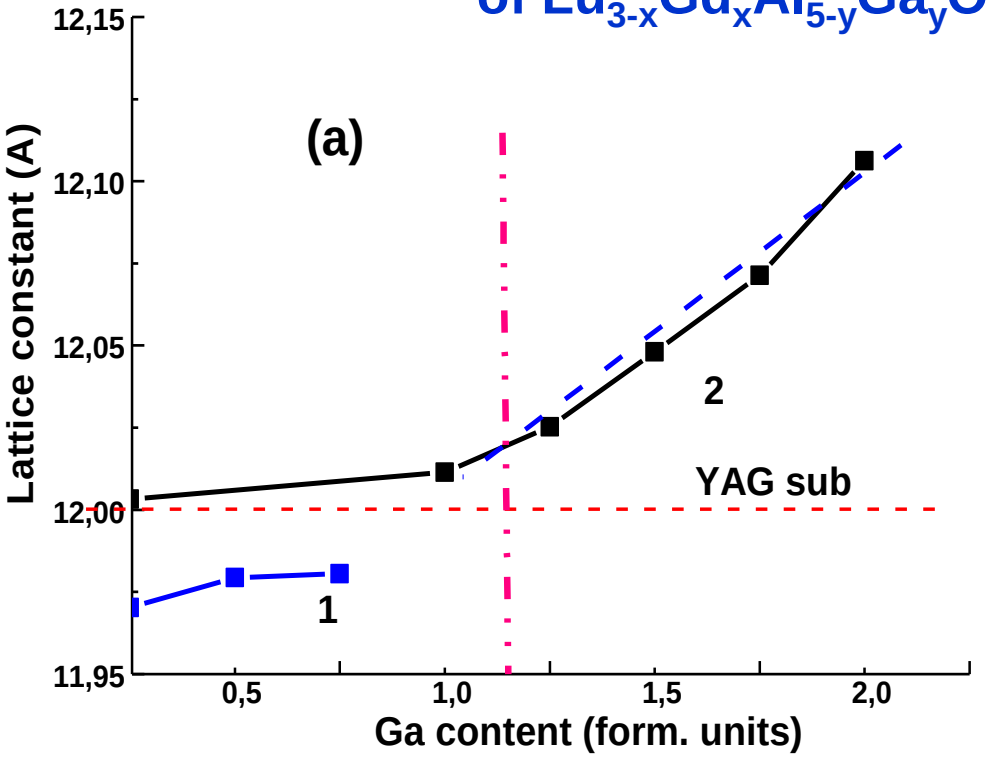

Complicated character of dependence of the SCF lattice constant on Ga content is caused by the preference in the Ga localization in tetrahedral sites and preference in Al substitution of octahedral sites of garnet host

(b, c) – dependence of the lattice constants (b) and misfit m (c) of $Lu_{3-x}Gd_xAG$ SCF on the Gd content x

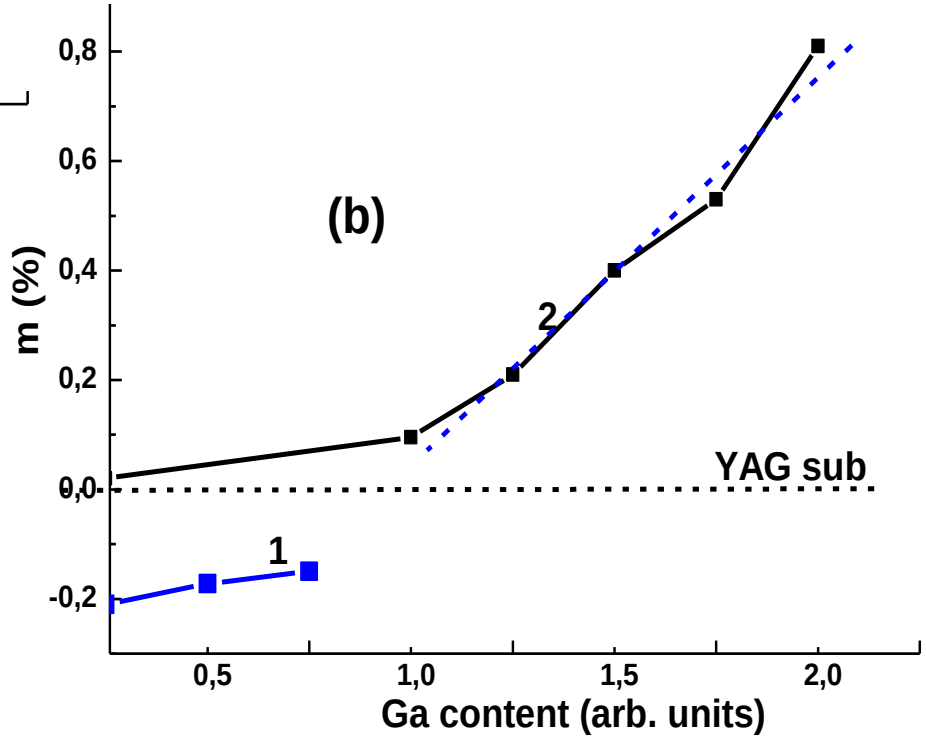

NMR spectroscopy of Ga ions in $Y_3Al_{5-x}Ga_xO_{12}$:Ce and $Y_3Al_{5-x}Ga_xO_{12}$:Ce crystals and SCF (performed by prof. V. Laguta)

Y_{dod} = 1.01 A

Ga_{oct}= 0.63 A
Al_{oct} = 0.53 A

Al_{tet} = 0.39 A
Ga_{tet}= 0.47 A

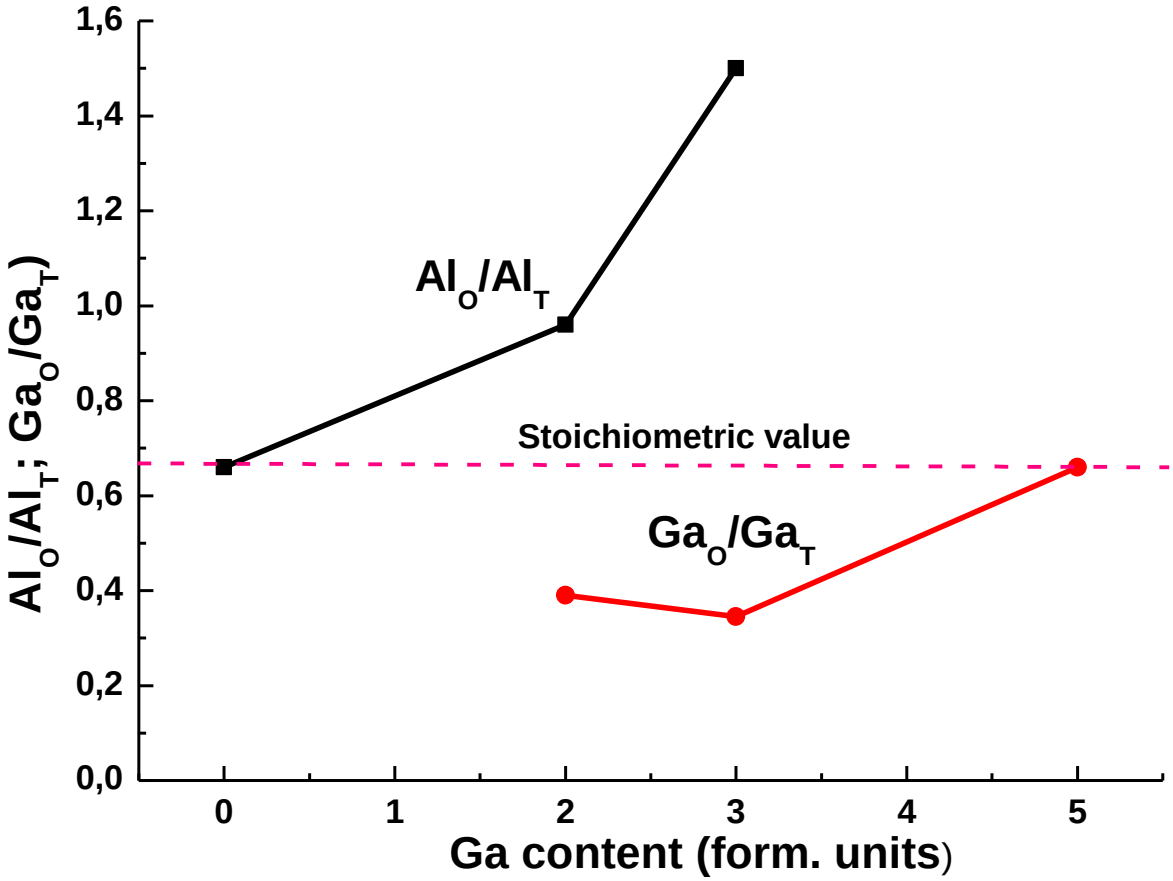

Local conclusions :

- Al^{3+} ions are preferable occupaid the octachedral position of garnet host;
- Ga^{3+} ions are preferable occupaid the tetrahedral position of garnet host;
- These conclusion are in contradict with typical preference in the occupation of crystalografic position depending on the dimension of ionic radii

SCF scintillators based on the mixed garnet compounds

Scintillators based on the $Gd_{3-x}Lu_xAl_{5-y}Ga_yO_{12}$:Ce SCF LPE grown onto GAGG substrates from PbO and BaO based flux

SCF of $Gd_{3-x}Lu_xAl_{5-y}Ga_yO_{12}$:Ce and $Gd_3Al_{5-y}Ga_yO_{12}$:Ce garnets LPE grown onto $Gd_{2.5}Ga_{2.5}Al_{2,5}O_{12}$ (GAGG) substrates at IF UKW in Bydgoszcz, Poland

LGAGG:Ce GAGG:Ce

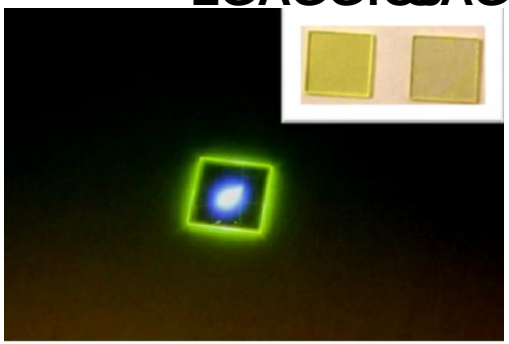

Laser λ_{ex}=360 nm excitation;

Yu. Zorenko, e. a., Physica Status Solidi RRL, 2015, V.9, No 8, P. 489–493.

Luminescent and scintillation properties of $Gd_{3-x}Lu_xAl_{5-y}Ga_yO_{12}$:Ce

Cathodoluminescence (CL) spectra

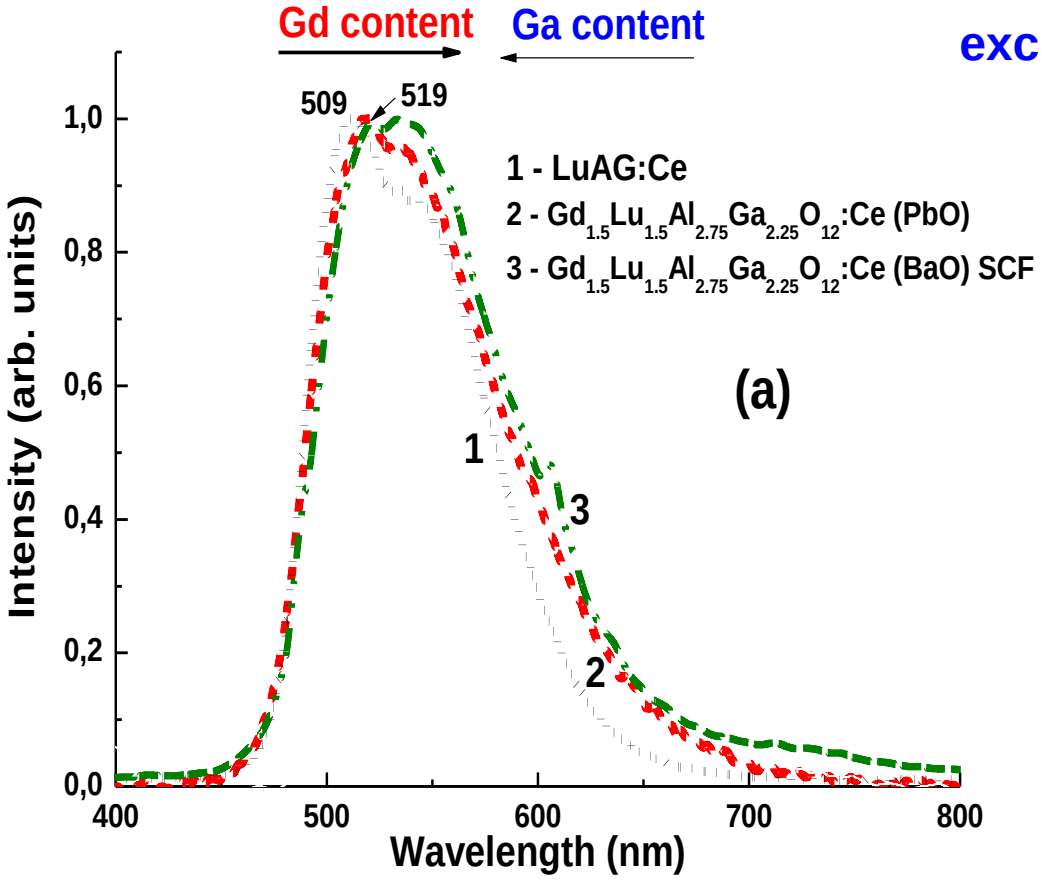

(a) - normalized CL spectra of $Gd_{1.5}Lu_{1.5}Al_{2.75}Ga_{2,25}O_{12}$:Ce (PbO) (1) and (BaO) (2) SCF in comparison with CL spectra of LuAG:Ce (PbO) SCF;

Scintillation decay kinetic under excitation by α–particles of Pu^{239} source

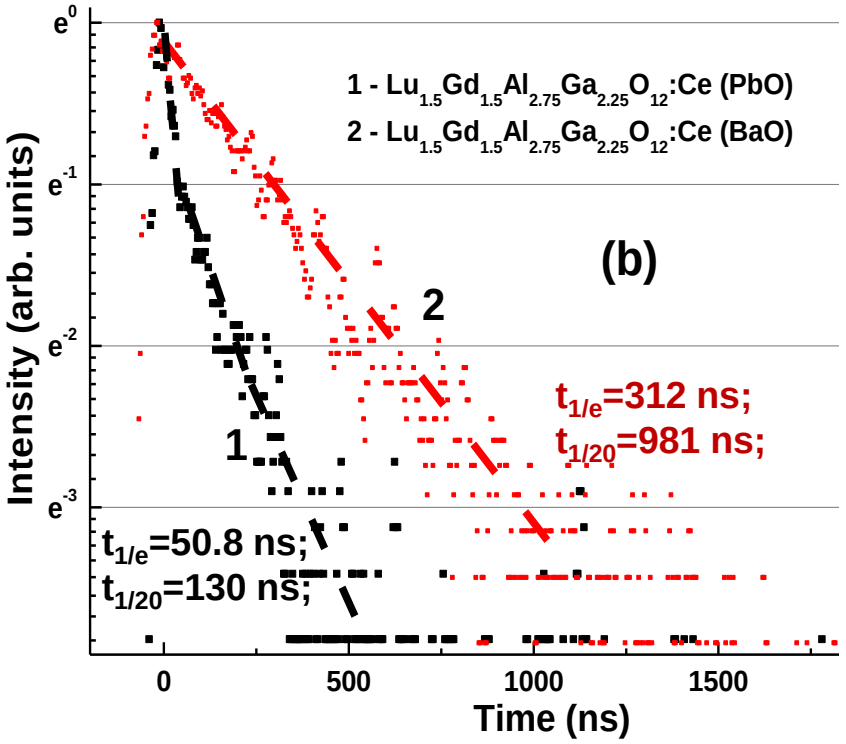

(b) – normalized decay kinetic of $Gd_{1.5}Lu_{1.5}Al_{2.75}Ga_{2.25}O_{12}$:Ce (PbO) (1) and (BaO) (2) SCF

$Gd_{3-x}Lu_xAl_{5-y}Ga_yO_{12}$:Ce SCFs, grown from PbO flux, shows more faster non-exponential decay kinetic then their counterparts, grown from BaO flux

Luminescent and scintillation properties of $Gd_3Al_{5-y}Ga_yO_{12}$:Ce SCFs

CL spectra

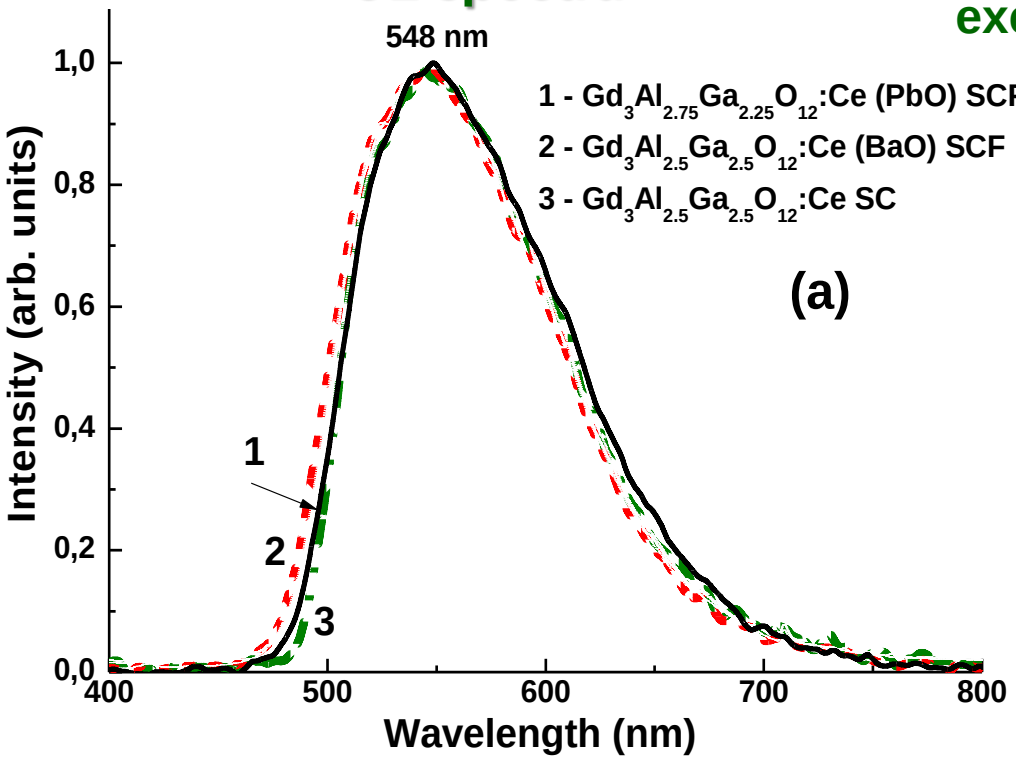

Scintillation decay kinetic under excitation by α–particles of Pu^{239} source

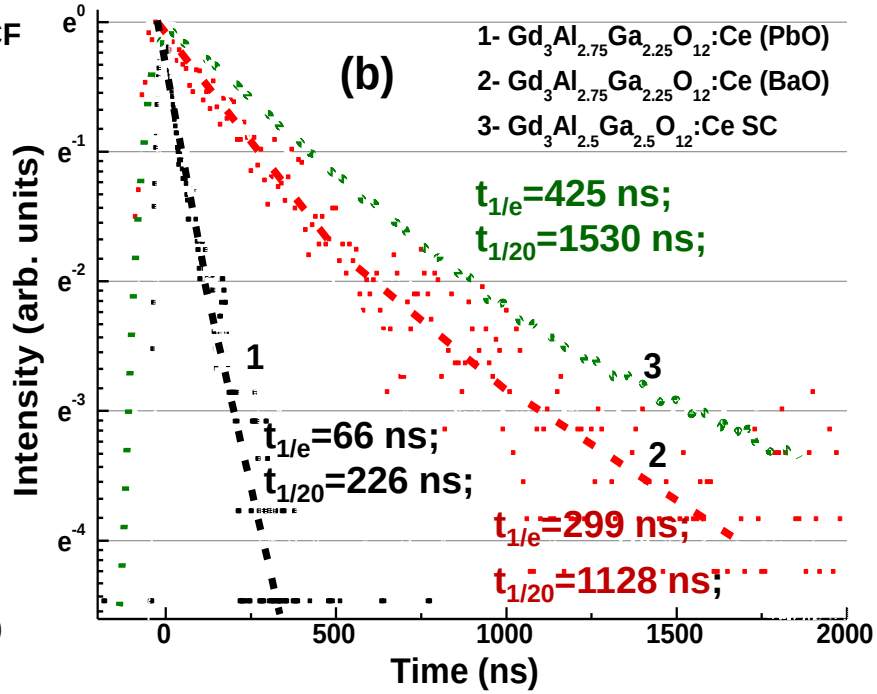

(a)- normalized CL spectra of $Gd_{1.5}Lu_{1.5}Al_{2.75}Ga_{2,25}O_{12}$:Ce (BaO) (1) and $Gd_3Al_{2.5}Ga_{2,5}O_{12}$:Ce (BaO) (2) SCF in comparison with CL spectra of $Gd_3Al_2Ga_3O_{12}$:Ce crystal;

(b) - decay kinetic of $Gd_3Al_{2,25}Ga_{2.25}O_{12}$:Ce (PbO) (1) and (BaO) (2) SCFs in comparison with decay kinetic of $Gd_3Al_{2.5}Ga_{2.5}O_{12}$:Ce (3) crystal counterparts;

1. $Gd_3Al_{5-y}Ga_yO_{12}$:Ce SCF grown from PbO based flux (Fig.a) also demonstrates faster decay kinetic then their SCF counterparts, grown from BaO based flux
2. Scintillation decay of $Gd_3Al_{2.75-2.5}Ga_{2.25-2.5}O_{12}$:Ce (BaO) SCF (Fig.b) is very close to that in $Gd_3Al_{2.5}Ga_{2.5}O_{12}$:Ce and $Gd_3Al_2Ga_3O_{12}$:Ce SC counterparts.

Luminescent and scintillation properties of $Gd_{3-x}Lu_xAl_{5-y}Ga_yO_{12}$:Ce SCFs

Table 1. Conditions of growth (type of flux and substrate; misfit **m** between lattice constant of SCF and substrate), maxima of emission spectra λ_{max}, scintillation decay time $t_{1/e}$,/ $t_{1/20}$ and LY of best samples in series of $(Gd,Lu)_3(Al,Ga)_5O_{12}$:Ce SCFs under excitation by Pu^{239} sources (measured with shaping time of 12 μs) in comparison with standard YAG:Ce SCF (360 phels/MeV) and LuAG:Ce SCF counterparts and standard $Gd_3Al_{2.5}Ga_{2.5}O_{12}$:Ce and $Gd_3Al_2Ga_3O_{12}$:Ce bulk crystals

Garnet content	Sub-strate	Type of flux	m, %	λ_{max}, nm	Decay time, $t_{1/e}/t_{1/20}$, ns	LY, %
$Y_3Al_5O_{12}$:Ce	YAG	PbO	-	535	57.3/ 171	100
$Lu_3Al_5O_{12}$:Ce	YAG	PbO	- 0.82	509	52.8 / 262	205
$Gd_{1.5}Lu_{1.5}Al_{2.75}Ga_{2.25}O_{12}$:Ce	GGAG	PbO	-0.73	519	50.8 / 130	145
$Gd_3Al_{2.75}Ga_{2.25}O_{12}$:Ce	GGAG	PbO	-0.32	547	66.2 / 226	55
$Gd_{1.5}Lu_{1.5}Al_{2.75}Ga_{2.25}O_{12}$:Ce	GGAG	BaO	-0.53	522	312 / 981	346
$Gd_3Al_{2.5}Ga_{2.5}O_{12}$:Ce	GGAG	BaO	-0.14	546	299 / 1128	347
$Gd_3Al_2Ga_3O_{12}$:Ce Yoshikawa group, Japan	-	-	-	549	275 / 830	318
$Gd_3Al_{2.5}Ga_{2.5}O_{12}$:Ce Sidletskiy, ISMA Kharkiv, Ukraine	-	-	-	547	425/1530	381

$Gd_{1.5}Lu_{1.5}Al_{2.75}Ga_{2.25}O_{12}$:Ce and $Gd_3Al_{2.5}Ga_{2.5}O_{12}$:Ce – novel and efficient SCF scintillators, grown both from PbO and BaO fluxes

SCF scintillators based on the mixed garnet compounds

Scintillators based on the $Tb_{3-x}Gd_xAl_{5-y}Ga_yO_{12}$:Ce SCF LPE grown onto GAGG substrates from PbO and BaO based flux

SCF of TAGG:Ce (PbO) and TAGG:Ce (BaO) garnets LPE grown onto $Gd_{2.5}Ga_{2.5}Al_{2,5}O_{12}$ (GAGG) substrates at IF UKW in Bydgoszcz, Poland

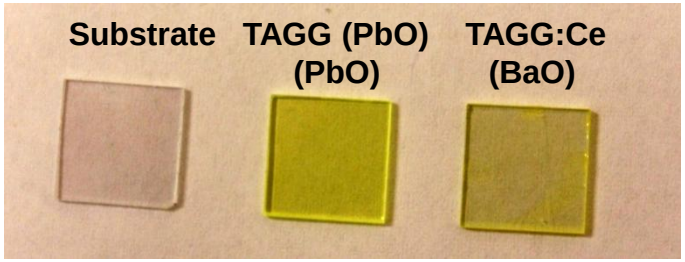

Yu. Zorenko, IEEE TNS, 2016, V.55(4), DOI: 10.1109/TNS.2015.2514.
Yu. Zorenko, e. a., Optical Materials, 2016; doi:10.1016/j.optmat.2016.03.031

Luminescent and scintillation properties of $Tb_{3-x}Gd_xAl_{5-y}Ga_yO_{12}$:Ce (PbO) SCF

CL spectra

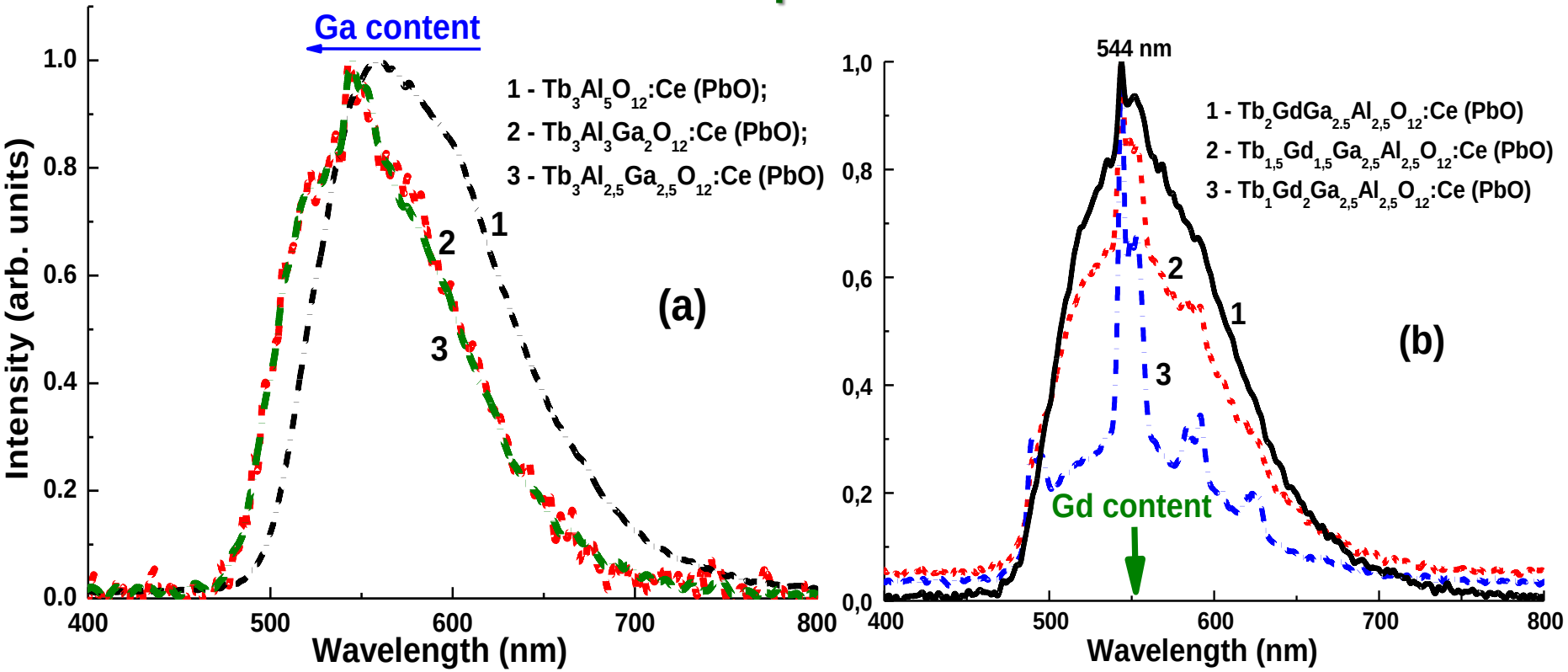

Normalized CL spectra of $Tb_{3-x}Gd_xAl_{5-y}Ga_yO_{12}$:Ce (PbO) SCF with different Ga (a) and Gd (b) content. T=300 K.

- Ga doping is shifted the CL spectra to blue range but also lead to notable decrease of the contribution of Ce^{3+} luminescence (Fig.a);
- Gd doping is shifted the CL spectra to red range and also lead to strong decrease of contribution of Ce^{3+} luminescence (Fig.b);

Luminescent and scintillation properties of $Tb_{3-x}Gd_xAl_{5-y}Ga_yO_{12}$:Ce (PbO) SCFs

Scintillation decay kinetic under excitation by α–particles of Pu^{239} source

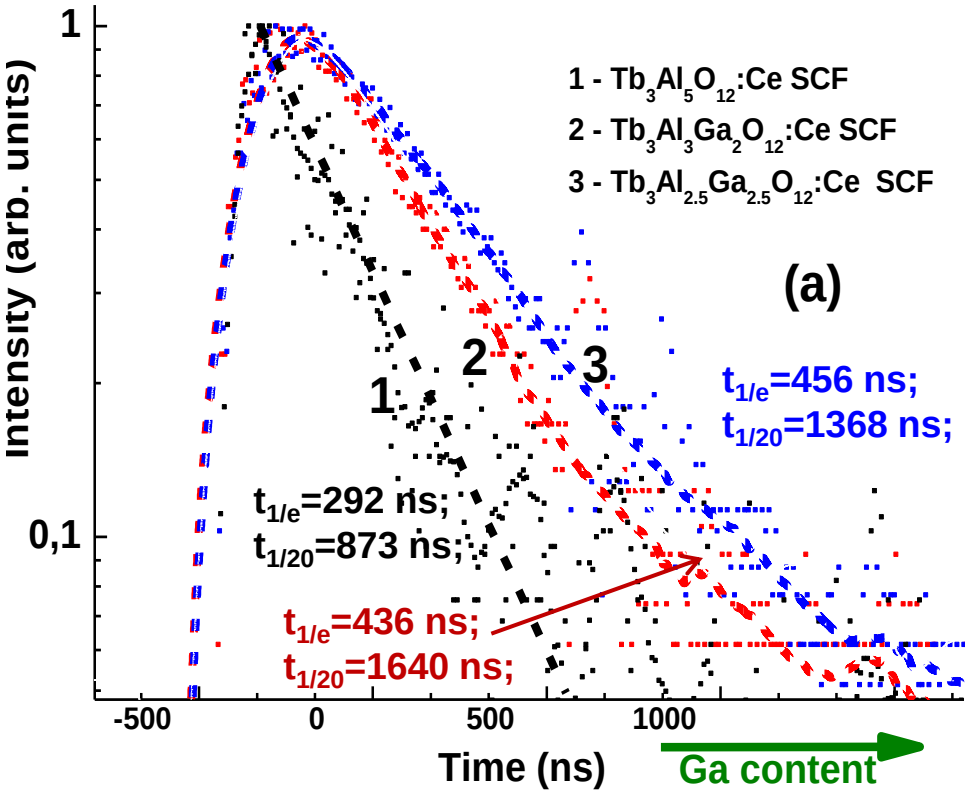

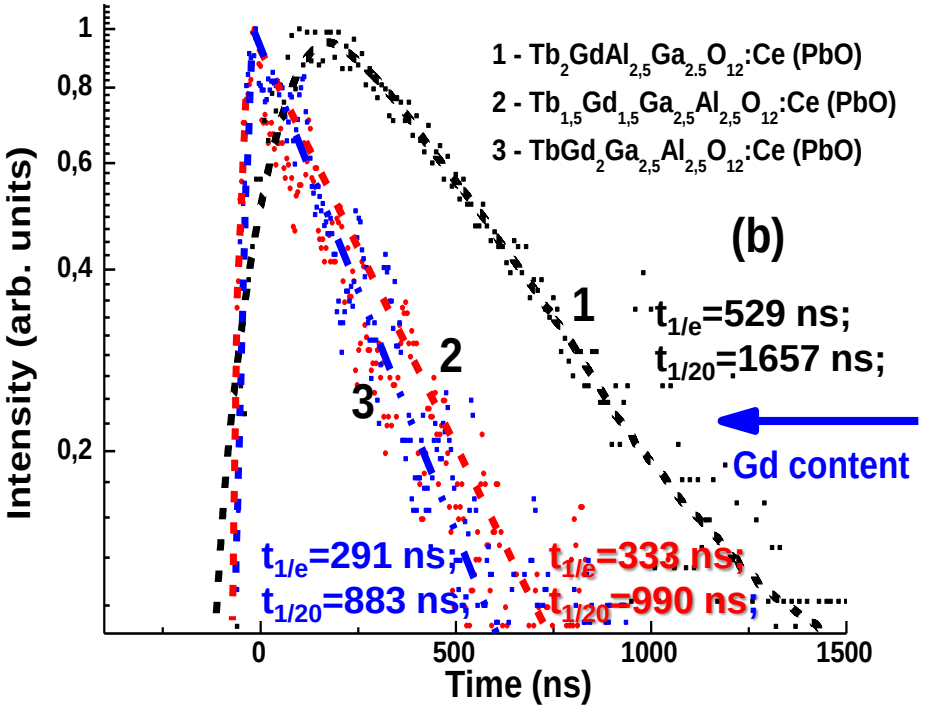

Normalized decay kinetic of $Tb_{3-x}Gd_xAl_{5-y}Ga_yO_{12}$:Ce (PbO) SCF with different content y of Ga cations (a) and different content x of Gd cations (b).

- **Ga doping in concentration y>2 in $Tb_3Al_{5-y}O_{12}$:Ce SCF leads to the notable delay of the scintillation decay most probably due to the termo-activated transitions from Ce^{3+} excited levels to the CB (Fig.a);**
- **Gd doping in concentration x>1.5 leads to the acceleration of the scintillation decay of $Tb_{3-x}Gd_xAl_{5-y}Ga_yO_{12}$:Ce SCF (Fig.b);**

Luminescent and scintillation properties of $Tb_{3-x}Gd_xAl_{5-y}Ga_yO_{12}$:Ce (BaO) SCFs

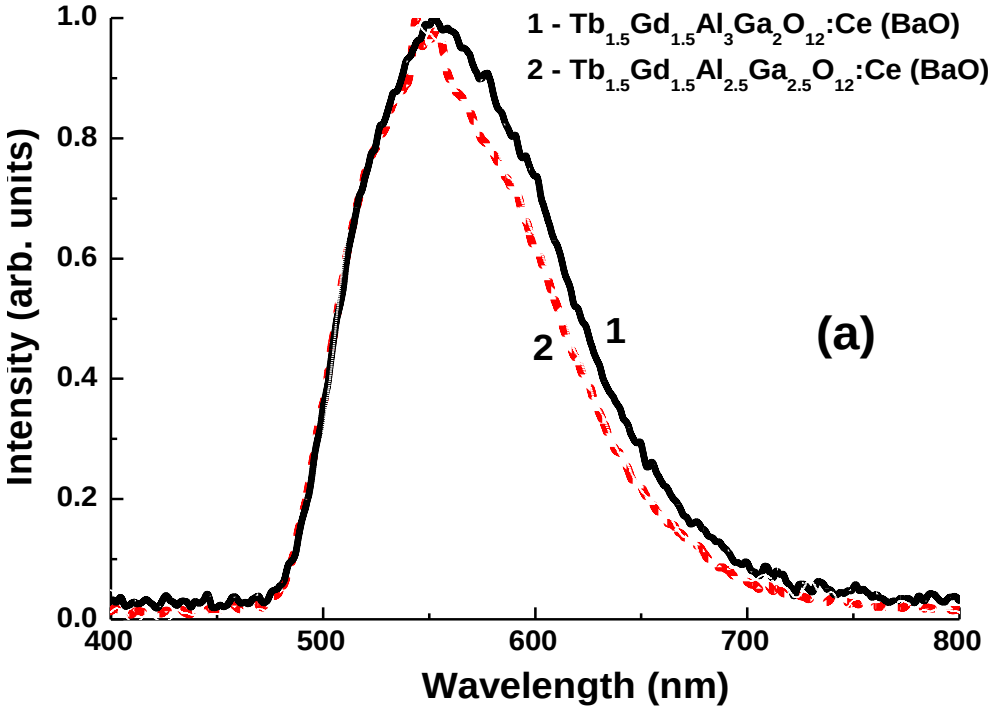

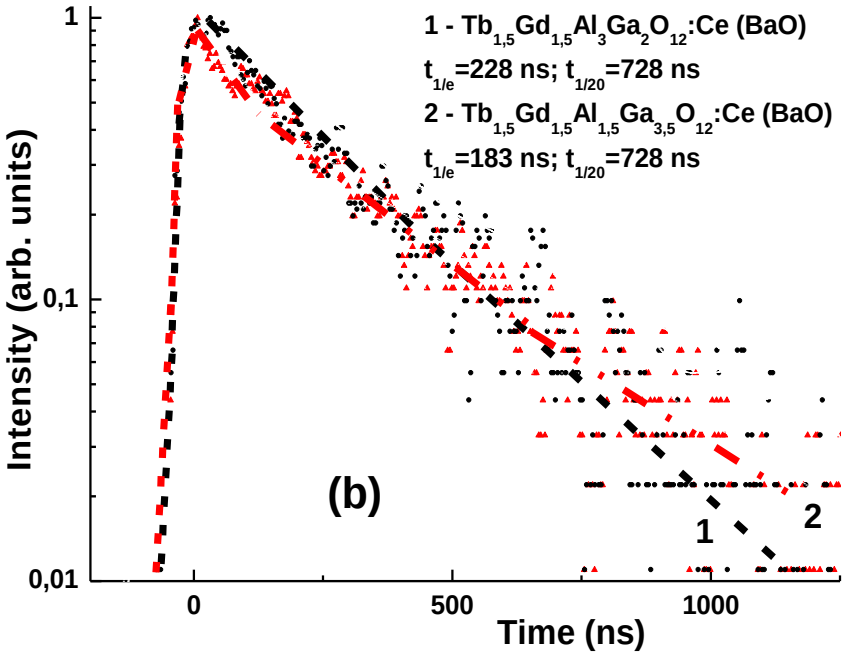

1. $Tb_{3-x}Gd_xAl_{5-y}Ga_yO_{12}$:Ce (BaO) SCF shows the relatively fast decay kinetic more close to exponential and very low TSL in the RT range

2. LY of $Tb_{1.5}Gd_{1.5}Al_{2-2.5}Ga_{3-2.5}O_{12}$:Ce (BaO) SCF is lagest from all developed garnet film scintillators

Luminescent and scintillation properties of $Tb_{3-x}Gd_xAl_{5-y}Ga_yO_{12}$:Ce SCFs

Table 1. Conditions of growth (type of flux and substrate; misfit **m** between lattice constant of SCF and substrate), maxima of emission spectra λ_{max}, scintillation decay time $t_{1/e}$,/ $t_{1/20}$ and LY of best samples in series of $(Tb,Gd)_3(Al,Ga)_5O_{12}$:Ce SCFs under excitation by Pu^{239} sources (measured with shaping time of 12 μs) in comparison with standard YAG:Ce SCF (360 phels/MeV) and LuAG:Ce SCF counterparts and standard $Gd_3Al_{2.5}Ga_{2.5}O_{12}$:Ce and $Gd_3Al_2Ga_3O_{12}$:Ce bulk crystals

Garnet content	Sub-strate	Type of flux	m, %	λ_{max}, nm	Decay time, $t_{1/e}/t_{1/20}$, ns	LY, %
$Y_3Al_5O_{12}$:Ce	YAG	PbO	-	535	57.3/ 171	100
$Lu_3Al_5O_{12}$:Ce	YAG	PbO	- 0.82	509	52.8 / 262	205
$Tb_3Al_5O_{12}$:Ce	YAG	PbO	+0.53	555	292 / 873	263
$Tb_3Al_3Ga_2O_{12}$:Ce	GGAG	PbO	-0.49	544	436 / 1340	230
$Tb_3Al_{2.5}Ga_{2.5}O_{12}$:Ce	GGAG	PbO	-0.44	544	456 / 1368	195
$Tb_2GdAl_{2.5}Ga_{2.5}O_{12}$:Ce	GGAG	PbO	-0.20	544	291 / 883	254
$Tb_{1.5}Gd_{1.5}Al_{2.5}Ga_{2.5}O_{12}$:Ce	GGAG	PbO	-0.12	544	333 / 990	340
$TbGd_2Al_{2.5}Ga_{2.5}O_{12}$:Ce	GGAG	PbO	-0.04	544	529/1657	160
$Tb_{1.5}Gd_{1.5}Al_3Ga_2O_{12}$:Ce	GGAG	BaO	- 1.3	560	228 / 728	380
$Tb_{1.5}Gd_{1.5}Al_{2.5}Ga_{2.5}O_{12}$:Ce	GGAG	BaO	-0.79	543	201/893	270
$Gd_3Al_2Ga_3O_{12}$:Ce Yoshikawa group, Japan	-	-	-	549	275/830	318
$Gd_3Al_{2.5}Ga_{2.5}O_{12}$:Ce ISM Kharkiv, Ukraine	-	-	-	547	425/1530	381

$Tb_3Al_5O_{12}$:Ce and $Tb_{1.5}Gd_{1.5}Al_{3-2.5}Ga_{2-2.5}O_{12}$:Ce garnets – novel and efficient SCF scintillators can be produced both from PbO and BaO based fluxes

Conclusions

The fast development of micro-imaging techniques using traditional X-sources and synchrotron radiation strongly demands single crystalline film (SCF) scintillating screens with high X-ray absorption for 2D/3D imaging with the micron-submicron spatial resolution.

For this purpose the SCF of YAG:Ce, LuAG:Ce, GGG:Tb and GGG:Eu garnets, LYSO:Ce,Tb orthosilicates and LuAP:Ce,Tb perovskites were successfully developed using the Liquid Phase Epitaxy (LPE) method in the last decade.

The novel concepts of the detectors for micro-tomography has been also proposed in the last years:

- **Using *hybrid multi-film scintillators* with the separate pathway for registration of the optical signal from each film scintillator.**
- **using *K–edge enginneering* of SCF scintillators based on the solid solution of Gd, Lu, Tb and Y containing mixed compounds grown onto the same known substrate.**

Such a novel concept requires creation of the efficient and heavy SCF scintillators which can be deposited by the LPE method onto the same luminescent or non-luminescent substrate.

Conclusions

- We report the creation of new heavy and efficient mixed $Gd_{1.5}Lu_{1.5}Al_{2.25}Ga_{2.75}O_{12}$:Ce, $Gd_3Al_{2.5}Ga_{2.5}O_{12}$:Ce, $Tb_3Al_5O_{12}$:Ce and $Tb_{1.5}Gd_{1.5}Al_{3-2.5}Ga_{2-2.5}O_{12}$:Ce SCF scintillators, grown by LPE method from PbO and BaO based fluxes, onto YAG and GAGG substrates, for different optoelectronic applications, first of all for microimaging detectors high spacial resolution.
- SCF of these garnets possess the very high LY, which exceed the LY of the best LuAG:Ce SCF samples, obtained from PbO based flux, and shows significantly lower afterglow, which is comparable with afterglow level of the best of LSO:Ce,Tb SCF sample usually used now for X ray imaging.
- Taking into account that the $Gd_{1.5}Lu_{1.5}Al_{2.25}Ga_{2.75}O_{12}$:Ce, $Tb_3Al_5O_{12}$:Ce and $Tb_{1.5}Gd_{1.5}Al_{3-2.5}Ga_{2-2.5}O_{12}$:Ce SCFs can be grown onto GAGG substrates, these SCFs and the high-quality $Gd_3Al_2Ga_3O_{12}$:Ce crystals can be used for creation using the LPE of the advanced ***"film-substrate" hybrid scintillators*** method for imaging applications.

Collaboration

V. Gorbenko, T. Zorenko, A. Iskalieva, K. Paprocki

EPI lab at Institute of Physics UKW in Bydgoszcz
Laboratory of Optoelectronic Materials (LOM), Department of Electronics
of Ivan Franko National University of Lviv, Ukraine

T. Martin, P.-A. Douishard, F. Riva
ESRF, Grenoble, France

C. Dujardin
Institute Lumiere Mateire
University Lyon 1

P. Bilski, A. Twardak, W. Gieszczyk
Institute for Nuclear Physics PAN
in Krakow, Poland

M. Nikl, V. Laguta, J.A. Mares,
A. Beitlerova, V. Jari, V. Babin
Institute of Physics, AS CzR,
Prague, Czech Republic

B. Grinyov, O. Sidletskiy, A. Fedorov
Institute for Scintillation Materials NAS
Ukraine, Kharkiv, Ukraine

Thank you for attention !

Grazie mille !

Dziękuję za uwagę !

Acknowledgement

The presentation was prepared based on the results of Polish National Science Center project No. 2012/07/B/ ST5/02376, NATO project No CBP.NUKR. CLG984305, Czech Science foundation project P204/12-0805 and Ministry Education and Science of Ukraine (projects No SF 20 and FK 64/34.

13.09.2016, Milan, Italy